# Dynamics and Control of Morphing Aircraft

Thomas Michael Seigler

Dissertation submitted to the Faculty of the
Virginia Polytechnic Institute and State University
in partial fulfillment of the requirements for the degree of

Doctor of Philosophy
in
Mechanical Engineering

Daniel J. Inman, Chair
Brian Sanders, Co-Chair
Harry H. Robertshaw
William H. Mason
Donald J. Leo
Craig C. Woolsey

August 2, 2005
Blacksburg, Virginia

Keywords: Morphing Aircraft, Flight Dynamics, Flight Control
Copyright 2005, Thomas Michael Seigler

# Dynamics and Control of Morphing Aircraft

by

Thomas Michael Seigler

(ABSTRACT)

The following work is directed towards an evaluation of aircraft that undergo structural shape change for the purpose of optimized flight and maneuvering control authority. Dynamical equations are derived for a morphing aircraft based on two primary representations; a general non-rigid model and a multi-rigid-body. A simplified model is then proposed by considering the altering structural portions to be composed of a small number of mass particles. The equations are then extended to consider atmospheric flight representations where the longitudinal and lateral equations are derived. Two aspects of morphing control are considered. The first is a regulation problem in which it is desired to maintain stability in the presence of large changes in both aerodynamic and inertial properties. From a baseline aircraft model various wing planform designs were constructed using Datcom to determine the required aerodynamic contributions. Based on nonlinear numerical evaluations adequate stabilization control was demonstrated using a robust linear control design. In maneuvering, divergent characteristics were observed at high structural transition rates. The second aspect considered is the use of structural changes for improved flight performance. A variable span aircraft is then considered in which asymmetric wing extension is used to effect the rolling moment. An evaluation of the variable span aircraft is performed in the context of bank-to-turn guidance in which an input-output control law is implemented.

"Education is an admirable thing, but it is well to remember from time to time that nothing worth knowing can be taught." -Oscar Wilde

# Acknowledgements

Much of my gratitude is owed to Dr. Daniel J. Inman for his guidance and friendship. I could not imagine working for a better advisor. I would like to thank my advisory committee Dr. Brian Sanders, Dr. Harry Robertshaw, Dr. William Mason, Dr. Donald Leo, and Dr. Craig Woolsey. I have great respect for each of them and always enjoy speaking with them on research an other unrelated matters.

During my time at Virginia Tech I have had the good fortune of friendship. I would especially like to acknowledge Nathan Siegel, Fernando Goncalves, and Mohammad Elahinia. I am thankful to have known them. I also thank my CIMSS colleagues, especially David Neal for his friendship. To Dr. Jae-Sung Bae I owe an especial gratitude for teaching me a bit of aerodynamics.

I would like to thank my parents and my sister. I hope that I have made them proud. And finally, I would like to thank my wife Amy. I am forever indebted to her for her love and support.

# Contents

**Acknowledgments** **iv**

**List of Figures** **vii**

**List of Tables** **x**

**1 Introduction** **1**

1.1 Background . . . . . 2

1.2 Aircraft Dynamics and Control . . . . . 6

1.3 Perspective and Overview . . . . . 9

**2 Dynamics of Morphing Aircraft** **12**

2.1 Kinematic Representations . . . . . 13

2.2 Coordinate Representations . . . . . 19

2.3 Dynamics of Lagrange, Kane, and Gibbs . . . . . 22

2.4 Morphing Aircraft Dynamics . . . . . 32

2.5 Summary . . . . . 40

**3 Equations of Atmospheric Flight** **41**

3.1 Stability and Wind Axis Equations . . . . . 42

3.2 Longitudinal Dynamics . . . . . 46
3.3 Lateral Dynamics . . . . . 47
3.4 Inertial Contributions . . . . . 49
3.5 Summary . . . . . 50

**4 Aerodynamic Modeling** **51**
4.1 Aerodynamic Derivatives . . . . . 51
4.2 Morphing Aircraft Model . . . . . 53
4.3 Variable Span Morphing . . . . . 59
4.4 Summary . . . . . 71

**5 Flight Control Design and Analysis** **73**
5.1 General Considerations . . . . . 74
5.2 Morphing Stabilization Analysis . . . . . 77
5.3 Nonlinear Navigation Control . . . . . 88
5.4 Summary . . . . . 105

**6 Conclusions and Recommendations** **107**
6.1 Conclusions . . . . . 107
6.2 Recommendations . . . . . 109

**Bibliography** **110**

**Appendix A - Flight Dynamics** **122**

**Appendix B - Datcom Aerodynamics** **125**

**Vita** **139**

# List of Figures


1.1 Variations in Modern Planform Design; (a) Northrop Grumman B-2 Stealth Bomber, (b) Grumman X-29, (c) Lockheed SR-71 Blackbird . . . . . 2

1.2 Morphing Aircraft Structures Conceptual Designs; (a) NextGen Aeronautics, (b) Lockheed Martin . . . . . 5

2.1 Adjacent Bodies with Relative Motion . . . . . 15

2.2 Kinematic Representation of a Constrained Multibody System . . . . . 17

2.3 Depiction of the Multibody Representation . . . . . 35

2.4 Depiction of the Multi-Mass Approximation . . . . . 39

4.1 Teledyne Ryan BQM-34 Firebee . . . . . 54

4.2 Morphing Planform Configurations; (a) Standard, (b) Loiter, (c) Dash, (d) Maneuver . . . . . 55

4.3 Variation in Lift Coefficient for Morphing Configurations . . . . . 56

4.4 Variation in Moment Coefficient for Morphing Configurations . . . . . 57

4.5 Aircraft with Variable Span Morphing . . . . . 60

4.6 Changes of Aspect Ratio and Wing Area . . . . . 66

4.7 Effects of Wingspan on Drag and Range . . . . . 66

4.8 Spanwise Lift Distribution . . . . . 67

4.9 Moment due to Left and Right Wing (right wing extended) . . . . . 68

4.10 Roll Producing Moment due to Wing Extension . . . . . 68
4.11 Spanwise Lift Distribution Due to Roll Speed $P$ . . . . . 69
4.12 Roll Damping Moment of Left and Right Wings (right wing extended) . . . 70
4.13 Total Roll Damping Moment due to Wing Extension . . . . . 70

5.1 Pitch Attitude Hold with Dynamic Compensation . . . . . 82
5.2 Root Locus for Loiter and Dash Configurations, $\theta(s)/u_{\delta_e}(s)$ . . . . . 82
5.3 Open-Loop Bode for Pitch-Attitude Compensators . . . . . 83
5.4 Step Response for Closed-Loop Pitch-Attitude Control . . . . . 83
5.5 Comparison of Linear and Nonlinear Simulations for Pitch-Attitude Control Design . . . . . 84
5.6 Configuration Change from Loiter to Dash Using Gain Scheduled Compensator; The Results Demonstrate the Effects of Transition Rate . . . . . 86
5.7 Configuration Change from Loiter to Dash While Maneuvering . . . . . 86
5.8 Configuration Change from Dash to Loiter Using Gain Scheduled Compensator; The Results Demonstrate the Effects of Transition Rate . . . . . 87
5.9 Configuration Change from Dash to Loiter While Maneuvering . . . . . 87
5.10 Geometry of Bank-to-turn Guidance . . . . . 91
5.11 Nominal I/O Linearization Control Tracking Stationary Commands . . . . . 97
5.12 Set-Point Guidance with Nominal I/O Linearization Control . . . . . 98
5.13 Nominal I/O Linearization Control Tracking Time-Varying Commands from Guidance System . . . . . 98
5.14 Optimal Allocation Scheme . . . . . 100
5.15 Comparison of Variable Span Control and Conventionally Actuated Designs Simulated 5% Error Applied to the Aerodynamic Coefficients . . . . . 101
5.16 Comparison of Variable Span Control and Conventionally Actuated Designs Simulated 10% Error Applied to the Aerodynamic Coefficients . . . . . 102

5.17 Conventional Aircraft Design Tracking ($\phi,\ \alpha\ \beta$) Commands from Proportional Navigation . . . . . 103

5.18 Variable Span Aircraft Design Tracking ($\phi,\ \alpha\ \beta$) Commands from Proportional Navigation . . . . . 103

5.19 X-Y Spacial Position of Aircraft Subjected to Proportional Navigation Tracking Commands . . . . . 104

# List of Tables

4.1 BQM-34C Baseline Specifications . . . . . 54

4.2 Datcom Aerodynamic Derivatives . . . . . 58

4.3 Baseline Wing Properties . . . . . 65

5.1 Morphing Aircraft Parameters . . . . . 81

# Chapter 1

# Introduction

Aircraft design has evolved at an extraordinary rate since the first manned flight in 1903. In only a century engineers have created aircraft that can travel at many times the speed of sound, traverse the earth's circumference without refueling, and even breach the atmosphere into space. Modern aircraft are capable of large payload transport, extreme-maneuverability, high speeds, high altitudes, and long ranges; they are capable of stealth, vertical take-off and landing, and long-range reconnaissance. Of course, no one design possesses all of these qualities. In fact, as demonstrated in Fig. (1.1), aircraft designs may be radically different depending on the operational requirements. To service the ever-growing mission requirements of the military, since 1970 no less than 36 new aircraft have been designed–all but 3 have been flight tested–under contract by the US Department of Defense. In the year 2000 there were 12 active aircraft production lines servicing the US arsenal, with one producing unmanned aircraft [1].

The reason for the varying aircraft types is that mission capabilities are a result of atmospheric interactions which are dictated predominantly by vehicle geometry. As a result, while an aircraft may be exceptional in some given flight regime, another can be found in which the aircraft performs poorly. An obvious remedy to this situation is to generate the capability of altering wing shape to enable a single aircraft to encompass a larger range of flight missions. This, however, has proved to be a very difficult problem.

Morphing aircraft are flight vehicles that change their shape to effectuate either a change in mission and/or to provide control authority for maneuvering, without the use of discrete control surfaces or seams. Aircraft constructed with morphing technology promise the dis-

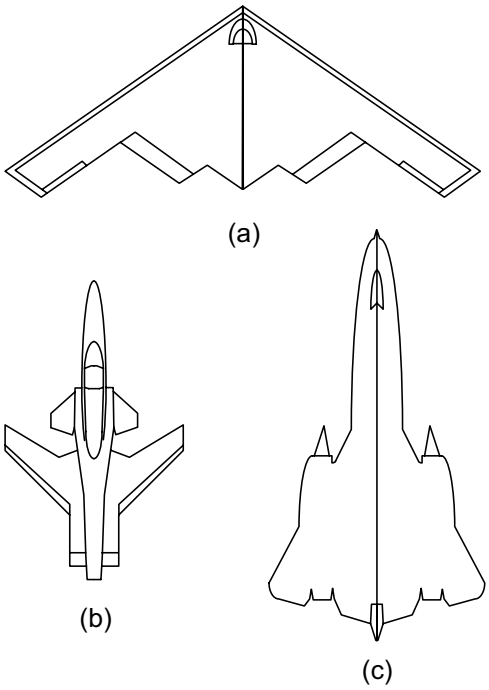



Figure 1.1: Variations in Modern Planform Design; (a) Northrop Grumman B-2 Stealth Bomber, (b) Grumman X-29, (c) Lockheed SR-71 Blackbird

tinct advantage of being able to fly multiple types of missions and to perform radically new maneuvers not possible with conventional control surfaces. Work in morphing aircraft is motivated by the US Air Force's move to rely more heavily on unmanned aircraft and also the desire to reduce the number of aircraft required for current demands–that is, the need for one aircraft to accomplish the goals of many. As almost all currently designed aircraft are centered around a fixed planform arrangement, the consideration of morphing calls for investigation into several research areas, including aerodynamic modeling, non-rigid dynamics, and flight control.

## 1.1 Background

The first planform changing aircraft design was the variable sweep wing. Both theory and experiments had shown that, while the straight wing was sufficient for most tasks, a swept wing is more ideal for high-speed flight, particularly at supersonic speeds. The first aircraft flown with the variable sweep design was the X-5 in 1951; later on, the F-111 and F-14 were

also equipped with variable swept wings. Ultimately, however, the additional weight of the mechanisms to accommodate the wing changes were found to be too costly with regards to fuel efficiency. It is this problem of weight that continues to be the largest difficulty in designing a feasible shape changing aircraft. Nonetheless, designers have continued to incorporate shape changing technology, albeit much smaller, into aircraft wings. Commercial transport aircraft alter chord and camber shape using leading and trailing edge flaps; the F-16 and F-18 also have leading edge flaps.

Wing shape changes currently in practice, while beneficial, provide only marginal improvements within a given flight regime. They can not, for instance, transform a fighter into a vehicle capable of long range and endurance. As an example, the F-16 has an aspect ratio of 3.2 while the RQ-4A Global Hawk has an aspect ratio of 25. Current designers seek to create the ability to alter the critical geometrical properties that would enable a single vehicle to accommodate multiple mission requirements. Such geometry changes are much more substantial than conventional methods and to accommodate large planform change while overcoming weight penalties requires significant advancements in both materials and actuator technology relative to what is currently applied in aircraft construction.

## Active Wing Programs

Developments in active material technology over the past several years have been accompanied by advanced concepts in aircraft design. Active materials such as piezoelectric/ electrostrictive ceramics and shape memory alloy (SMA) were deemed as suitable replacements for conventional actuation devices given their impressive energy density. Some of the first work in the field of adaptive aerodynamic surface actuation was conducted by Crawley *et al* who explored the beneficial coupling properties of active aeroelastic structures [2]. This sort of aerodynamic tailoring was first suggested by Weisshaar, who showed the capacity for improved control authority [3]. Later developments in active material technology applied to flight vehicles have included the development of a bimorph piezoelectric hinged flap [4], a trailing edge flap actuator for helicopter rotors [5, 6], and flexspar actuators for missile fins [7, 8].

As a result of previous successes, government sponsored research programs have sought to investigate shape changing aircraft technology. The first of these was the Defense Advanced Research Projects Agency/NASA/Air Force Research Laboratory (AFRL)/Northrop Grum-

man sponsored Smart Wing Program [9, 10, 11, 12, 13]. Begun in 1996, the Smart Wing program consisted of two phases culminating in wind tunnel testing of an aircraft wing outfitted with a shape memory alloy (SMA) actuated, hingeless, smoothly contoured trailing edge. Some benefits were a 15% increase in rolling moment and 11% increase in lift relative to the untwisted conventional wing.

The second program, started in 1996, was the Active Aeroelastic Wing (AAW) program, a joint program sponsored by DARPA/NASA/AFRL/Boeing Phantom Works [14, 15, 16]. The goal of this program was to demonstrate the advantages of active aeroelastic wing technology. The final result of the project was the flight testing of a full-size aircraft (F/A-18) equipped with flexible wings. Roll control was achieved by a differential deflection of the inboard and outboard leading-edge flaps. In addition to significant aerodynamic improvements, it was shown that active aeroelastic wing technology could reduce aircraft wing weight of up to 20 percent.

Yet another program is the Active Aeroelastic Aircraft Structures (3AS) project in Europe [17]. Under this program various active aeroelastic concepts have been developed and demonstrated. Of note, Amprikidis *et al* investigated internal actuation methods to continuously adjust wing shape while maintaining an optimal lift-drag ratio [18, 19, 20].

## Morphing Aircraft Structures (MAS) Program

The program under which the current study is funded is the DARPA Morphing Aircraft Structures (MAS) program. This program was initiated with goal of researching larger wing shape changes than have been previously investigated. Under the MAS program a *morphing* aircraft was defined as a multirole platform that:

- Changes its state substantially to adapt to changing mission environments.
- Provides superior system capability not possible without reconfiguration.
- Uses a design that integrates innovative combinations of advanced materials, actuators, flow controllers, and mechanisms to achieve the state change

The program originally funded three main contractors: NextGen Aeronautics, Raytheon Missile Systems, and Lockheed Martin. Several university partners were also included in the

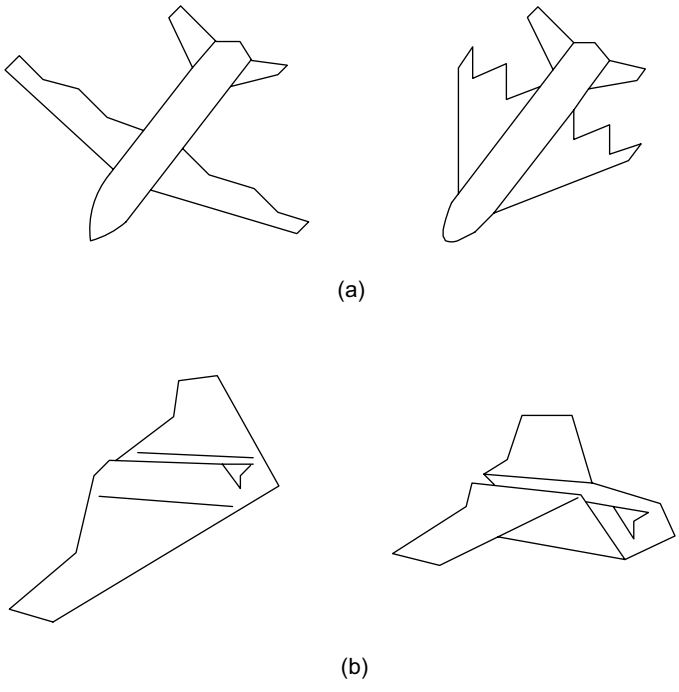



Figure 1.2: Morphing Aircraft Structures Conceptual Designs; (a) NextGen Aeronautics, (b) Lockheed Martin

program resulting in numerous fundamental theoretical and experimental studies of material applications and methods of altering structural geometry to obtain improvements in flight performance. One of the first concepts from this program was an extension of leading and trailing edge control surfaces to fully adaptive wings; that is, a wing capable of changing its camber-shape at each section along the span of the wing. Like a bird's wing, such a desgin would be devoid of control surfaces, achieving flight control authority by changing wing shape. Of note, Gern *et al* performed a structural and aeroelastic analysis of an unmanned combat aerial vehicle (UCAV) with morphing airfoils [21, 22]. Petit *et al* performed similar evaluations [23] and Bae *et al* investigated the 2-dimensional aeroelastic effects of a variable camber wing. Since shaping a wing to achieve a desired control authority has non-unique solutions, several researchers have investigated optimizing wing shape to minimize actuator energy [24, 25, 26]. Others have investigated the methods to actuate morphing wing sections; novel methods such as *compliant mechanisms* have been studied extensively [27, 28, 29].

The MAS program has recently focused on the development of aircraft that are capable of significant planform alterations. Stated goals include a 200% change in aspect ratio, 50% change in wing area, 50% change in wing twist, and 20-degree change in wing sweep.

Furthermore, it is expected that the weight of the resulting wing should be no greater than that of a conventional aircraft. Such a design could be optimized for a given flight regime, such as loiter or take-off. Efforts to create these types of morphing aircraft are currently underway. The concept morphing aircraft designs for NextGen and Lockheed [30] are depicted in Fig. (1.2). Supporting research at the university level has included investigation into various wing morphing designs. Bae *et al* performed an aeroelastic analysis of a variable span wing for cruise missiles [31, 32]. Blondeau *et al* developed an inflatable telescopic spar and performed wind-tunnel test of a variable-span wing [33], and Neal *et al* developed a scaled morphing aircraft for wind-tunnel testing capable of variable span, sweep, and wing twist [34].

## 1.2 Aircraft Dynamics and Control

Beyond the actual methods employed to generate the required shape changes, there are also obstacles to overcome in the area of flight control. A morphing aircraft requires flight control laws capable of high performance while maintaining stability in the presence of large variations in aerodynamic forces, moments of inertia, and mass center. These requirements lead to underlying research aspects involving the interaction between the environment, aircraft structure, and flight control system. Specifically, the issues are the identification and approximation of the transient aerodynamic forces and moments of significant consequence, and methods of dynamic/aerodynamic modeling that are suitable for analysis and control design. The following is an overview of previous research that has been conducted in the both aircraft flight dynamics and control.

### Flight Dynamics

The standard rigid body equations of flight were first developed by Bryan in 1911 [35]. Almost 100 years later, these equations continue to be used in the analysis, simulation, and design of almost every modern aircraft. This is of course no surprise since the laws of motion developed by Newton, Euler, Lagrange, and Hamilton continue to be valid for such rigid-body evaluations. The more important contribution of Bryan was the extraction of the longitudinal equations from the six-degree-of-freedom dynamics and furthermore, the incorporation of the applied aerodynamic forces and moments via the *stability derivatives*. The

result was a set of time-invariant ordinary differential equations that could be evaluated by existing methods of stability analysis. Most notable is Routh's stability criterion, developed in the early 1900's. Over the years the flight equations have evolved into a standardized dimensionless form with the small perturbation motions being characterized by five modes: phugoid, longitudinal short period, dutch roll, roll, and spiral. Along the way there have been numerous contributions in both theory and experiment, a summary of which can be found in the text by Abzug and Larrabee [36].

The first inclusion of nonrigid components, as an addendum to the standard rigid body equations, came from the desire to introduce the effects of spinning elements, such as propellers or the rotors of a jet engine. This was accomplished by simply adding the resulting angular momentum of the spinning rotors to the angular momentum of the rigid body. After several years of research in the field of aeroelasticity [37], the importance of such effects on rigid body motions became apparent [38, 39]. The first link of the two, seemingly separate, fields was produced by Bisplinghoff and Ashley who derived the equations of motion for an unrestrained flexible body [40]. Later Milne extended the former concepts of aircraft stability to include aeroelastic effects [41]. Corrections and additions to the flexible aircraft equations were made by several contributers [42, 43, 44]. Most recently, Meirovitch *et al* presented a unified theory of flight dynamics and aeroelasticity [45]; this work was later extended to a derivation of the explicit equations of motion in body-fixed coordinates [46, 47].

In the 1960's, stemming from the need to model complex satellites and spacecraft, the new field of multibody dynamics emerged. With the advancements in computer technology, as well as numerical techniques, many previously intractable problems became approachable. One of the first was the problem of simulating the motion of an arbitrary number of connected rigid bodies [48]. Advancements also allowed the formulation of connected flexible bodies. Methods currently available in multibody dynamics, and their contributers, are covered in reviews by Huston [49], Shabana [50], and Schiehlen [51]. A substantial contribution to the field of multibody dynamics is credited to Kane, and his method–generally termed "Kane's Method"–was first formulated in 1965 [52]. Kane's method provides a simple method of formulating dynamic equations of both nonconservative and nonholonomic systems without using energy methods or Lagrange multipliers. Similar to the Gibbs-Appell equations [53, 54], Kane's method constitutes a very different approach than previously established methods (i.e., Newton, Lagrange, and Hamilton). Applications of Kane's method include complex spacecraft [55], robotics [56, 57], and dynamic computational methods [58, 59, 60].

Nevertheless, many researchers continued the advancement of the more traditional methods. Meirovitch *et al* derived the equations–coupled ordinary and partial differential equations–of motion for a flexible body using Lagrange's Equations for quasi-coordinates and the Extended Hamilton's Principle [61, 62]; this work was later extended to flexible multibody systems [63, 64]. Also, Woolsey derived the Hamiltonian description of a rigid body in a fluid coupled to a moving mass particle [65].

## Flight Control

The elements of classical and modern control theory can be attributed to a long and growing list of researchers; a comprehensive review of the subject was performed by Lewis [66]. The key elements of aircraft control are performance and robustness. According to Dorato [67], robust control is divided into *classical* (1927-1960), *state-variable* (1960 to 1975), and *modern robust* (1975-Present) periods. This division is used to outline the methods of aircraft control.

Methods stemming from the classical period are based on single-input single-output (SISO) transfer function descriptions of the dynamic system represented in the frequency and Laplace domain. They rely on the graphical methods such as the Nyquist, Bode, Nichols and root-locus plots; robustness is accounted for by gain/phase margin and the sensitivity function. Classical control has been implemented with great success for decades, however, the methods generally do not extend well to multi-input multi-output (MIMO) systems. For MIMO systems the classical approach is an iterative process–relying on both experience and intuition–of designing a control law for each transfer function of the system. The underlying assumption is that if the individual subsystems are well-behaved, then the total system will also comply. Examples have been shown to the contrary.

State-variable control is based on *system theory* of dynamic systems represented in state-space. During this period Kalman introduced key concepts of controllability, observability, optimal state feedback, and optimal state estimation [67]. Linear system theory became the basis for analysis; control theory was viewed as the altering of a system's dynamic structure via the eigenvalues and eigenvectors. In contrast to classical methods where control gains are chosen, state-variable control allowed for the gains to be calculated based on more precise analytical and numerical *optimal* methods–two major contributers are Bellman [68] and Pontryagin [69]. Although in most ways deemed superior to classical control, state-variable methods have lacked some of the useful tools of robust design.

Viewed as a blending of new and old, modern robust control design introduced methods using multivariable frequency domain approaches. The singular value was established as an important criterion in analyzing stability, coprime matrix factorization was introduced as a design tool, and the small gain theorem was utilized extensively. Some important contributions of this period can be attributed to MacFarlane and Postlethwaite [70], Doyle and Stein [71], and Safonov *et al* [72], to name only a few. In addition to linear methods there has also been an increased development of nonlinear analysis in flight control–this might be considered an addendum to the modern robust period. Nonlinear methods of analysis are based on the stability theorems of Lyapunov and include, most notably for aircraft applications, a technique of *feedback linearization* termed *dynamic inversion* [73, 74]. Dynamic inversion is a mathematically elegant method of control that allows for the consideration of nonlinear characteristics of a dynamic system. However, it lacks many of the powerful design tools of linear theory that can be used for stability and robustness analysis– the field of linear system theory, where much is known, is only a small subset of nonlinear systems, where much more is not.

## 1.3 Perspective and Overview

Because aircraft control is model based, and the aerodynamic forces can change significantly and with a degree of uncertainty, an enormous amount of information is required in the design process. For a rigid aircraft the implementation of a flight control system involves an extensive process of aerodynamic testing, analytical design, numerical simulation, and flight testing. For a multi-configuration aircraft it is apparent that the task of control design becomes more involved. The overwhelming majority of conventional control design employs linear methods that are optimized at various operating points. Therefore, considering a variable planform aircraft, these methods would require a robust, optimized design for each operating point and for each aircraft configuration. The design process then becomes equivalent to developing a flight control system for several different aircraft types.

In addition, there is also the question of the transient phase of morphing; that is, control of the aircraft during the transition from one structural state to the next. Although modern aircraft certainly contain various moving components, in the majority of cases the effect of these components can be considered negligible due to small displacements and low relative mass. As a result, the inertial forces caused by the moving components can be approximated

as constant without significant consequence. For an aircraft undergoing large structural changes, however, standard rigid body analysis is insufficient. If the changes are slow, then a quasi-steady dynamic and aerodynamic approximation may be sufficient. If, alternatively the changes are desired to be very fast or while maneuvering, and the moving components are of substantial mass, then it is uncertain whether this assumption is sufficient for ensuring stable and high performance flight.

To begin to approach some of these problems requires an adequate state-variable description (i.e. the equations of atmospheric flight) of the morphing aircraft. An important consideration in generating this model is its level of complexity. This issue is addressed succinctly by Zhou [75]:

> "A good model should be simple enough to facilitate design, yet complex enough to give the engineer confidence that designs based on the model will work on the true plant."

With this in mind, Chapters 2 through 4 are concerned with modeling the transient dynamics of an aircraft undergoing large planform changes. In Chapter 2 a kinematic framework is first developed as a means to describe both the gross aircraft motion and the relative translation and rotation of moving components–the notation employed is similar to that of Roberson [76]. Dynamic equations are then derived by Kane's method based on the chosen kinematic description. The choice of the quasi-coordinates uniquely determines the form of the dynamic equations of motion. A particular set of coordinates are chosen so that the dynamics can be expressed in detail. Two basic models are presented: a non-rigid body model and a multi-rigid body model. As a compromise between the difficulties that result from these two approaches, a rigid-body multi-point-mass model is derived. Using the models derived in Chapter 2, the atmospheric flight equations are derived in Chapter 3. For reference, the full scalar equations are given in Appendix A. Chapter 4 presents a framework to account for the applied aerodynamic forces. Quasi-steady conditions are assumed, and the aerodynamic derivatives that result from this assumption are evaluated using Datcom–input and output files are provided in Appendix B. Similar to the research conducted by NextGen Aeronautics [77], the planform of the Teledyne Ryan BQM-34 "Firebee" is used as a baseline aircraft.

There are two basic approaches to controlling a morphing aircraft. The first is to consider the structural changes as additional dynamic/aerodynamic forcing inputs that can be controlled; this will involve a complex interaction between inertial forces and applied aerodynamic forces.

In this scheme, structural changes would be controlled in an efficient manner by feedback, thus taking into account the dynamic state of the aircraft. Besides morphing applications researchers have begun to investigate making use of inertial forces to obtain better control authority. Moving mass control has been explored for underwater vehicles [78, 79], space structures [80, 81], kinetic warheads [82], and re-entry vehicles [83]. The second approach is to change shape in an open-loop manner, without consideration of the overall vehicle state. The objective is then control in spite of the structural changes, making the subject more similar to the study of flexible aircraft control [45, 46]. The first approach is referred to as *control morphing* and the second as *planform morphing*. In Chapter 5, both methods of control are addressed. In particular, an investigation into the stabilizing a morphing aircraft is presented using classical methods. Finally, control morphing–maneuvering using variable span wings–is investigated using the nonlinear technique of dynamic inversion.

This thesis is concluded with the Chapter 6, which discusses the main results and provides suggestions for further research.

# Chapter 2

# Dynamics of Morphing Aircraft

The goal of this chapter is to develop the equations of motion for a morphing aircraft that is in the process of undergoing large planform changes. A kinematic framework is first developed as a means to describe both the gross aircraft motion and the relative translation and rotation of moving components. Kane's method is then derived, alongside Lagrange's equations and the Gibbs-Appell equations, from D'Alambert's principle to demonstrate the relationship between the three "energy type" methods–to the author's knowledge these relationships have never been explicitly demonstrated in the literature. Furthermore, methods of dealing with non-homogenous constraints, in the form of specified motion, are discussed. Dynamic equations are then derived by Kane's method based on the chosen kinematic description. Specifically, the choice of the quasi-coordinate vector uniquely determines the form of the dynamic equations of motion; a particular set of coordinates are chosen so that the dynamics can be expressed in detail. Two basic models are presented: a non-rigid body model and a multi-rigid body model. In choosing a particular model there exists a trade-off in one complexity for another. In particular, the non-rigid body model is amenable to decoupling, although the resulting equations are nonautonomous. Alternatively, the multi-body approach has the capacity of time-invariance, but at the cost of a larger degree of complexity. As an alternative to either of these derivations, we consider modeling the aircraft as a single body coupled to a small number of moving masses. This approach can be thought of as a compromise between the non-rigid and multi-body approaches.

## 2.1 Kinematic Representations

We begin in the typical manner by defining two euclidean spaces: an inertial coordinate frame $\mathcal{F}^0(\mathbb{R})$ composed of origin and a dextral orthonormal basis set $\{O^0, \mathrm{e}^0\}$, and a moving body coordinate frame $\mathcal{F}^i(\mathbb{R})$, corresponding to body $B_i$, with $\{O^i, \mathrm{e}^i\}$. The motion of $\mathcal{F}^i$ with respect to $\mathcal{F}^0$ can be determined by the location of $O^i$ with respect to $O^0$, given by the Cartesian vector $\boldsymbol{b}^{0i}$, and the relative orientation of $\mathbf{e}^i$ with respect to $\mathbf{e}^0$, determined by the components of the operator $\mathbf{A}^{0i} \in SO(3)$.

### Rotational Kinematics

By definition, the component vectors of $\mathrm{e}^0 = \{\mathbf{e}_1^0, \mathbf{e}_2^0, \mathbf{e}_3^0\}$ can be written as a linear combination of the vectors of $\mathrm{e}^i = \{\mathbf{e}_1^i, \mathbf{e}_2^i, \mathbf{e}_3^i\}$. Letting $\mathbf{e}^i = (\mathbf{e}_1^i, \mathbf{e}_2^i, \mathbf{e}_3^i)$ and $\mathbf{e}^0 = (\mathbf{e}_1^0, \mathbf{e}_2^0, \mathbf{e}_3^0)$ the previous statement indicates that

$$\mathbf{e}^0 = \mathbf{A}^{0i}\ \mathbf{e}^i \tag{2.1}$$

where $\mathbf{A}^{0i}$ is a non-unique matrix representation whose components are parameterized in any convenient manner. In flight dynamics the parameterization is typically chosen as a set of three Euler angles, although this is not always the case [84]. Due to the requirement that the two bases be orthonormal $\mathbf{A}^{0i}$ is necessarily orthonormal (it is also unitary); that is $(\mathbf{A}^{0i})^{-1} = (\mathbf{A}^{0i})^T \triangleq \mathbf{A}^{i0}$. Operators of this type belong to the special orthogonal group $SO(3)$. The inverse transformation is then

$$\mathbf{e}^i = \mathbf{A}^{i0}\ \mathbf{e}^0 \tag{2.2}$$

As a result of Eqs. (2.1) and (2.2), a vector represented by its components $\boldsymbol{r}^i \in \mathcal{F}^i$ can be alternatively expressed as $\boldsymbol{r}^0 \in \mathcal{F}^0$ by the operation

$$\boldsymbol{r}^0 = \mathbf{A}^{0i}\ \boldsymbol{r}^i \tag{2.3}$$

and the inverse operation by

$$\boldsymbol{r}^i = \mathbf{A}^{i0}\ \boldsymbol{r}^0 \tag{2.4}$$

By Poisson's kinematical equation, it can be shown that

$$\dot{\mathbf{A}}^{i0} = -\tilde{\boldsymbol{\omega}}^{i0}\mathbf{A}^{i0} \tag{2.5}$$

or

$$\dot{\mathbf{A}}^{0i} = \mathbf{A}^{0i}\tilde{\boldsymbol{\omega}}^{i0} \tag{2.6}$$

where $\boldsymbol{\omega}^{i0} \in \mathcal{F}^i$ is the angular velocity vector and $(\sim)$ denotes the operator that transforms a vector into its skew symmetric matrix representation (i.e., $\tilde{\mathbf{x}}\boldsymbol{y} = \boldsymbol{x} \times \boldsymbol{y}\ \forall\ \boldsymbol{x},\boldsymbol{y} \in \mathbb{R}^3$).

Now consider two bodies, $B_i$ and $B_j$, as shown in Fig. (1). By analogy to Eq. (2.4) the transformation of a vector between frames, $\mathcal{F}^j \to \mathcal{F}^i$, can be found by

$$\boldsymbol{r}^i = \mathbf{A}^{ij}\boldsymbol{r}^j$$

Similarly, Poisson's equation for adjacent bodies is

$$\dot{\mathbf{A}}^{ji} = -\tilde{\boldsymbol{\omega}}^{ji}\mathbf{A}^{ji} \tag{2.7}$$

or

$$\dot{\mathbf{A}}^{ij} = \mathbf{A}^{ij}\tilde{\boldsymbol{\omega}}^{ji} \tag{2.8}$$

Note that in choosing the parameterization of $\mathbf{A}^{ij}$ it is important to consider the limits on the relative motion of adjoining bodies. The Eulerian angles, as with any three dimensional parameterization, introduce a singularity in the kinematic equations. The reason for this is that it is not possible to find a global diffeomorphism between $SO(3)$ and $\mathbb{R}^3$ [85]. Thus to avoid choosing multiple Eulerian angle sets that accommodate the relative rotation of each adjoining body a four dimensional parameterization, such as Quaternions or Euler parameters, may be appropriate. A discussion of the the many parameterizations on $SO(3)$ can be found in [86, 87].

Letting $L(i)$ be the lower body array [87]–that is, the index of the adjoining lower numbered body of $B_i$–the transformation operator between any basis $\mathbf{e}^i$ and the inertial basis $\mathbf{e}^0$ can

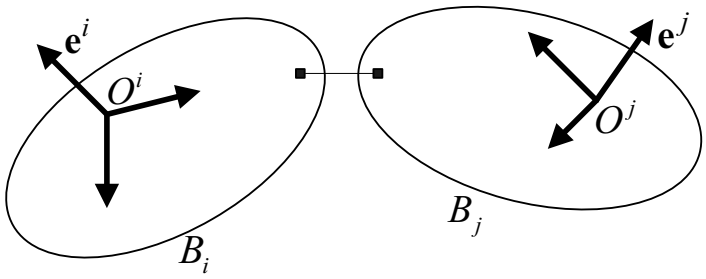



Figure 2.1: Adjacent Bodies with Relative Motion

be found by

$$\mathbf{A}^{i0} = \prod_i \mathbf{A}^{iL(i)} \tag{2.9}$$

By application of Eq. (2.9), the transformation of, for example, $\mathbf{A}^{20}$ can be expressed as

$$\mathbf{A}^{20} = \mathbf{A}^{21}\mathbf{A}^{10}$$

and the derivative is evaluated by

$$\dot{\mathbf{A}}^{20} = \dot{\mathbf{A}}^{21}\mathbf{A}^{10} + \mathbf{A}^{21}\dot{\mathbf{A}}^{10}$$

From Eq. (2.7) this can be reduced as follows:

$$\begin{aligned}
\dot{\mathbf{A}}^{20} &= -\tilde{\boldsymbol{\omega}}^{21}\mathbf{A}^{21}\mathbf{A}^{10} - \mathbf{A}^{21}\tilde{\boldsymbol{\omega}}^{10}\mathbf{A}^{10} \\
&= -\tilde{\boldsymbol{\omega}}^{21}\mathbf{A}^{20} - \mathbf{A}^{20}(\mathbf{A}^{01}\tilde{\boldsymbol{\omega}}^{10}\mathbf{A}^{10}) \\
&= -\tilde{\boldsymbol{\omega}}^{21}\mathbf{A}^{20} - \mathbf{A}^{20}(\mathbf{A}^{01}\boldsymbol{\omega}^{10})^{\sim}\mathbf{A}^{02}\mathbf{A}^{20} \\
&= -\tilde{\boldsymbol{\omega}}^{21}\mathbf{A}^{20} - (\mathbf{A}^{20}\mathbf{A}^{01}\boldsymbol{\omega}^{10})^{\sim}\mathbf{A}^{20} \\
&= -(\boldsymbol{\omega}^{21} + \mathbf{A}^{21}\boldsymbol{\omega}^{10})^{\sim}\mathbf{A}^{20}
\end{aligned}$$

By Eq. (2.8) the inverse operation is

$$\dot{\mathbf{A}}^{02} = \mathbf{A}^{02}(\boldsymbol{\omega}^{21} + \mathbf{A}^{21}\boldsymbol{\omega}^{10})^{\sim}$$

Comparing the previous two equations with Eqs. (2.7) and (2.8) it is apparent that

$$\boldsymbol{\omega}^{20} = \boldsymbol{\omega}^{21} + \mathbf{A}^{21}\boldsymbol{\omega}^{10}$$

With the goal of finding a more general expression we consider, for example, the case of $i = \{1, 2, 3, 4, 5, ...\}$ and $L(i) = \{0, 1, 1, 2, 3, ...\}$ represented by Fig. (2.2). We let $L^0(5) = 5$, $L^1(5) = L(5) = 3$, $L^2(5) = L(L(5)) = L(3) = 1$, and finally $L^3(5) = L(L(L(5))) = L(1) = 0$. Using this notation, the transformation between any $\mathbf{e}^i$ and $\mathbf{e}^{L^r(i)}$, for any $r \in i$, can be found by the operation

$$\mathbf{A}^{iL^r(i)} = \prod_{k=0}^{r-1} \mathbf{A}^{L^k(i)L^{k+1}(i)} \tag{2.10}$$

Then by repeated application of Eqs. (2.7) and (2.10) the angular velocity $\boldsymbol{\omega}^{iL^p(i)} \in \mathcal{F}^i$ of basis $\mathbf{e}^{L^p(i)}$ relative to basis $\mathbf{e}^i$ can be found by

$$\boldsymbol{\omega}^{iL^r(i)} = \boldsymbol{\omega}^{iL(i)} + \sum_{h=1}^{r-1} \left[ \left( \prod_{m=0}^{h-1} \mathbf{A}^{L^m(i)L^{m+1}(i)} \right) \boldsymbol{\omega}^{L^h(i)L^{h+1}(i)} \right] \tag{2.11}$$

Then, from Eq. (2.8)

$$\dot{\mathbf{A}}^{L^r(i)i} = \mathbf{A}^{L^r(i)i}\tilde{\boldsymbol{\omega}}^{iL^r(i)},$$

The usefulness of Eq. (2.11) becomes apparent when the dynamic equations are defined relative to a single main body, but the constraint equations by motion of connected bodies.

## Translational Kinematics

Again referring to Fig. (2.2), the Cartesian vector $\boldsymbol{r}_k^0$ and $\boldsymbol{\rho}_k^i$ locate the same point in $\mathbb{R}^3$ relative to $O^0$ and $O^i$, respectively. The location of this point can be expressed as

$$\boldsymbol{r}_k^0 = \boldsymbol{b}^{0i} + \mathbf{A}^{0i}\boldsymbol{\rho}_k^i \tag{2.12}$$

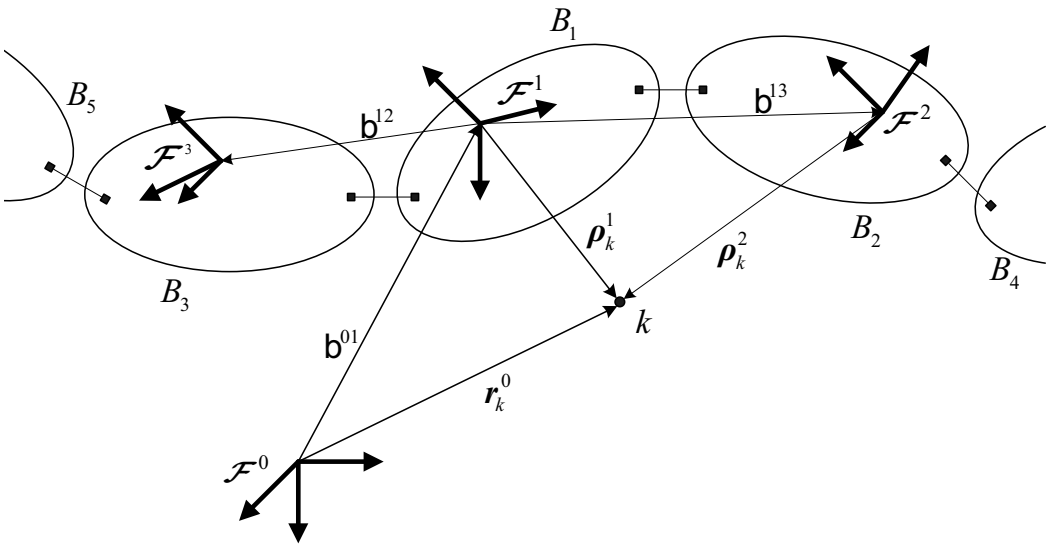



Figure 2.2: Kinematic Representation of a Constrained Multibody System

where $\boldsymbol{b}^{0i}$ locates origin $O^i$ with respect to $O^0$. With reference to Eq. (2.5), the time derivative is

$$\dot{\boldsymbol{r}}_k^0 = \dot{\boldsymbol{b}}^{0i} - \mathbf{A}^{0i}\tilde{\boldsymbol{\rho}}_k^i\boldsymbol{\omega}^{i0} + \mathbf{A}^{0i}\dot{\boldsymbol{\rho}}_k^i \tag{2.13}$$

Note that $\dot{\boldsymbol{b}}^{0i}$ is the derivative as seen by an observer in the inertial frame and $\dot{\boldsymbol{\rho}}_k^i$ implies differentiation as seen in the frame of $\mathcal{F}^i$. To be completely clear, the notation should include some indication to both the basis in which the vector is expressed and in which the derivative is taken. However, since the notation is somewhat cumbersome and the kinematic equations are well established, the frame of reference is assumed to be implied.

Taking the second derivative with respect to time results in

$$\ddot{\boldsymbol{r}}_k^0 = \ddot{\boldsymbol{b}}^{0i} - \mathbf{A}^{0i}\tilde{\boldsymbol{\omega}}^{i0}\tilde{\boldsymbol{\rho}}_k^i\boldsymbol{\omega}^{i0} - 2\mathbf{A}^{0i}\dot{\tilde{\boldsymbol{\rho}}}_k^i\boldsymbol{\omega}^{i0} - \mathbf{A}^{i0}\tilde{\boldsymbol{\rho}}_k^i\dot{\boldsymbol{\omega}}^{i0} + \mathbf{A}^{0i}\ddot{\boldsymbol{\rho}}_k^i \tag{2.14}$$

From Eq. (2.4), this can be expressed in $\mathcal{F}^i$ as

$$\ddot{\boldsymbol{r}}_k^i = \mathbf{A}^{i0}\ddot{\boldsymbol{b}}^{0i} - \tilde{\boldsymbol{\omega}}^{i0}\tilde{\boldsymbol{\rho}}_k^i\boldsymbol{\omega}^{i0} - 2\dot{\tilde{\boldsymbol{\rho}}}_k^i\boldsymbol{\omega}^{i0} - \tilde{\boldsymbol{\rho}}_k^i\dot{\boldsymbol{\omega}}^i + \ddot{\boldsymbol{\rho}}_k^i \tag{2.15}$$

Defining $\boldsymbol{v}^i = \mathbf{A}^{i0}\dot{\boldsymbol{b}}^{0i}$, Eq. (2.15) becomes

$$\ddot{\boldsymbol{r}}_k^i = \dot{\boldsymbol{v}}^i + \tilde{\boldsymbol{\omega}}^{i0}\boldsymbol{v}^i - \tilde{\boldsymbol{\omega}}^{i0}\tilde{\boldsymbol{\rho}}_k^i\boldsymbol{\omega}^{i0} - 2\dot{\tilde{\boldsymbol{\rho}}}_k^i\boldsymbol{\omega}^{i0} - \tilde{\boldsymbol{\rho}}_k^i\dot{\boldsymbol{\omega}}^{i0} + \ddot{\boldsymbol{\rho}}_k^i \tag{2.16}$$

Equation (2.16) is therefore the inertial acceleration of a mass particle expressed entirely in body frame coordinates. Note that for a rigid body $\dot{\boldsymbol{\rho}}_k^i = \ddot{\boldsymbol{\rho}}_k^i = \mathbf{0}$. Due to the manner in which the applied aerodynamic forces are specified in flight mechanics, it is beneficial to work with a set of coordinates that identify the motion of the aircraft relative to the wind. The relative wind velocity vector $\boldsymbol{v}_r^i$ is defined as

$$\boldsymbol{v}_r^i = \boldsymbol{v}^i - \mathbf{A}^{i0}\boldsymbol{\gamma}_w^0$$

where $\boldsymbol{\gamma}_w^0$ is the velocity of the wind relative to the inertial basis. After some substitution, the inertial acceleration of $O^i$ can be expressed as

$$\mathbf{A}^{i0}\ddot{\boldsymbol{b}}^{0i} = \dot{\boldsymbol{v}}_r^i + \tilde{\boldsymbol{\omega}}^{i0}\boldsymbol{v}_r^i + \mathbf{A}^{i0}\dot{\boldsymbol{\gamma}}_w^0 \tag{2.17}$$

If the wind speed is assumed to be non-accelerating ($\dot{\boldsymbol{\gamma}}_w^0 = \mathbf{0}$), then $\dot{\boldsymbol{v}}_r^i$ and $\dot{\boldsymbol{v}}^i$ are equal and thus interchangeable in Eq. (2.16).

As an alternative to Eq. (2.12) we could also choose the representation

$$\boldsymbol{r}_k^0 = \boldsymbol{b}^{0i} + \mathbf{A}^{0i}\left(\boldsymbol{b}^{ij} + \mathbf{A}^{ij}\boldsymbol{\rho}_k^i\right) \tag{2.18}$$

in which motion of a point in $B_j$ is described relative to the frame $\mathcal{F}^i$; if $B_i$ is the lower adjoining body of $B_j$ then $i = L(j)$. Alternatively, if $i = L^r(j)$, then by repeated application of Eq. (2.10)

$$\boldsymbol{b}^{L^r(j)j} = \boldsymbol{b}^{L(j)j} + \sum_{h=1}^{r-1}\left[\left(\prod_{k=0}^{n-1}\mathbf{A}^{L^{k+1}(j)L^k(j)}\right)\boldsymbol{b}^{L^{h+1}(j)L^h(j)}\right] \tag{2.19}$$

Equation (2.19) is the translational equivalent of the rotational equation given by Eq. (2.11). Taking the first time derivative gives

$$\dot{\boldsymbol{r}}_k^0 = \dot{\boldsymbol{b}}^{0i} - \mathbf{A}^{0i}\left(\boldsymbol{b}^{ij} + \mathbf{A}^{ij}\boldsymbol{\rho}_k^i\right)^{\sim}\boldsymbol{\omega}^{i0} + \mathbf{A}^{0i}\left(\dot{\boldsymbol{b}}^{ij} - \mathbf{A}^{ij}\tilde{\boldsymbol{\rho}}_k^i\boldsymbol{\omega}^{ji}\right) \tag{2.20}$$

where a rigid body has been assumed; i.e., $\dot{\boldsymbol{\rho}}_k^i = 0$. Letting $\tilde{\mathbf{s}}_k^{ij} = (\boldsymbol{b}^{ij} + \mathbf{A}^{ij}\boldsymbol{\rho}_k^i)^{\sim}$, the second

time derivative, again expressed in the coordinates of $\mathcal{F}^i$, is

$$\begin{aligned}\ddot{\boldsymbol{r}}_k^i &= \dot{\boldsymbol{v}}^i + \tilde{\boldsymbol{\omega}}^{i0}\boldsymbol{v}^i - \tilde{\mathbf{s}}_k^{ij}\dot{\boldsymbol{\omega}}^{i0} - \tilde{\boldsymbol{\omega}}^{i0}\tilde{\mathbf{s}}_k^{ij}\boldsymbol{\omega}^{i0} + \ddot{\boldsymbol{b}}^{ij} + 2\tilde{\boldsymbol{\omega}}^{i0}\dot{\boldsymbol{b}}^{ij} \\ &- \left(2\tilde{\boldsymbol{\omega}}^{i0}\mathbf{A}^{ij}\tilde{\boldsymbol{\rho}}_k^i + \mathbf{A}^{ij}\tilde{\boldsymbol{\omega}}^{ji}\tilde{\boldsymbol{\rho}}_k^i\right)\boldsymbol{\omega}^{ji} - \mathbf{A}^{ij}\tilde{\boldsymbol{\rho}}_k^i\dot{\boldsymbol{\omega}}^{ji} \end{aligned} \tag{2.21}$$

where, for the general case of $i = L^r(j)$, $\boldsymbol{\omega}^{ji}$ is determined by Eq. (2.11) and $\boldsymbol{b}^{ij}$ by Eq. (2.19).

## 2.2 Coordinate Representations

For a dynamic system with $n$ degrees of freedom, its configuration can be described by, at least, $n$ generalized coordinates while the kinematics are described by the derivatives of these generalized coordinates. The choice of coordinates used to describe the motion of a system uniquely determines the form of the dynamic equations of motion.

### Rigid Body Coordinates

Considering an unconstrained rigid body $B_i$, its configuration can be quantified by the Cartesian vector $\boldsymbol{b}^{0i} = (X^{0i}, Y^{0i}, Z^{0i})$ and the relative orientation of the bases $\mathbf{e}^i$ and $\mathbf{e}^0$. Assuming that orientation is defined by a particular Euler angle set, composed of the elements of the scalar array $\Theta^{0i} = (\phi^{0i}, \theta^{0i}, \psi^{0i})$, an adequate choice for the generalized coordinates is $(q_1, q_2, q_3, q_4, q_5, q_6) = (X^{0i}, Y^{0i}, Z^{0i}, \phi^{0i}, \theta^{0i}, \psi^{0i})$ so that configuration space is the Cartesian product $\mathbb{R}^3 \times SO(3)$. The kinematics are then given by the coordinate derivatives $\dot{\boldsymbol{q}} = (\dot{\boldsymbol{b}}^{0i}, \dot{\Theta}^{0i})$. For Euler angle sets, the rotational kinematics are

$$\boldsymbol{\omega}^{i0} = \mathbf{D}^{i0}(\Theta^{0i})\ \dot{\Theta}^{0i} \tag{2.22}$$

where, unlike $\mathbf{A}^{0i}$, the operator $\mathbf{D}^{i0}$ is not unitary and its inverse always contains a singularity. Equation (2.22) is typically referred to as *Euler's kinematical equations*, or the *strapdown*

*equations* [88]. For the standard 3-2-1 Euler angle representation the transformation is

$$\mathbf{D}^{i0} = \begin{bmatrix} 1 & 0 & -\sin\theta \\ 0 & \cos\phi & \sin\phi\cos\theta \\ 0 & -\sin\phi & \cos\phi\cos\theta \end{bmatrix}$$

Expressing Eq. (2.13) in terms of the generalized coordinates gives

$$\dot{\boldsymbol{r}}_p^0 = \begin{bmatrix} \mathbb{1} & -\mathbf{A}^{0i}\tilde{\boldsymbol{\rho}}_p^i\mathbf{D}^{i0} \end{bmatrix} \dot{q} \tag{2.23}$$

where $\dot{\boldsymbol{\rho}}_p^i = \mathbf{0}$ for a rigid body. To avoid singularities associated with Eulerian angles, it may be advantageous to employ Euler parameters $\epsilon^{0i} = (\epsilon_1^{0i}, \epsilon_2^{0i}, \epsilon_3^{0i}, \epsilon_4^{0i})$ in which case the rotational kinematics are

$$\boldsymbol{\omega}^{i0} = 2\mathbf{E}^{i0}(\epsilon^{0i})\ \dot{\epsilon}^{0i}$$

In flight dynamics it is typically more useful to work with, not the generalized coordinate derivatives $\dot{q}$, but a set of coordinates that can be easily measured using an on board sensor array. This sensor array, composed of accelerometers and gyroscopes, is referred to as a *strapdown inertial navigation system* (INS)–hence the terminology *strapdown equations* of Eq. (2.22). The coordinates measured by the INS are $\ddot{\boldsymbol{y}} \triangleq (\dot{\boldsymbol{v}}^i, \dot{\boldsymbol{\omega}}^{i0})$ and the relationship between the coordinates $\dot{\boldsymbol{y}} = (\boldsymbol{v}^i, \boldsymbol{\omega}^{i0})$ and the generalized coordinate velocities is

$$\dot{\boldsymbol{q}} = \mathbf{H}\dot{\boldsymbol{y}} \tag{2.24}$$

where for the case of Eulerian angles

$$\mathbf{H} = \begin{bmatrix} \mathbf{A}^{0i} & \mathbf{0} \\ \mathbf{0} & \mathbf{D}^{0i} \end{bmatrix}$$

where $\mathbf{D}^{0i} \triangleq (\mathbf{D}^{i0})^{-1}$. Expressing Eq. (2.13) in terms of the quasi-coordinates results in

$$\dot{\boldsymbol{r}}_k^i = \begin{bmatrix} \mathbb{1} & -\tilde{\boldsymbol{\rho}}_k^i \end{bmatrix} \dot{\boldsymbol{y}} \tag{2.25}$$

Furthermore, rewriting Eq. (2.16) in terms of $\dot{\boldsymbol{y}}$ and $\ddot{\boldsymbol{y}}$ gives

$$\ddot{\boldsymbol{r}}_k^i = \begin{bmatrix} \mathbb{1} & -\tilde{\boldsymbol{\rho}}_k^i \end{bmatrix} \ddot{\boldsymbol{y}} + \begin{bmatrix} \tilde{\boldsymbol{\omega}}^{i0} & -\tilde{\boldsymbol{\omega}}^{i0}\tilde{\boldsymbol{\rho}}_k^i \end{bmatrix} \dot{\boldsymbol{y}} \tag{2.26}$$

The components of $\dot{\boldsymbol{y}}$ are generally referred to as *generalized velocities* or *generalized speeds* [89, 90, 87]. Instead of "coordinates", the terminology *quasi-coordinates* is often used due to the fact that, unlike the generalized coordinates, the generalized velocities are not the derivative of any underlying physical quantity [91, 92, 93].

## Non-rigid Body Coordinates

For a general non-rigid body the configuration becomes harder to describe because each of the elements may be moving with respect to one another in such a manner that velocity and attitude become difficult to define. This difficulty is somewhat alleviated if some of the elements are stationary with respect to one another in that the origin of the reference frame can be fixed relative to these elements and confined to translate and rotate with them. The body would then be partially rigid having non-rigid elements. There are several ways to describe such a system of particles. One method is to consider a single non-rigid body–$B_1$ with $\mathcal{F}^1 = \{O^1, \mathbf{e}^1\}$– of $N$ elements where it is assumed that the components of each $\tilde{\boldsymbol{\rho}}_k^1$ $(k = 1, 2, ..., N)$ is known as an explicit function of time, not to be solved for, belonging to the class of twice differentiable functions $\mathcal{C}_2$. Under these conditions the configuration can, as with the rigid body, be parameterized by the coordinates $\dot{\boldsymbol{y}} = (\boldsymbol{v}^1, \boldsymbol{\omega}^{10})$; the equations of motion would be accompanied by $N$ time-varying constraint equations for each $\tilde{\boldsymbol{\rho}}_k^1$. From Eq. (2.13), the velocity can be expressed in terms of the quasi-coordinates by

$$\dot{\boldsymbol{r}}_k^1 = \begin{bmatrix} \mathbb{1} & -\tilde{\boldsymbol{\rho}}_k^1 \end{bmatrix} \dot{\boldsymbol{y}} + \dot{\boldsymbol{\rho}}_k^1 \tag{2.27}$$

and from Eq. (2.16) the acceleration may be expressed as

$$\ddot{\boldsymbol{r}}_k^1 = \begin{bmatrix} \mathbb{1} & -\tilde{\boldsymbol{\rho}}_k^1 \end{bmatrix} \ddot{\boldsymbol{y}} + \begin{bmatrix} \tilde{\boldsymbol{\omega}}^{10} & -(\tilde{\boldsymbol{\omega}}^{10}\tilde{\boldsymbol{\rho}}_k^1 + 2\dot{\tilde{\boldsymbol{\rho}}}_k^1) \end{bmatrix} \dot{\boldsymbol{y}} + \ddot{\boldsymbol{\rho}}_k^1 \tag{2.28}$$

## Multi-Rigid Body Coordinates

Now considering a collection of $\mu$ rigid bodies, $B_i$ and $B_j$, the relative rotation of the corresponding body reference frames $\mathcal{F}^i$ and $\mathcal{F}^j$ can be determined by Euler's kinematical equation:

$$\boldsymbol{\omega}^{ji} = \mathbf{D}^{ji}(\Theta^{ij})\ \dot{\Theta}^{ij} \tag{2.29}$$

where $\Theta^{ij}$ contains the three Euler angles that give the orientation of $\mathbf{e}^j$ relative to $\mathbf{e}^i$. Similarly, using the Euler parameters, the rotational kinematics are

$$\boldsymbol{\omega}^{ji} = 2\mathbf{E}^{ji}(\epsilon^{ij})\ \dot{\epsilon}^{ij}$$

Instead of describing motion in terms of inertial coordinates, as in Sec. (2.2), we may also choose the relative coordinates $\dot{\boldsymbol{y}} = (\boldsymbol{v}^i, \boldsymbol{\omega}^{i0}, \dot{\boldsymbol{b}}^{ij}, \boldsymbol{\omega}^{ji})$. Thus, Eq. (2.20) becomes

$$\dot{\boldsymbol{r}}_k^i = \begin{bmatrix} \mathbb{1} & -\left(\boldsymbol{b}^{ij} + \mathbf{A}^{ij}\boldsymbol{\rho}_k^j\right)^{\sim} & \mathbb{1} & -\mathbf{A}^{ij}\tilde{\boldsymbol{\rho}}_k^j \end{bmatrix} \dot{\boldsymbol{y}} \tag{2.30}$$

and Eq. (2.21) may be written as

$$\begin{aligned} \ddot{\boldsymbol{r}}_k^i &= \begin{bmatrix} \mathbb{1} & -\left(\boldsymbol{b}^{ij} + \mathbf{A}^{ij}\boldsymbol{\rho}_k^j\right)^{\sim} & \mathbb{1} & -\mathbf{A}^{ij}\tilde{\boldsymbol{\rho}}_k^j \end{bmatrix} \ddot{\boldsymbol{y}} \\ &+ \begin{bmatrix} \tilde{\boldsymbol{\omega}}^{i0} & -\tilde{\boldsymbol{\omega}}^{i0}\left(\boldsymbol{b}^{ij} + \mathbf{A}^{ij}\boldsymbol{\rho}_k^j\right)^{\sim} - 2\tilde{\boldsymbol{\omega}}^{i0}\mathbf{A}^{ij}\tilde{\boldsymbol{\rho}}_k^j & 2\tilde{\boldsymbol{\omega}}^{i0}\dot{\boldsymbol{b}}^{ij} & -\mathbf{A}^{ij}\tilde{\boldsymbol{\omega}}^{ji}\tilde{\boldsymbol{\rho}}_k^j \end{bmatrix} \dot{\boldsymbol{y}} \end{aligned} \tag{2.31}$$

where, in general, $j = L^r(i)$, $r \in i$. Comparing this result with the representation of Eq. (2.26), it is apparent a representation using relative coordinates is more complex. The reason for using the more complex representation is that it is more natural to define the motion of one body with respect its adjoining body. In computer simulations the representation is arbitrary since transformations between reference frames are made with ease. However, as will be demonstrated, the relative coordinates provide a more useful means of creating time-invariant state-space representations of the dynamic equations of motion.

## 2.3 Dynamics of Lagrange, Kane, and Gibbs

Lagrange's form of d'Alembert's principle is the well-known scalar equation

$$\sum_{k=1}^{N} \left[\mathbf{f}_k^0 + \bar{\mathbf{f}}_k^0 - m_k\ddot{\boldsymbol{r}}_k^0\right] \cdot \delta\boldsymbol{r}_k^0 = 0 \tag{2.32}$$

where $\boldsymbol{r}_k^0$ is the inertial position vector locating the $k^{th}$ of $N$ particles, having mass $m_k$; $\delta\boldsymbol{r}_k^0$ is the virtual displacement, $\mathbf{f}_k^0$ is applied force, and $\bar{\mathbf{f}}_k^0$ is the constraint force.

## Dynamics of Generalized Coordinates

Supposing that each position vector can be written as a function of $n$ generalized coordinates and time, $\boldsymbol{r}_k^0 = \boldsymbol{r}_k^0(q_1, q_2, ..., q_n, t)$, then

$$\dot{\boldsymbol{r}}_k^0 = \sum_{r=1}^{n} \frac{\partial \boldsymbol{r}_k^0}{\partial q_r}\dot{q}_r + \frac{\partial \boldsymbol{r}_k^0}{\partial t} \tag{2.33}$$

where the vector coefficients $\partial \boldsymbol{r}_k^0/\partial q_r$ and $\partial \boldsymbol{r}_k^0/\partial t$ are termed *partial velocities*. Equation (2.33) can also be expressed as

$$\dot{\boldsymbol{r}}_k^0 = \frac{\partial \boldsymbol{r}_k^0}{\partial \boldsymbol{q}}\dot{\boldsymbol{q}} + \frac{\partial \boldsymbol{r}_k^0}{\partial t} \tag{2.34}$$

where $\boldsymbol{q}$ is an $n \times 1$ array and thus $\partial \boldsymbol{r}_k^0/\partial \boldsymbol{q}$ is a $3 \times n$ rectangular array. Note that $\boldsymbol{q}$ is not in general a vector quantity since its components may include rotational elements. Rotation can not be expressed as a vector quantity, failing to commute under the operation of vector addition [94]. The time derivative of rotation, however, is a vector–that is, $\dot{\boldsymbol{q}} \in \mathbb{R}^n$. From Eq. (2.34), the virtual displacement is

$$\delta \boldsymbol{r}_k^0 = \frac{\partial \boldsymbol{r}_k^0}{\partial \boldsymbol{q}}\delta \boldsymbol{q} \tag{2.35}$$

Therefore, a restatement of Eq. (2.32) in generalized coordinates is

$$\sum_{k=1}^{N} \left[ \frac{\partial \boldsymbol{r}_k^0}{\partial \boldsymbol{q}} \cdot \left( \mathbf{f}_k^0 + \bar{\mathbf{f}}_k^0 \right) - m_k \frac{\partial \boldsymbol{r}_k^0}{\partial \boldsymbol{q}} \cdot \ddot{\boldsymbol{r}}_k^0 \right] \cdot \delta \boldsymbol{q} = 0 \tag{2.36}$$

From Eq. (2.36) Lagrange's equations of motion can be derived in terms of the kinetic energy scalar function, $T = T(\dot{\boldsymbol{q}}, \boldsymbol{q})$ [92]. The resulting equations, for a holonomic system, are

$$\left[ \frac{d}{dt}\left( \frac{\partial T}{\partial \dot{\boldsymbol{q}}} \right) - \frac{\partial T}{\partial \boldsymbol{q}} \right]^T = \boldsymbol{Q} + \bar{\boldsymbol{Q}} \tag{2.37}$$

where the *generalized active force* ($\boldsymbol{Q}$) and *generalized constraint force* ($\bar{\boldsymbol{Q}}$) are defined as

$$\boldsymbol{Q} = \sum_{k=1}^{N} \frac{\partial \boldsymbol{r}_k^0}{\partial \boldsymbol{q}} \cdot \mathbf{f}_k^0, \quad \bar{\boldsymbol{Q}} = \sum_{k=1}^{N} \frac{\partial \boldsymbol{r}_k^0}{\partial \boldsymbol{q}} \cdot \bar{\mathbf{f}}_k^0$$

Proceeding toward an alternative expression for the dynamic equations of motion consider the total derivative of Eq. (2.34):

$$\ddot{\boldsymbol{r}}_k^0 = \frac{\partial \dot{\boldsymbol{r}}_k^0}{\partial \boldsymbol{q}} \dot{\boldsymbol{q}} + \frac{\partial \boldsymbol{r}_k^0}{\partial \boldsymbol{q}} \ddot{\boldsymbol{q}} + \frac{\partial \dot{\boldsymbol{r}}_k^0}{\partial t} \tag{2.38}$$

From Eqs. (2.38) and (2.34) we note that

$$\frac{\partial \ddot{\boldsymbol{r}}_k^0}{\partial \ddot{\boldsymbol{q}}} = \frac{\partial \dot{\boldsymbol{r}}_k^0}{\partial \dot{\boldsymbol{q}}} = \frac{\partial \boldsymbol{r}_k^0}{\partial \boldsymbol{q}}$$

Therefore, Eq. (2.36) can be written as

$$\sum_{k=1}^{N} \left[ \frac{\partial \boldsymbol{r}_k^0}{\partial \boldsymbol{q}} \cdot \left( \mathbf{f}_k^0 + \bar{\mathbf{f}}_k^0 \right) - m_k \frac{\partial \ddot{\boldsymbol{r}}_k^0}{\partial \ddot{\boldsymbol{q}}} \cdot \ddot{\boldsymbol{r}}_k^0 \right] \cdot \delta \boldsymbol{q} = 0 \tag{2.39}$$

and assuming that the generalized coordinates are independent, then

$$\sum_{k=1}^{N} m_k \frac{\partial \ddot{\boldsymbol{r}}_k^0}{\partial \ddot{\boldsymbol{q}}} \cdot \ddot{\boldsymbol{r}}_k^0 = \boldsymbol{Q} + \bar{\boldsymbol{Q}} \tag{2.40}$$

Defining the *generalized inertial force* ($\boldsymbol{Q}^*$) as

$$\boldsymbol{Q}^* = \sum_{k=1}^{N} m_k \frac{\partial \ddot{\boldsymbol{r}}_k^0}{\partial \ddot{\boldsymbol{q}}} \cdot \ddot{\boldsymbol{r}}_k^0 \tag{2.41}$$

then Eq. (2.40) may be expressed as

$$\boldsymbol{Q}^* = \boldsymbol{Q} + \bar{\boldsymbol{Q}} \tag{2.42}$$

Attributed to Kane [52], these equations produce $n$ second-order ordinary differential equations–in terms of the $n$ generalized coordinates–that are equivalent to those produced by Lagrange's equations. We may proceed further to generate an expression similar to Lagrange's equations by defining the acceleration energy

$$G = \frac{1}{2} \sum_{k=1}^{N} \left( m_k \ddot{\boldsymbol{r}}_k^0 \cdot \ddot{\boldsymbol{r}}_k^0 \right) \tag{2.43}$$

also known as the *Gibbs function* [91]–more precisely it is a *functional*. Note that since

$$\ddot{\boldsymbol{r}}_k^i \cdot \ddot{\boldsymbol{r}}_k^i = (\ddot{\boldsymbol{r}}_k^0)^T \mathbf{A}^{0i} \mathbf{A}^{i0} \ddot{\boldsymbol{r}}_k^0 = \ddot{\boldsymbol{r}}_k^0 \cdot \ddot{\boldsymbol{r}}_k^0$$

the Gibbs equation is equal in value, but different in form, when expressed in either inertial or body coordinates. From Eq. (2.43),

$$\frac{\partial G}{\partial \ddot{\boldsymbol{q}}} = \sum_{k=1}^{N} m_k \ddot{\boldsymbol{r}}_k^0 \cdot \frac{\partial \ddot{\boldsymbol{r}}_k^0}{\partial \ddot{\boldsymbol{q}}}$$

so that Eq. (2.39) can be written in terms of the Gibbs function as

$$\left[ \boldsymbol{Q} + \bar{\boldsymbol{Q}} - \left( \frac{\partial G}{\partial \ddot{\boldsymbol{q}}} \right)^T \right] \cdot \delta \boldsymbol{q} = 0 \tag{2.44}$$

Again, assuming that the coordinates variations are independent results in

$$\left( \frac{\partial G}{\partial \ddot{\boldsymbol{q}}} \right)^T = \boldsymbol{Q} + \bar{\boldsymbol{Q}} \tag{2.45}$$

These equations are known as the *Gibbs-Appell equations* and yield $n$ second-order differential equations in terms of the generalized coordinates [53, 54]. Analogous to Lagrange's equations being expressed as a function of kinetic energy, the Gibbs-Appell equations are expressed in terms of the acceleration energy, or Gibbs function. Finally, comparing Eqs. (2.37), (2.40), and (2.45) it is apparent that the relationship between Lagrange's, Kane's, and Gibbs' equations for generalized coordinates is

$$\frac{d}{dt} \left( \frac{\partial T}{\partial \dot{\boldsymbol{q}}} \right) - \frac{\partial T}{\partial \boldsymbol{q}} = \frac{\partial G}{\partial \ddot{\boldsymbol{q}}} = (\boldsymbol{Q}^*)^T$$

The principal criteria for choosing the method of formulation is typically based on the objective of simplicity [55], although there may be other factors. For example, it may be necessary to construct the energy expressions, in particular the kinetic and potential functionals, when energy based control methods are employed [95].

## Dynamics of Quasi-Coordinates

To find an expression in terms of the quasi-coordinates, $\dot{\boldsymbol{y}}$, we begin by noting the relationship between the generalized velocity and quasi-coordinates. From Eq. (2.24) the virtual displacement of $\boldsymbol{q}$ is

$$\delta \boldsymbol{q} = \mathbf{H}\ \delta \boldsymbol{y} \tag{2.46}$$

Substituting this expression into (2.35) gives

$$\delta \boldsymbol{r}_k^0 = \left( \frac{\partial \boldsymbol{r}_k^0}{\partial \boldsymbol{q}} \mathbf{H} \right)\ \delta \boldsymbol{y} \tag{2.47}$$

The fundamental equation, Eq. (2.32), then becomes

$$\sum_{k=1}^{N} \left[ \left( \frac{\partial \boldsymbol{r}_k^0}{\partial \boldsymbol{q}} \mathbf{H} \right) \cdot \left( \mathbf{f}_k^0 + \bar{\mathbf{f}}_k^0 \right) - m_k \left( \frac{\partial \boldsymbol{r}_k^0}{\partial \boldsymbol{q}} \mathbf{H} \right) \cdot \ddot{\boldsymbol{r}}_k^0 \right] \cdot \delta \boldsymbol{y} = 0 \tag{2.48}$$

Taking the first and second derivatives of $\boldsymbol{r}_k^0$ in terms of the quasi-coordinates results in

$$\dot{\boldsymbol{r}}_k^0 = \frac{\partial \boldsymbol{r}_k^0}{\partial \boldsymbol{q}} \mathbf{H} \dot{\boldsymbol{y}} + \frac{\partial \boldsymbol{r}_k^0}{\partial t} \tag{2.49}$$

Using this expression, and assuming that the kinetic energy can be expressed as $\bar{T} = \bar{T}(\boldsymbol{q}, \dot{\boldsymbol{y}}, t)$–note that $\bar{T} \neq T$–the following can be verified:

$$\left[ \frac{d}{dt} \left( \frac{\partial T}{\partial \dot{\boldsymbol{y}}} \right) - \frac{\partial T}{\partial \dot{\boldsymbol{y}}} \mathbf{H}^T \dot{\mathbf{H}} - \frac{\partial T}{\partial \boldsymbol{q}} \mathbf{H} \right]^T = \sum_{k=1}^{N} m_k \left( \frac{\partial \boldsymbol{r}_k^0}{\partial \boldsymbol{q}} \mathbf{H} \right) \cdot \ddot{\boldsymbol{r}}_k$$

Note that $\mathbf{H}$ may be reduced further [93]. Defining the generalized applied and constraint forces in terms of quasi-coordinates

$$\boldsymbol{F} = \sum_{k=1}^{N} \frac{\partial \dot{\boldsymbol{r}}_k^0}{\partial \dot{\boldsymbol{y}}} \cdot \mathbf{f}_k^0 = \mathbf{H}^T \boldsymbol{Q}, \quad \bar{\boldsymbol{F}} = \sum_{k=1}^{N} \frac{\partial \dot{\boldsymbol{r}}_k^0}{\partial \dot{\boldsymbol{y}}} \cdot \bar{\mathbf{f}}_k^0 = \mathbf{H}^T \bar{\boldsymbol{Q}} \tag{2.50}$$

results in the reformulation of Lagrange's equations given by

$$\left[ \frac{d}{dt} \left( \frac{\partial T}{\partial \dot{\boldsymbol{y}}} \right) - \frac{\partial T}{\partial \dot{\boldsymbol{y}}}\ \mathbf{H}^T \dot{\mathbf{H}} - \frac{\partial T}{\partial \boldsymbol{q}} \mathbf{H} \right]^T = \boldsymbol{F} + \bar{\boldsymbol{F}} \tag{2.51}$$

These are Lagrange's equations in terms of quasi-coordinates [93], also referred to as the *Boltzmann-Hamel* equations [55].

To arrive at Kane's equations for quasi-coordinates, same approach is taken as in the previous section; that is, by taking the second derivative

$$\ddot{\boldsymbol{r}}_k^0 = \left(\frac{\partial \dot{\boldsymbol{r}}_k^0}{\partial \boldsymbol{q}}\mathbf{H}\right)\dot{\boldsymbol{y}} + \left(\frac{\partial \boldsymbol{r}_k^0}{\partial \boldsymbol{q}}\dot{\mathbf{H}}\right)\dot{\boldsymbol{y}} + \left(\frac{\partial \boldsymbol{r}_k^0}{\partial \boldsymbol{q}}\mathbf{H}\right)\ddot{\boldsymbol{y}} + \frac{\partial \dot{\boldsymbol{r}}_k^0}{\partial t} \tag{2.52}$$

and noting that

$$\frac{\partial \ddot{\boldsymbol{r}}_k^0}{\partial \ddot{\boldsymbol{y}}} = \frac{\partial \dot{\boldsymbol{r}}_k^0}{\partial \dot{\boldsymbol{y}}} = \frac{\partial \boldsymbol{r}_k^0}{\partial \boldsymbol{q}}\mathbf{H} \tag{2.53}$$

Therefore, Eq. (2.48) takes the form

$$\sum_{k=1}^{N}\left[\frac{\partial \dot{\boldsymbol{r}}_k^0}{\partial \dot{\boldsymbol{y}}}\cdot\left(\mathbf{f}_k^0 + \bar{\mathbf{f}}_k^0\right) - m_k\frac{\partial \ddot{\boldsymbol{r}}_k^0}{\partial \ddot{\boldsymbol{y}}}\cdot\ddot{\boldsymbol{r}}_k^0\right]\cdot\delta\boldsymbol{y} = 0 \tag{2.54}$$

which is Lagrange's form of d'Alembert's principle expressed in quasi-coordinates. Upon defining the generalized inertial force in terms of quasi-coordinates

$$\boldsymbol{F}^* = \sum_{k=1}^{N} m_k\frac{\partial \ddot{\boldsymbol{r}}_k^0}{\partial \ddot{\boldsymbol{y}}}\cdot\ddot{\boldsymbol{r}}_k^0 \tag{2.55}$$

then Kane's equation in terms of quasi-coordinates is

$$\boldsymbol{F}^* = \boldsymbol{F} + \bar{\boldsymbol{F}} \tag{2.56}$$

If the Gibbs function is expressed in terms of the quasi-coordinates then

$$\frac{\partial G}{\partial \ddot{\boldsymbol{y}}} = \sum_{k=1}^{N} m_k\ddot{\boldsymbol{r}}_k^0\cdot\frac{\partial \ddot{\boldsymbol{r}}_k^0}{\partial \ddot{\boldsymbol{y}}}$$

Therefore, the Gibbs-Appell equations in terms of the quasi-coordinates is

$$\left(\frac{\partial G}{\partial \ddot{\boldsymbol{y}}}\right)^T = \boldsymbol{F} + \bar{\boldsymbol{F}} \tag{2.57}$$

Comparing this form with Eq. (2.45) it can be seen that the Gibbs-Appell equations take

the same form when expressed in either generalized coordinates or quasi-coordinates. This is not the case for Lagrange's equations. Comparing Eqs. (2.56) and (2.57), both are derived from Eq. (2.54), the difference being the defining of the Gibbs function. Although the Gibbs-Appell form was discovered first, it was Kane who recognized the usefulness of the preceding form of the equation. In particular, the Gibbs-Appell equations require that the acceleration vector be squared resulting in an unnecessary increase in complexity. More important distinctions, although not apparent in this work, of Kane's equations can be found in the literature [96, 97, 98, 99, 100]. Of particular note, Kane's method provides for the efficient formulation of the equations of motion for nonholonomic systems [101]. Other comparisons of Kane's method and the Gibbs-Appell equations can be found in [102, 103].

Finally, a comparison of the methods of Lagrange, Kane, and Gibbs gives the relation

$$\frac{d}{dt}\left(\frac{\partial T}{\partial \dot{\boldsymbol{y}}}\right) - \frac{\partial T}{\partial \dot{\boldsymbol{y}}}\,\mathbf{H}^T\dot{\mathbf{H}} - \frac{\partial T}{\partial \boldsymbol{q}}\mathbf{H} = \frac{\partial G}{\partial \ddot{\boldsymbol{y}}} = (\boldsymbol{F}^*)^T$$

Each method results in an identical set of $2n$-first-order differential equations. However, the cost of producing these equations is different. In terms of the calculation effort for complex systems, Kane's equations provides an efficient means of derivation. For this reason, Kane's method will be employed in subsequent development.

## Constrained Equations

In developing the dynamic equations of the previous section, it was assumed that both the generalized coordinates and the quasi-coordinate variations ($\delta\boldsymbol{q}$ and $\delta\boldsymbol{y}$) are independent, such that for a system with $\nu$ degrees of freedom, $\delta\boldsymbol{q} \in \mathbb{R}^\nu$ and $\delta\boldsymbol{y} \in \mathbb{R}^\nu$. This assumption allowed further development of Eqs. (2.39), (2.44), (2.48), and (2.54). For a constrained system, however, these variations are not independent and to remedy the situation, independent virtual displacements must be determined. The following will only consider quasi-coordinate constraints, however a similar development can be achieved for generalized coordinate constraints.

A set of $m$ independent constraint equations are taken to be of the form

$$\mathbf{B}\; d\boldsymbol{y} - \mathbf{g}\; dt = \mathbb{0} \tag{2.58}$$

where $\mathbf{B} \in \mathbb{R}^{m \times n}$. In order to be consistent with the constraints it is necessary that

$$\mathbf{B}\ \delta \boldsymbol{y} = \mathbb{0} \tag{2.59}$$

Therefore, $\delta \boldsymbol{y}$ belongs to the null-space of $\mathbf{B}$ and is perpendicular to the range of $\mathbf{B}$. That is, $\mathbf{B}$ constitutes a matrix representation of a linear operator $\mathcal{B} : \mathbb{R}^n \rightarrow \mathbb{R}^m$ where $\delta \boldsymbol{y} \in \ \ker(\mathcal{B})$ and $\delta \boldsymbol{y} \perp \ \text{Ran}(\mathcal{B})$, where $E \triangleq \ \text{Ker}(\mathcal{B})$ is a linear subspace (or linear manifold) of $\mathbb{R}^n$ and $\text{Ran}(\mathcal{B})$ is a linear subspace of $\mathbb{R}^m$ [104]. The number of degrees of freedom of the system is equal to dimension of the null-space of $\mathcal{B}$ (termed the *nullity* of $\mathcal{B}$) which can be found by a well-known theorem of linear algebra:

$$\begin{aligned} \text{nullity}(\mathcal{B}) &= \dim(\mathbb{R}^n) - \ \text{rank}(\mathcal{B}) \\ &= n - m \end{aligned}$$

The dynamic system, therefore, has $n-m$ degrees of freedom which are being represented by $n$ coordinates. The task is then to determine an independent set of virtual displacements $\delta \boldsymbol{y}'$. To accomplish this consider constructing a basis set $\ \mathrm{C} = \{\mathbf{c}_1, ..., \mathbf{c}_{n-m}\}$ of $E$ in which the vector components of $\ \mathrm{C}$ must, by definition, be linearly independent and span the null-space of $E$. The vector $\delta \boldsymbol{y}$ may be expressed in the basis of $\ \mathrm{C}$ by the operation

$$\delta \boldsymbol{y} = \mathbf{C}\ \delta \boldsymbol{y}'$$

where $\mathbf{C}$ is a matrix whose columns are the basis vectors of $\ \mathrm{C}$ and $\delta \boldsymbol{y}'$ is an arbitrary vector of length $n - m$. The important contribution to this development is the operator $\mathbf{C} \in \mathbb{R}^{n \times (n-m)}$. From Eq. (2.54), and considering the definitions of Eqs. (2.50) and (2.55), d'Alembert's principle may be stated as

$$\left[\boldsymbol{F} + \bar{\boldsymbol{F}} - \boldsymbol{F}^*\right] \cdot \delta \boldsymbol{y} = 0$$

which according to the previous development may be written

$$\mathbf{C}^T \left[\boldsymbol{F} + \bar{\boldsymbol{F}} - \boldsymbol{F}^*\right] \cdot \delta \boldsymbol{y}' = 0$$

Since $\delta \boldsymbol{y}'$ is arbitrary, then it is true that

$$\mathbf{C}^T \boldsymbol{F}^* = \mathbf{C}^T \left(\boldsymbol{F} + \bar{\boldsymbol{F}}\right)$$

Although, expressed in quasi-coordinates and in the nomenclature of Kane's method, the procedure for arriving at this form can be attributed to Maggi [105, 106]; when derived in terms of generalized coordinates the resulting equations are known as Maggi's equations.

The basis set C is, of course, not unique and may be chosen at one's convenience. There are several ways of constructing this basis set; an excellent reference regarding this topic is the work by Kurdila, et. al. [106]. An important feature of $C$ can be deduced by substituting for Eq. (2.59):

$$\mathbf{B}\ \delta\boldsymbol{y} = \mathbf{BC}\ \delta\boldsymbol{y}' = \mathbb{0} \tag{2.60}$$

where it is apparent that $\mathbf{BC} = \mathbb{0}$. Therefore, the vector components of $C$ belong to the orthogonal complement of $E$. The orthogonal complement of $E$ is the set of all vectors orthogonal to $E$ and is denoted $E^{\perp}$ [104]. That is, $\mathbf{c}_1, ..., \mathbf{c}_{n-m} \in E^{\perp}$. Methods of generating sets of vectors belonging to the orthogonal complement of an inner product space include singular value decomposition, eigenvector decomposition, and the generalized inverse [87, 107]. For simplicity, the method chosen here is to make use of the zero eigenvectors of $\mathbf{B}^T\mathbf{B}$. More specifically, $\mathbf{B}^T\mathbf{B}$ is a square matrix $(n \times n)$ with rank $m$–the same rank as $\mathbf{B}$–and has $n - m$ eigenvectors $\boldsymbol{\zeta}_1$, ..., $\boldsymbol{\zeta}_{n-m}$, corresponding to same number of zero-valued eigenvalues. Therefore, from the standard eigen-problem

$$\begin{aligned} \left(\mathbf{B}^T\mathbf{B}\right)\boldsymbol{\zeta}_1 &= \mathbf{0} \\ &\vdots \\ \left(\mathbf{B}^T\mathbf{B}\right)\boldsymbol{\zeta}_{n-m} &= \mathbf{0} \end{aligned}$$

Letting these zero eigenvectors be the components of the basis set $C$ (i.e. $\mathbf{C} = \begin{bmatrix}\boldsymbol{\zeta}_1 & ... & \boldsymbol{\zeta}_{n-m}\end{bmatrix}^T$) then

$$\left(\mathbf{B}^T\mathbf{B}\right)\mathbf{C} = \mathbb{0}$$

which requires that $\mathbf{BC} = \mathbb{0}$

The generalized constraint force $\bar{\boldsymbol{F}}$, results from imposed constraints on configuration of the body. For morphing applications the imposed constraints are manifested by actuators that either inhibit or generate motion of the moving portion of the aircraft. In general, the actuation forces and moments are difficult to specify and, to complicate matters, they will be

resisted by workless constraints whose form depends on the nature of the joint interactions [108]. Therefore, it is typically more convenient to either solve for the constraint forces and moments or to eliminate them from the equations of motion. The generalized constraint force can be related to the constraint equations by

$$\bar{\boldsymbol{F}} = \mathbf{B}^T \lambda \tag{2.61}$$

where $\lambda$ is a $m \times 1$ array of unknown values; the validity of Eq. (2.61) has been demonstrated by Huston and Wang [87, 107]. Substituting this new expression into Kane's equations results in

$$\mathbf{C}^T \boldsymbol{F}^* = \mathbf{C}^T \left( \boldsymbol{F} + \mathbf{B}^T \lambda \right) \tag{2.62}$$

Defining $\boldsymbol{K} = \mathbf{C}^T \boldsymbol{F}$ and $\boldsymbol{K}^* = \mathbf{C}^T \boldsymbol{F}^*$, since $\mathbf{C}^T \mathbf{B}^T = \mathbb{0}$, Eq. (2.62) reduces to

$$\boldsymbol{K}^* = \boldsymbol{K} \tag{2.63}$$

The terms $\boldsymbol{K}^*$ and $\boldsymbol{K}$ are denoted, respectively, as the *constrained inertial force* and the *constrained applied force*. In constructing the basis set $C$, the constraint forces have been eliminated from the equations of motion. The remaining $m$ equations come from differentiating Eq. (2.58):

$$\mathbf{B}\ddot{\boldsymbol{y}} = \dot{\mathbf{g}} - \dot{\mathbf{B}}\dot{\boldsymbol{y}} \tag{2.64}$$

where $\mathbf{g}$ is a $m \times 1$, possibly time dependent, array that acts as a kinematic input. The constrained inertial force may be expressed in the general form

$$\boldsymbol{K}^* = \boldsymbol{\Lambda}\ddot{\boldsymbol{y}} + \boldsymbol{\Omega}\dot{\boldsymbol{y}} + \boldsymbol{k}$$

and the total constrained equations of motion become

$$\begin{bmatrix} \boldsymbol{\Lambda} \\ \mathbf{B} \end{bmatrix} \ddot{\boldsymbol{y}} = - \begin{bmatrix} \boldsymbol{\Omega} \\ \dot{\mathbf{B}} \end{bmatrix} \dot{\boldsymbol{y}} + \begin{bmatrix} \boldsymbol{K} + \boldsymbol{k} \\ \dot{\mathbf{g}} \end{bmatrix} \tag{2.65}$$

In general, these constitute a set of $n$ nonlinear, nonautonomous, first-order differential equations.

## 2.4 Morphing Aircraft Dynamics

In the following sections, three methods of modeling variable planform aircraft are presented. The first case develops a general non-rigid description, the second a multi-rigid model, and the final case approximates the multi-body system by a collection of concentrated masses. In deriving the flight equations it is typically advantageous to make some simplifying assumptions to reduce the complexity of the dynamics. As such, it is assumed that the aircraft of interest flies at a speed sufficiently slow such that the rotation of the earth may be neglected. Furthermore, the aircraft traverses a sufficiently small distance so that the earth may be considered flat. These assumptions produce the so-called *flat-earth* equations of motion [88].

### Non-Rigid Model

For a general non-rigid body analysis, a single body $B_1$ with frame $\{O^1, \mathbf{e}^1\}$ is considered. The position of body elements is given by Eq. (2.12) where each $\boldsymbol{\rho}_k^1$ $(k = 1, 2, ..., N_1)$ is considered to be a known function of time. From Eq. (2.16), and repeated from Eq. (2.28), the acceleration may be expressed in the coordinates $\boldsymbol{y} = (\boldsymbol{v}^1, \boldsymbol{\omega}^{10})$ by

$$\ddot{\boldsymbol{r}}_k^1 = \begin{bmatrix} \mathbb{1} & -\tilde{\boldsymbol{\rho}}_k^1 \end{bmatrix} \ddot{\boldsymbol{y}} + \begin{bmatrix} \tilde{\boldsymbol{\omega}}^{10} & -(\tilde{\boldsymbol{\omega}}^{10}\tilde{\boldsymbol{\rho}}_k^1 + 2\dot{\tilde{\boldsymbol{\rho}}}_k^1) \end{bmatrix} \dot{\boldsymbol{y}} + \ddot{\boldsymbol{\rho}}_k^1$$

Noting that

$$\frac{\partial \ddot{\boldsymbol{r}}_k^0}{\partial \ddot{\boldsymbol{y}}} \cdot \ddot{\boldsymbol{r}}_k^0 = \mathbf{A}^{0i} \frac{\partial \ddot{\boldsymbol{r}}_k^i}{\partial \ddot{\boldsymbol{y}}} \cdot \mathbf{A}^{0i} \ddot{\boldsymbol{r}}_k^i = \frac{\partial \ddot{\boldsymbol{r}}_k^i}{\partial \ddot{\boldsymbol{y}}} \cdot \ddot{\boldsymbol{r}}_k^i$$

and carrying out the operation from Eq. (2.55) results in

$$\boldsymbol{F}^* = \sum_{k=1}^{N_1} m_k \left( \begin{bmatrix} \mathbb{1} & -\tilde{\boldsymbol{\rho}}_k^1 \\ \tilde{\boldsymbol{\rho}}_k^1 & -\tilde{\boldsymbol{\rho}}_k^1 \tilde{\boldsymbol{\rho}}_k^1 \end{bmatrix} \ddot{\boldsymbol{y}} + \begin{bmatrix} \tilde{\boldsymbol{\omega}}^{10} & -(\tilde{\boldsymbol{\omega}}^{10}\tilde{\boldsymbol{\rho}}_k^1 + 2\dot{\tilde{\boldsymbol{\rho}}}_k^1) \\ \tilde{\boldsymbol{\rho}}_k^1 \tilde{\boldsymbol{\omega}}^{10} & -\tilde{\boldsymbol{\rho}}_k^1 (\tilde{\boldsymbol{\omega}}^{10}\tilde{\boldsymbol{\rho}}_k^1 + 2\dot{\tilde{\boldsymbol{\rho}}}_k^1) \end{bmatrix} \dot{\boldsymbol{y}} + \begin{bmatrix} \ddot{\boldsymbol{\rho}}_k^1 \\ \tilde{\boldsymbol{\rho}}_k^1 \ddot{\boldsymbol{\rho}}_k^1 \end{bmatrix} \right)$$

The basis superscripts have been excluded since all vectors are expressed in $\mathcal{F}^1$. Respectively defining the zeroth, first, and second moments of inertia as

$$\begin{aligned}
\mathbf{M}_i &= \mathbb{1}\sum_{k=1}^{N_i} m_k \\
\mathbf{S}_i &= \sum_{k=1}^{N_i} m_k \tilde{\boldsymbol{\rho}}_k^i \\
\mathbf{J}_i &= -\sum_{k=1}^{N_i} m_k \tilde{\boldsymbol{\rho}}_k^i \tilde{\boldsymbol{\rho}}_k^i
\end{aligned}$$

the inertial force can be written in the form

$$\boldsymbol{F}^* = \begin{bmatrix} \mathbf{M}_1 & -\mathbf{S}_1 \\ \mathbf{S}_1 & \mathbf{J}_1 \end{bmatrix} \ddot{\boldsymbol{y}} + \begin{bmatrix} \mathbf{M}_1\tilde{\boldsymbol{\omega}}^{10} & -(\tilde{\boldsymbol{\omega}}^{10}\mathbf{S}_1 + 2\dot{\mathbf{S}}_1) \\ \mathbf{S}_1\tilde{\boldsymbol{\omega}}^{10} & \tilde{\boldsymbol{\omega}}^{10}(\mathbf{J}_1 - 2\sum \tilde{\boldsymbol{\rho}}_k^1\dot{\tilde{\boldsymbol{\rho}}}_k^1) \end{bmatrix} \dot{\boldsymbol{y}} + \begin{bmatrix} \sum m_k\ddot{\boldsymbol{\rho}}_k^1 \\ \sum m_k\tilde{\boldsymbol{\rho}}_k^1\ddot{\boldsymbol{\rho}}_k^1 \end{bmatrix} \tag{2.66}$$

Derived by Meirovitch [62] using Lagrange's equations for quasi-coordinates, Eq. (2.66) is nonautonomous in nature since $\mathbf{S}_1$ and $\mathbf{J}_1$ are considered to be explicit functions of time. The time dependence is in contrast to the coupled form produced by Meirovitch in which the small motions of each $\boldsymbol{\rho}_k^1$ was determined by considering the elastic properties of the body. Here, the motions are considered to be much larger and directly controlled.

Note that $\mathbf{J}_i$ and $\mathbf{S}_i$ have been defined about an origin whose location is arbitrary. The inertia tensors may also be expressed with reference to the center of mass by

$$\begin{aligned}
\mathbf{S}_i &= \mathbf{S}_i^c + \mathbf{M}_i\tilde{\boldsymbol{\rho}}_c^i = \mathbf{M}_i\tilde{\boldsymbol{\rho}}_c^i \\
\mathbf{J}_i &= \mathbf{J}_i^c - \mathbf{M}_i\tilde{\boldsymbol{\rho}}_c^i\tilde{\boldsymbol{\rho}}_c^i = \mathbf{J}_i^c - \mathbf{M}_i[\boldsymbol{\rho}_c^i(\boldsymbol{\rho}_c^i)^T - \mathbb{1}(\boldsymbol{\rho}_c^i)^T\boldsymbol{\rho}_c^i]
\end{aligned} \tag{2.67}$$

where $\mathbf{S}_i^c$ and $\mathbf{J}_i^c$ are the inertial moments measured about the center of mass which is located relative to $O^i$ by the vector $\boldsymbol{\rho}_c^i$–by definition, $\mathbf{S}_i' = 0$.

The generalized applied force from Eq. (2.50) can be written in terms of force and moment couple, expressed in frame $\mathcal{F}^1$, by

$$\begin{aligned}
\boldsymbol{F} &= \sum_{k=1}^{N} \mathbf{A}^{10}\frac{\partial\dot{\boldsymbol{r}}_k^0}{\partial\dot{\boldsymbol{y}}} \cdot \mathbf{A}^{10}\mathbf{f}_k^0 = \sum_{k=1}^{N}\left(\frac{\partial\boldsymbol{v}^1}{\partial\dot{\boldsymbol{y}}} - \tilde{\boldsymbol{\rho}}_k^1\frac{\partial\boldsymbol{\omega}^{10}}{\partial\dot{\boldsymbol{y}}}\right)\cdot\mathbf{f}_k^1 \\
&= \frac{\partial\boldsymbol{v}^1}{\partial\dot{\boldsymbol{y}}}\cdot\mathbf{f}^1 + \frac{\partial\boldsymbol{\omega}^{10}}{\partial\dot{\boldsymbol{y}}}\cdot\mathbf{m}^1
\end{aligned} \tag{2.68}$$

where $\mathbf{f}^1 = \sum_{k=1}^{N_1} \mathbf{f}_k^1$ and $\mathbf{m}^1 = \sum_{k=1}^{N_1} \tilde{\boldsymbol{\rho}}_k^1 \mathbf{f}_k^1$. Therefore, the generalized applied force is

$$\boldsymbol{F} = \begin{bmatrix} \mathbf{f}^1 & \mathbf{m}^1 \end{bmatrix}^T \tag{2.69}$$

where again the basis notation has, again, been excluded. Since there are no constraints involving the coordinates $\boldsymbol{y}$, the generalized constraint force is $\bar{\boldsymbol{F}} = \mathbf{B}^T \lambda = \mathbf{0}$. Physically, this means that the the constraint forces are internal with each force being equal and opposite and thus the summation is zero. Since the constraint the generalized constraint force is zero, $\boldsymbol{F}^* = \boldsymbol{K}^*$ and $\boldsymbol{F} = \boldsymbol{K}$. The components of Eq. (2.65) are then

$$\begin{aligned} \boldsymbol{\Lambda} &= \begin{bmatrix} \mathbf{M} & -\mathbf{S} \\ \mathbf{S} & \mathbf{J} \end{bmatrix} \\ \boldsymbol{\Omega} &= \begin{bmatrix} \mathbf{M}\tilde{\boldsymbol{\omega}} & -(\tilde{\boldsymbol{\omega}}\mathbf{S} + 2\dot{\mathbf{S}}) \\ \mathbf{S}\tilde{\boldsymbol{\omega}} & (\tilde{\boldsymbol{\omega}}\mathbf{J} + 2\sum \tilde{\boldsymbol{\rho}}_k \dot{\tilde{\boldsymbol{\rho}}}_k) \end{bmatrix} \\ \boldsymbol{k} &= \begin{bmatrix} \sum m_k \ddot{\boldsymbol{\rho}}_k \\ \sum m_k \tilde{\boldsymbol{\rho}}_k \ddot{\boldsymbol{\rho}}_k \end{bmatrix} \\ \mathbf{B} &= \dot{\mathbf{B}} = \mathbb{0} \end{aligned} \tag{2.70}$$

These dynamics consist of a set of 6 nonlinear time-varying differential equations, in which $\mathbf{S}$, $\mathbf{J}$, and $\boldsymbol{k}$ are explicitly defined functions of time.

## Multi-Rigid Body System

As depicted in Fig. (2.3), a body is composed of a set of $\mu$ rigid bodies where a reference frame origin $O^i$ within $B_i$. The location of $O^i$ with respect to $O^1$–considered to be the origin of the main body $B_1$–is specified by the vector $\mathbf{b}^{1i}$. Furthermore, the angular velocity of the basis $\mathbf{e}^i$ with respect to $\mathbf{e}^1$ is specified by $\boldsymbol{\omega}^{1i}$. The $6(\mu - 1)$ constraint equations of Eq. (2.58) can be written

$$\begin{bmatrix} \dot{\mathbf{b}}^{12} & \boldsymbol{\omega}^{21} & \cdots & \dot{\mathbf{b}}^{1\mu} & \boldsymbol{\omega}^{\mu 1} \end{bmatrix}^T = \mathbf{g} \tag{2.71}$$

These type of constraints, where the motions are specified, are generally termed *program constraints* or *servocontraints*. An interesting problem that stems from partly specified motion is that of determining the actuation forces required to achieve the desired motions

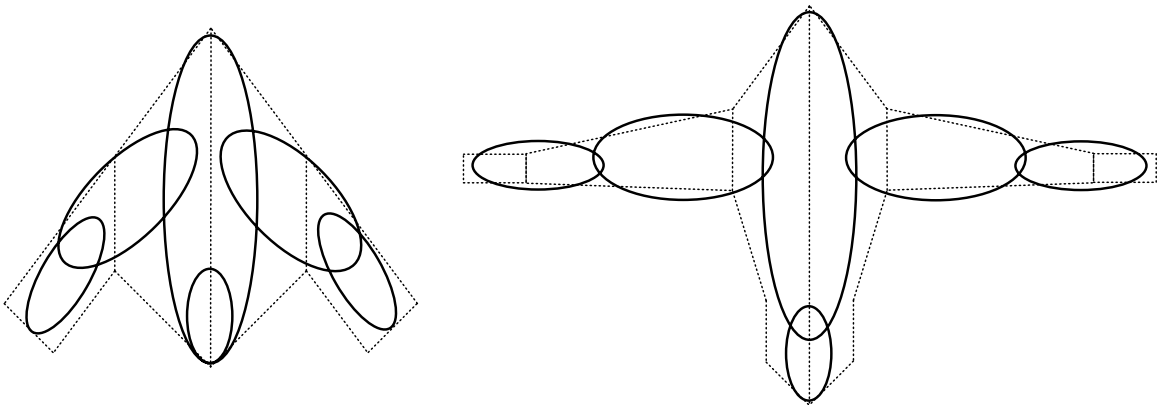


Figure 2.3: Depiction of the Multibody Representation

[109, 110, 108]. Here we do not consider such problems; that is, the program constraints are achieved independent of external influence.

Choosing the coordinates $\boldsymbol{y} = (\boldsymbol{v}^1, \boldsymbol{\omega}^{10}, \dot{\mathbf{b}}^{12}, \boldsymbol{\omega}^{21}, ..., \dot{\mathbf{b}}^{1\mu}, \boldsymbol{\omega}^{\mu 1})$ results in the $m \times n$ ($m = 6(\mu - 1)$ and $n = 6\mu$) constraint array

$$\mathbf{B} = \begin{bmatrix} \mathbb{0} & \mathbb{0} & \mathbb{1} & \mathbb{0} & \cdots & \mathbb{0} & \mathbb{0} \\ \mathbb{0} & \mathbb{0} & \mathbb{0} & \mathbb{1} & \cdots & \mathbb{0} & \mathbb{0} \\ \vdots & \vdots & \vdots & \vdots & \ddots & \vdots & \vdots \\ \mathbb{0} & \mathbb{0} & \mathbb{0} & \mathbb{0} & \cdots & \mathbb{1} & \mathbb{0} \\ \mathbb{0} & \mathbb{0} & \mathbb{0} & \mathbb{0} & \cdots & \mathbb{0} & \mathbb{1} \end{bmatrix}$$

As previously discussed, elimination of the constraint forces is accomplished by constructing a basis set for the null-space of $\mathbf{B}$. This basis set, $C$, is composed of vectors which belong to the orthogonal complement of this null space. As such, the matrix $\mathbf{C}$ is generally termed an orthogonal complement of $\mathbf{B}$, although the terminology is not precise. To construct the orthogonal complement, the columns of $\mathbf{C}$ are set equal to the zero eigenvectors of $\mathbf{B}^T\mathbf{B}$ resulting in

$$\mathbf{C}^T = \begin{bmatrix} \mathbb{1} & \mathbb{0} & \mathbb{0} & \mathbb{0} & \cdots & \mathbb{0} & \mathbb{0} \\ \mathbb{0} & \mathbb{1} & \mathbb{0} & \mathbb{0} & \cdots & \mathbb{0} & \mathbb{0} \end{bmatrix}$$

From Eq. (2.16) the acceleration of an element of $B_1$ can be expressed by

$$\ddot{\boldsymbol{r}}_k^1 = \begin{bmatrix} \mathbb{1} & -\tilde{\boldsymbol{\rho}}_k^1 \end{bmatrix} \begin{bmatrix} \dot{\boldsymbol{v}}^1 \\ \dot{\boldsymbol{\omega}}^{10} \end{bmatrix} + \begin{bmatrix} \tilde{\boldsymbol{\omega}}^{10} & -\tilde{\boldsymbol{\omega}}^{10}\tilde{\boldsymbol{\rho}}_k^1 \end{bmatrix} \begin{bmatrix} \boldsymbol{v}^1 \\ \boldsymbol{\omega}^{10} \end{bmatrix}$$

in which case the constrained inertial force of $B_1$ is

$$\mathbf{K}_1^* = \begin{bmatrix} \mathbf{M}_1 & -\mathbf{S}_1 & \mathbb{0} & \cdots & \mathbb{0} \\ \mathbf{S}_1 & \mathbf{J}_1 & \mathbb{0} & \cdots & \mathbb{0} \end{bmatrix} \dot{\boldsymbol{y}} + \begin{bmatrix} \mathbf{M}_1\tilde{\boldsymbol{\omega}}^{10} & -\tilde{\boldsymbol{\omega}}^{10}\mathbf{S}_1 & \mathbb{0} & \cdots & \mathbb{0} \\ \mathbf{S}_1\tilde{\boldsymbol{\omega}}^{10} & \tilde{\boldsymbol{\omega}}^{10}\mathbf{J}_1 & \mathbb{0} & \cdots & \mathbb{0} \end{bmatrix} \boldsymbol{y} \tag{2.72}$$

If the reference frame origin $O^1$ is placed at the center of mass of $B_1$, then by definition $\mathbf{S}_1 = \mathbb{0}$. From Eq. (2.21), the acceleration of a point belonging to any $B_i \neq B_1$ can be expressed relative to the origin of $B_1$ by

$$\begin{aligned} \ddot{\boldsymbol{r}}_k^1 &= \begin{bmatrix} \mathbb{1} & -\tilde{\mathbf{s}}_k^{1i} & \mathbb{1} & -\mathbf{A}^{1i}\tilde{\boldsymbol{\rho}}_k^i \end{bmatrix} \begin{bmatrix} \dot{\boldsymbol{v}}^1 \\ \dot{\boldsymbol{\omega}}^{10} \\ \ddot{\mathbf{b}}^{1i} \\ \dot{\boldsymbol{\omega}}^{i1} \end{bmatrix} \\ &+ \begin{bmatrix} \tilde{\boldsymbol{\omega}}^{10} & -\tilde{\boldsymbol{\omega}}^{10}\tilde{\mathbf{s}}_k^{1i} & 2\tilde{\boldsymbol{\omega}}^{10} & -2\tilde{\boldsymbol{\omega}}^{10}\mathbf{A}^{1i}\tilde{\boldsymbol{\rho}}_k^i - \mathbf{A}^{1i}\tilde{\boldsymbol{\omega}}^{i1}\tilde{\boldsymbol{\rho}}_k^i \end{bmatrix} \begin{bmatrix} \boldsymbol{v}^1 \\ \boldsymbol{\omega}^{10} \\ \dot{\mathbf{b}}^{1i} \\ \boldsymbol{\omega}^{i1} \end{bmatrix} \end{aligned}$$

The constrained inertial force, $\mathbf{K}_i^*$, contributed by $B_i$ is then

$$\mathbf{K}_i^* = \boldsymbol{\Lambda}_i \begin{bmatrix} \dot{\boldsymbol{v}}^1 \\ \dot{\boldsymbol{\omega}}^{10} \\ \ddot{\mathbf{b}}^{1i} \\ \dot{\boldsymbol{\omega}}^{i1} \end{bmatrix} + \boldsymbol{\Omega}_i \begin{bmatrix} \boldsymbol{v}^1 \\ \boldsymbol{\omega}^{10} \\ \dot{\mathbf{b}}^{1i} \\ \boldsymbol{\omega}^{i1} \end{bmatrix}, \qquad \mathrm{i} = 2, ..., \mu$$

where

$$\begin{aligned} \boldsymbol{\Lambda}_i &= \begin{bmatrix} \mathbf{M}_i & -\hat{\mathbf{S}}_i & \mathbf{M}_i & \mathbb{0} \\ \hat{\mathbf{S}}_i & \hat{\mathbf{J}}_i & \mathbf{M}_i\tilde{\mathbf{b}}^{1i} & -\mathbf{A}^{1i}\mathbf{J}_i \end{bmatrix} \\ \boldsymbol{\Omega}_i &= \begin{bmatrix} \mathbf{M}_i\tilde{\boldsymbol{\omega}}^{10} & -\tilde{\boldsymbol{\omega}}^{10}\hat{\mathbf{S}}_i & 2\mathbf{M}_i\tilde{\boldsymbol{\omega}}^{10} & \mathbb{0} \\ \mathbf{M}_i\tilde{\mathbf{b}}^{1i}\tilde{\boldsymbol{\omega}}^{10} & \tilde{\boldsymbol{\omega}}^{10}\hat{\mathbf{J}}_i & \hat{\mathbf{S}}_i\tilde{\boldsymbol{\omega}}^{10} & (2\mathbf{I}_i - \mathbf{A}^{1i}\tilde{\boldsymbol{\omega}}^{i1}\mathbf{J}_i) \end{bmatrix} \end{aligned}$$

with the additionally defined terms

$$\begin{aligned}\hat{\mathbf{S}}_i &= \mathbf{M}_i\tilde{\mathbf{b}}^{1i} \\ \hat{\mathbf{J}}_i &= -\mathbf{M}_i\tilde{\mathbf{b}}^{1i}\tilde{\mathbf{b}}^{1i} - \mathbf{A}^{1i}\mathbf{J}_i\mathbf{A}^{i1} \\ \mathbf{I}_i &= -\sum_{k=1}^{N_i}\mathbf{A}^{1i}\tilde{\boldsymbol{\rho}}_k^i\mathbf{A}^{i1}\tilde{\boldsymbol{\omega}}^{10}\mathbf{A}^{1i}\tilde{\boldsymbol{\rho}}_k^i\end{aligned}$$

The total inertial force is

$$\mathbf{K}^* = \sum_{i=1}^{\mu}\mathbf{K}_i^* = \sum_{i=1}^{\mu}\boldsymbol{\Lambda}_i\ddot{\boldsymbol{y}} + \boldsymbol{\Omega}_i\dot{\boldsymbol{y}}$$

Forces and moments applied to $B_1$ contribute to the generalized applied force as given by Eq. (2.68). Forces and moments applied to $B_i$ may be expressed as

$$\boldsymbol{F}_i = \sum_{k=1}^{N}\left(\mathbf{A}^{i1}\frac{\partial\boldsymbol{v}^1}{\partial\boldsymbol{y}} - \mathbf{A}^{i1}\left(\mathbf{b}^{1i} + \mathbf{A}^{1i}\boldsymbol{\rho}_k^i\right)^{\sim}\frac{\partial\boldsymbol{\omega}^{10}}{\partial\boldsymbol{y}} + \mathbf{A}^{i1}\frac{\partial\dot{\mathbf{b}}^{1i}}{\partial\boldsymbol{y}} - \boldsymbol{\rho}_k^i\frac{\partial\boldsymbol{\omega}^{i1}}{\partial\boldsymbol{y}}\right)\cdot\boldsymbol{f}_k^i$$

For a system of $\mu$ bodies the constrained generalized force is

$$\mathbf{K} = \mathbf{C}^T\boldsymbol{F} = \left[\begin{array}{cc}\left(\mathbf{f}^1 + \sum_{i=2}^{\mu}\mathbf{A}^{1i}\mathbf{f}^i\right) & \left(\mathbf{m}^1 + \sum_{i=2}^{\mu}\tilde{\mathbf{b}}^{1i}\mathbf{A}^{1i}\mathbf{f}^i\right)\end{array}\right]^T$$

where the forces and moments are defined at the center of mass of each body. In flight dynamics the applied forces and moments will be dependent on both the configuration and kinematic states; that is, $\mathbf{f}^i = \mathbf{f}^i(\boldsymbol{v}^i, \boldsymbol{\omega}^{i0}, \epsilon^{0i})$ and $\mathbf{m}^i = \mathbf{m}^i(\boldsymbol{v}^i, \boldsymbol{\omega}^{i0}, \epsilon^{0i})$. The common practice is to define the aerodynamics about a single origin, the location being at a point within the main fueselage (i.e., $O^1$). This means that only the gravitational contribution need be considered for the remaining bodies of aircraft. Hence, Eq. (2.73) becomes

$$\mathbf{K} = \left[\begin{array}{cc}\left(\mathbf{f}^1 + \bar{m}g\mathbf{A}^{10}\mathbf{e}_z^0\right) & \left(\mathbf{m}^1 + g\hat{\mathbf{S}}\mathbf{A}^{10}\mathbf{e}_z^0\right)\end{array}\right]^T$$

There remains the matter of relating $\mathbf{g}$ to the desired planform changes. This relationship will be specific to the design of the morphing structure. In general, the planform changes required for optimal regime flight will involve a complex kinematical interaction among the moving portions of the aircraft.

For an "open tree" structure, such as depicted in Fig. (2.2), in which the motion of each

body is controlled by its lower adjoining body, the components of $\mathbf{g}$ may be determined by Eqs. (2.19) and (2.11)–Eq. (2.19) requires a time derivative and Eq. (2.11) requires the specification of each $\epsilon^{1i}$. The morphing control equations would then be of the form

$$\begin{bmatrix} \dot{\mathbf{b}}^{L(i)i} \\ \dot{\epsilon}^{L(i)i} \end{bmatrix} = \boldsymbol{f}(\mathbf{b}^{L(i)i}, \dot{\epsilon}^{L(i)i}, \boldsymbol{u}) \qquad i = 2, ..., \mu \tag{2.73}$$

Summarized for convenience, the complete dynamics for the multi-rigid body system are again given by Eq. (2.65) where

$$\begin{aligned}
\boldsymbol{\Lambda} &= \begin{bmatrix} \mathbf{M} & (\mathbf{S}_1 + \hat{\mathbf{S}}) \\ -(\mathbf{S}_1 + \hat{\mathbf{S}}) & \mathbf{J}_1 + \hat{\mathbf{J}} \\ \mathbf{M}_2 & \mathbb{0} \\ \mathbf{M}_2\tilde{\mathbf{b}}^{12} & -\mathbf{A}^{12}\mathbf{J}_2 \\ \vdots & \vdots \\ \mathbf{M}_\mu & \mathbb{0} \\ \mathbf{M}_\mu\tilde{\mathbf{b}}^{1\mu} & -\mathbf{A}^{1\mu}\mathbf{J}_\mu \end{bmatrix}^T, \quad \boldsymbol{\Omega} = \begin{bmatrix} \mathbf{M}\tilde{\boldsymbol{\omega}}^{10} & \left(\mathbf{S}_1 + \hat{\mathbf{S}}\right)\tilde{\boldsymbol{\omega}}^{10} \\ -\tilde{\boldsymbol{\omega}}^{10}\left(\mathbf{S}_1 + \hat{\mathbf{S}}\right) & \tilde{\boldsymbol{\omega}}^{10}\left(\mathbf{J}_1 + \hat{\mathbf{J}}\right) \\ 2\mathbf{M}_2\tilde{\boldsymbol{\omega}}^{10} & \hat{\mathbf{S}}_2\tilde{\boldsymbol{\omega}}^{10} \\ \mathbb{0} & (2\mathbf{I}_2 - \mathbf{A}^{12}\tilde{\boldsymbol{\omega}}^{21}\mathbf{J}_2) \\ \vdots & \vdots \\ 2\mathbf{M}_\mu\tilde{\boldsymbol{\omega}}^{10} & \hat{\mathbf{S}}_\mu\tilde{\boldsymbol{\omega}}^{10} \\ \mathbb{0} & (2\mathbf{I}_\mu - \mathbf{A}^{1\mu}\tilde{\boldsymbol{\omega}}^{\mu 1}\mathbf{J}_\mu) \end{bmatrix}^T \\
\mathbf{K} &= \begin{bmatrix} (\mathbf{f}^1 + \bar{m}g\mathbf{A}^{10}\mathbf{e}_3^0) & (\mathbf{m}^1 + g\hat{\mathbf{S}}\mathbf{A}^{10}\mathbf{e}_3^0) \end{bmatrix}^T, \quad \boldsymbol{k} = \mathbf{0} \\
\mathbf{B} &= \begin{bmatrix} \mathbb{0} & \mathbb{0} & \mathbb{1} & \mathbb{0} & \cdots & \mathbb{0} & \mathbb{0} \\ \mathbb{0} & \mathbb{0} & \mathbb{0} & \mathbb{1} & \cdots & \mathbb{0} & \mathbb{0} \\ \vdots & \vdots & \vdots & \vdots & \ddots & \vdots & \vdots \\ \mathbb{0} & \mathbb{0} & \mathbb{0} & \mathbb{0} & \cdots & \mathbb{1} & \mathbb{0} \\ \mathbb{0} & \mathbb{0} & \mathbb{0} & \mathbb{0} & \cdots & \mathbb{0} & \mathbb{1} \end{bmatrix}, \quad \dot{\mathbf{g}} = \frac{d}{dt}\begin{bmatrix} \boldsymbol{f}(\mathbf{b}^{L(2)2}, \dot{\epsilon}^{L(2)2}, \boldsymbol{u}) \\ \vdots \\ \boldsymbol{f}(\mathbf{b}^{L(\mu)\mu}, \dot{\epsilon}^{L(\mu)\mu}, \boldsymbol{u}) \end{bmatrix}
\end{aligned} \tag{2.74}$$

## Point Mass Approximation

As depicted in Fig. (2.4), the multi-rigid body is approximated by a system composed of a single rigid body ($B_1$) and a set of ($\mu - 1$) point masses each capable of motion relative to the main body. A body-fixed frame $\{O^1, \mathbf{e}^1\}$ is placed at the center of mass of the rigid body and the position of each mass, $m_i$ ($i = 2, 3, ..., \mu$), is located with respect $O^1$ by the vector $\mathbf{b}^{1i}$. The equations of motion are developed in the same manner as the rigid body case. Choosing $\boldsymbol{y} = (\boldsymbol{v}^1, \tilde{\boldsymbol{\omega}}^{10}, \dot{\mathbf{b}}^{12}, ..., \dot{\mathbf{b}}^{1\mu})$ and ignoring the rotational terms from Eqs. (2.72)

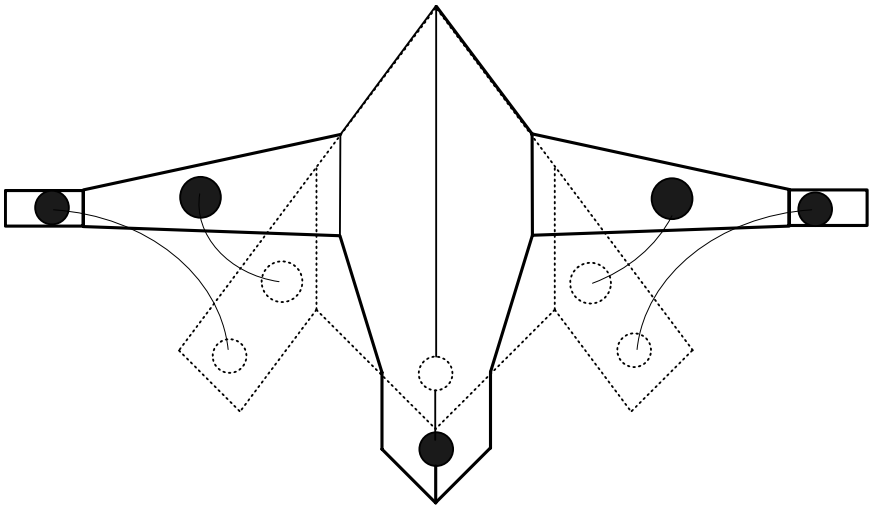


Figure 2.4: Depiction of the Multi-Mass Approximation

and (2.73), the constrained inertial force is

$$\begin{aligned}\mathbf{K}^* &= \begin{bmatrix} \mathbf{M} & -\hat{\mathbf{S}} & \mathbf{M}_2 & \cdots & \mathbf{M}_\mu \\ \hat{\mathbf{S}} & \mathbf{J}_1 + \hat{\mathbf{J}} & \mathbf{M}_2\tilde{\mathbf{b}}^{12} & \cdots & \mathbf{M}_\mu\tilde{\mathbf{b}}^{1\mu} \end{bmatrix} \ddot{\boldsymbol{y}} \\ &+ \begin{bmatrix} \mathbf{M}\tilde{\boldsymbol{\omega}}^{10} & -\tilde{\boldsymbol{\omega}}^{10}\hat{\mathbf{S}} & \mathbf{M}_2\tilde{\boldsymbol{\omega}}^{10} & \cdots & \mathbf{M}_\mu\tilde{\boldsymbol{\omega}}^{10} \\ \hat{\mathbf{S}}\tilde{\boldsymbol{\omega}}^{10} & \tilde{\boldsymbol{\omega}}^{10}(\mathbf{J}_1 + \hat{\mathbf{J}}) & \mathbf{M}_2\tilde{\mathbf{b}}^{12}\tilde{\boldsymbol{\omega}}^{10} & \cdots & \mathbf{M}_\mu\tilde{\mathbf{b}}^{1\mu}\tilde{\boldsymbol{\omega}}^{10} \end{bmatrix} \dot{\boldsymbol{y}} \end{aligned} \tag{2.75}$$

If the aerodynamic forces are defined about $O^1$, then the only external force applied to the moving masses is gravity. The constrained inertial force is then

$$\mathbf{K} = \begin{bmatrix} \mathbf{f}^1 + gm_T\mathbf{A}^{10}\mathbf{e}_z^0 & \mathbf{m}^1 + g\mathbf{A}^{10}\hat{\mathbf{S}}\mathbf{e}_z^0 \end{bmatrix}^T \tag{2.76}$$

Note that by choosing to approximate each body as a point mass, one of the major difficulties in multibody dynamics has been eliminated; that being the problems associated with quantifying relative rotation. This representation combines the more favorable features of the non-rigid and multibody representations; the non-rigid representation having a less complex form–in terms of the length of the equations–and the multibody representation having the capacity for time-invariance. It is then left to determine whether, and under what circumstances, the approximation is insufficient.

## 2.5 Summary

Equations of motion for evaluating the dynamics of variable geometry aircraft were presented in this chapter. A kinematic framework was first developed to account for various desired dynamical representations. Specifically equations were developed to calculate the rotation of any basis relative to another. Such development is thought to be useful when the dynamic equations are defined relative to a single main body, but the constraint equations by motion of connected bodies.

Kane's method is derived based on variational principles. Kane's method is also explicitly compared with both the Gibbs-Appell equations and Lagrange's equations of motion. To account for constraints, Maggi's equations were derived in terms of quasi-coordinates. It was shown that through the use of an orthogonal complement the dynamical equations could be expressed without the appearance of constraint forces. Using Kane's method two different models were derived. The first is a nonrigid body model in which only one body-fixed basis is defined and the motion of the aircraft is defined about this point. The nonlinear model leads to terms that are difficult to define explicitly, particularly for complex structural changes. The resulting model is considered to be time-varying, including the first and second inertial moments, in that the shape changes of the aircraft are assumed to be a known function of time. Development of an autonomous model was performed by considering the aircraft structure to be composed of a finite number of rigid bodies. Explicit state equations were developed to identify the motion of the total aircraft relative to the main body-fixed frame. Finally, as a compromise between the time-varying nonrigid equations and the complex multibody expression, a point mass approximation was presented. The resulting form produces autonomous equations of significantly reduced form relative to the multibody approach.

# Chapter 3

# Equations of Atmospheric Flight

Before the advent of computer technology, the process of investigating the behavior of rigid aircraft involved the concept of *steady state flight*, which was was introduced by G. H. Bryan in 1911 [35]. The steady state condition allows the nonlinear equations of flight to be decoupled into *longitudinal* and *lateral* equations. Furthermore, linearizing these equations produces a set of state equations that are amenable to the application of the many tools of analysis and design provided by linear system theory. In modern times, the process of linearizing the nonlinear equations of motion is based upon sophisticated numerical techniques [88]. This process requires a very specific knowledge of the aircraft design in that all of the parameters, such as moments of inertia and aerodynamic forces/moments, must be known with some degree of certainty. For this reason, the concept of steady-state flight continues to be of use in analyzing fundamental aspects of aircraft and aircraft control design.

The process of decoupling the nonlinear flight equations involves choosing a steady-state condition in which all of the applied forces and moments are constant (perhaps zero) in the body fixed frame. For instance, in the condition of steady wings-level flight this results in a constant configuration; if the configuration is described with the Eulerian angles, then the time derivative of these angles must be constant ($\dot{\phi} = 0, \dot{\theta} = 0, \dot{\psi} = 0$). Strictly speaking, the configuration may not be steady for a morphing aircraft. In particular, for the mutlibody description presented in the previous section, the configuration of the various morphing components of the aircraft may be allowed to change at a non-constant rate. Therefore, in speaking of steady-state conditions, it is implied that the main part of the aircraft (i.e. the fuselage) is steady; from the previous nomenclature, the fuselage is always identified by

body $B_x$. The un-steadiness of the morphing sections of the aircraft can be resolved by the implementation of state feedback control, in which the planform error–the difference between the planform and its desired configuration–is chosen as a configuration state. This will be further explained in subsequent development.

As a brief note on notation, in keeping with the standard practices of flight dynamics [88, 111, 112] the body translational velocity is defined as $\boldsymbol{v} = (U, V, W)$, the wind-relative velocity is $\boldsymbol{v}_r = (U', V', W')$, and the body angular velocity is $\boldsymbol{\omega} = (P, Q, R)$. Other variables will be defined as the need arises.

## 3.1 Stability and Wind Axis Equations

Thus far the dynamics have been derived in terms of a set of body-axis quasi-coordinates, namely $\boldsymbol{v}$ and $\boldsymbol{\omega}$. However, due to the manner in which the applied aerodynamic forces are specified in flight mechanics, it is beneficial–the benefit will be demonstrated later–to work with kinematic expressions in either the *stability-axis* or *wind-axis* frame, or a combination of the two. These frames are defined as follows. A vector belonging to $\mathcal{F}^i$ is transformed to the wind axis by two successive rotations, $\alpha$ and $\beta$. The basis $\mathbf{e}^i$ is transformed, via the *angle of attack* ($\alpha$), to the basis of the stability axis frame $\mathbf{e}^s$, which is then transformed to the wind-axis basis $\mathbf{e}^w$ by the sideslip angle ($\beta$). The basis transformations are

$$\begin{aligned} \mathbf{e}^s &= \mathbf{A}^{si}\mathbf{e}^i \\ \mathbf{e}^w &= \mathbf{A}^{ws}\mathbf{e}^s \end{aligned}$$

and, therefore

$$\mathbf{e}^w = \mathbf{A}^{ws}\mathbf{A}^{si}\mathbf{e}^i = \mathbf{A}^{wi}\mathbf{e}^i$$

The transformation matrices are given as

$$\mathbf{A}^{si} = \begin{bmatrix} c\alpha & 0 & s\alpha \\ 0 & 1 & 0 \\ -s\alpha & 0 & c\alpha \end{bmatrix}, \quad \mathbf{A}^{ws} = \begin{bmatrix} c\beta & s\beta & 0 \\ -s\beta & c\beta & 0 \\ 0 & 0 & 1 \end{bmatrix} \tag{3.1}$$

The relative rotation of these bases results in the angular velocity vectors $\boldsymbol{\omega}^{si}$, $\boldsymbol{\omega}^{ws}$, and $\boldsymbol{\omega}^{wi}$; these vectors are

$$\begin{aligned} \boldsymbol{\omega}^{si} &= [0 \quad -\dot{\alpha} \quad 0]^T \\ \boldsymbol{\omega}^{wi} &= [-s\beta\ \dot{\alpha} \quad -c\beta\ \dot{\alpha} \quad \dot{\beta}]^T \end{aligned}$$

where $\boldsymbol{\omega}^{ws} = \boldsymbol{\omega}^{wi} - \mathbf{A}^{ws}\boldsymbol{\omega}^{si}$. Since the vector $\mathbf{e}_x^w$ is always oriented into the wind, the wind-relative aircraft velocity is $\boldsymbol{v}_r^w = V_T\ \mathbf{e}_x^w = (V_T, 0, 0)$. A transformation into the basis of $\mathcal{F}^i$ gives

$$\boldsymbol{v}_r^i = \mathbf{A}^{iw}\boldsymbol{v}_r^w = \begin{bmatrix} V_T\ \cos\alpha\ \cos\beta \\ V_T\ \sin\beta \\ V_T\ \sin\alpha\ \cos\beta \end{bmatrix} \tag{3.2}$$

The relative velocity in the stability frame is

$$\boldsymbol{v}_r^s = \mathbf{A}^{sw}\boldsymbol{v}_r^w = \begin{bmatrix} \cos\beta\ V_T \\ \sin\beta\ V_T \\ 0 \end{bmatrix}$$

Assuming that the wind velocity is constant (i.e. $\boldsymbol{v}^i = \boldsymbol{v}_r^i$), the acceleration of the origin $O^i$ is

$$\boldsymbol{a}^i \triangleq \mathbf{A}^{i0}\ddot{\boldsymbol{b}}^{0i} = \dot{\boldsymbol{v}}^i + \tilde{\boldsymbol{\omega}}^{i0}\boldsymbol{v}^i = \dot{\boldsymbol{v}}_r^i + \tilde{\boldsymbol{\omega}}^{i0}\boldsymbol{v}_r^i$$

By substituting for the relative velocity and implementing Poisson's kinematical equation, the inertial acceleration becomes

$$\begin{aligned} \boldsymbol{a}^i &= \frac{d}{dt}(\mathbf{A}^{iw}\boldsymbol{v}_r^w) + \tilde{\boldsymbol{\omega}}^{i0}\mathbf{A}^{iw}\boldsymbol{v}_r^w \\ &= \dot{\mathbf{A}}^{iw}\boldsymbol{v}_r^w + \mathbf{A}^{iw}\dot{\boldsymbol{v}}_r^w + \tilde{\boldsymbol{\omega}}^{i0}\mathbf{A}^{iw}\boldsymbol{v}_r^w \\ &= \mathbf{A}^{iw}\left[\dot{\boldsymbol{v}}_r^w + \left(\tilde{\boldsymbol{\omega}}^{wi} + \mathbf{A}^{wi}\tilde{\boldsymbol{\omega}}^{i0}\mathbf{A}^{iw}\right)\boldsymbol{v}_r^w\right] \\ &= \mathbf{A}^{iw}\ \boldsymbol{a}^w \end{aligned} \tag{3.3}$$

or in terms of the stability frame

$$\begin{aligned} \boldsymbol{a}^i &= \mathbf{A}^{is}\left[\dot{\boldsymbol{v}}_r^s + \left(\tilde{\boldsymbol{\omega}}^{si} + \mathbf{A}^{si}\tilde{\boldsymbol{\omega}}^{i0}\mathbf{A}^{is}\right)\boldsymbol{v}_r^s\right] \\ &= \mathbf{A}^{is}\,\boldsymbol{a}^s \end{aligned} \tag{3.4}$$

In the development of the previous section the dynamics were constructed based on the particular choice of the quasi-coordinates. In all cases, the dynamic equations can be put in the form

$$\begin{bmatrix} \mathbf{M}\left(\dot{\boldsymbol{v}}^1 + \tilde{\boldsymbol{\omega}}^{10}\boldsymbol{v}^1\right) \\ \mathbf{J}_1\dot{\boldsymbol{\omega}}^{10} + \tilde{\boldsymbol{\omega}}^{10}\mathbf{J}_1\boldsymbol{\omega}^{10} \end{bmatrix} = \begin{bmatrix} \boldsymbol{h}_v(\ddot{\boldsymbol{y}}, \dot{\boldsymbol{y}}, t) \\ \boldsymbol{h}_\omega(\ddot{\boldsymbol{y}}, \dot{\boldsymbol{y}}, t) \end{bmatrix} + \begin{bmatrix} \mathbf{f}^1 + gm_T\mathbf{A}^{10}\mathbf{e}_z^0 \\ \mathbf{m}^1 + g\mathbf{A}^{10}\hat{\mathbf{S}}\mathbf{e}_z^0 \end{bmatrix} \tag{3.5}$$

where the functions $\boldsymbol{h}_v$ and $\boldsymbol{h}_\omega$ result from the inertial forces and will depend on the chosen formulation. Note that the dependence on time will not be apparent in all formulations.

The task is to determine expressions for the dynamics in the stability and wind axes, $\mathcal{F}^s$ and $\mathcal{F}^w$, respectively. Using Eqs. (3.3) and (3.4) the right side of Eq. (3.5) may be expressed as

$$\begin{aligned} \mathbf{M}\left(\dot{\boldsymbol{v}}^1 + \tilde{\boldsymbol{\omega}}^{10}\boldsymbol{v}^1\right) &= \mathbf{A}^{1s}\mathbf{M}\left(\dot{\boldsymbol{v}}_r^s + \tilde{\boldsymbol{\omega}}^{s1}\boldsymbol{v}_r^s + \mathbf{A}^{s1}\tilde{\boldsymbol{\omega}}^{10}\mathbf{A}^{1s}\boldsymbol{v}_r^s\right) \\ &= \mathbf{A}^{1w}\mathbf{M}\left(\dot{\boldsymbol{v}}_r^w + \tilde{\boldsymbol{\omega}}^{w1}\boldsymbol{v}_r^w + \mathbf{A}^{w1}\tilde{\boldsymbol{\omega}}^{10}\mathbf{A}^{1w}\boldsymbol{v}_r^w\right) \end{aligned}$$

Moving on to the rotational equations, let ${}^s\boldsymbol{\omega}^{10} = \mathbf{A}^{s1}\ \boldsymbol{\omega}^{10}$ (note that ${}^s\boldsymbol{\omega}^{10} \in \mathcal{F}^s$) be the body-fixed rotational velocity expressed in the coordinates of the stability axis:

$${}^s\boldsymbol{\omega}^{10} \triangleq \begin{bmatrix} P_s \\ Q_s \\ R_s \end{bmatrix} = \begin{bmatrix} P\cos\alpha + R\sin\alpha \\ Q \\ R\cos\alpha - P\sin\alpha \end{bmatrix} \tag{3.6}$$

Also let ${}^w\boldsymbol{\omega}^{10} = \mathbf{A}^{w1}\ \boldsymbol{\omega}^{10}$ (note that ${}^w\boldsymbol{\omega}^{10} \in \mathcal{F}^w$) be the body-fixed rotational velocity expressed in the coordinates of the stability axis:

$${}^w\boldsymbol{\omega}^{10} \triangleq \begin{bmatrix} P_w \\ Q_w \\ R_w \end{bmatrix} = \begin{bmatrix} P\cos\alpha\cos\beta + R\sin\alpha\cos\beta + Q\sin\beta \\ Q\cos\beta - (P\cos\alpha + R\sin\alpha)\sin\beta \\ R\cos\alpha - P\sin\alpha \end{bmatrix} \tag{3.7}$$

Note that $\tilde{\boldsymbol{\omega}}^{10}$ can now be replaced by either $(\mathbf{A}^{1s}\ {}^s\boldsymbol{\omega}^{10})^\sim = \mathbf{A}^{1s}\ {}^s\tilde{\boldsymbol{\omega}}^{10}\mathbf{A}^{s1}$ or $(\mathbf{A}^{1w}\ {}^w\boldsymbol{\omega}^{10})^\sim =$

$\mathbf{A}^{1w}\ {}^{w}\tilde{\boldsymbol{\omega}}^{10}\mathbf{A}^{w1}$ depending on the desired representation. Taking the derivatives

$$ {}^{s}\dot{\boldsymbol{\omega}}^{10} = \mathbf{A}^{s1}\dot{\boldsymbol{\omega}}^{10} - \tilde{\boldsymbol{\omega}}^{s1}\ {}^{s}\boldsymbol{\omega}^{10}, \quad {}^{w}\dot{\boldsymbol{\omega}}^{10} = \mathbf{A}^{w1}\dot{\boldsymbol{\omega}}^{10} - \tilde{\boldsymbol{\omega}}^{w1}\ {}^{w}\boldsymbol{\omega}^{10} $$

and substituting into the rotational portion of Eq. (3.5) results in

$$ \begin{aligned} \mathbf{J}_1\dot{\boldsymbol{\omega}}^{10} + \tilde{\boldsymbol{\omega}}^{10}\mathbf{J}_1\boldsymbol{\omega}^{10} &= \mathbf{A}^{1s}\left(\mathbf{J}_1^s\ {}^{s}\dot{\boldsymbol{\omega}}^{10} + \mathbf{J}_1^s\tilde{\boldsymbol{\omega}}^{s1}\ {}^{s}\boldsymbol{\omega}^{10} + \ {}^{s}\tilde{\boldsymbol{\omega}}^{10}\mathbf{J}_1^s\ {}^{s}\boldsymbol{\omega}^{10}\right) \\ &= \mathbf{A}^{1w}\left(\mathbf{J}_1^w\ {}^{w}\dot{\boldsymbol{\omega}}^{10} + \mathbf{J}_1^w\tilde{\boldsymbol{\omega}}^{w1}\ {}^{w}\boldsymbol{\omega}^{10} + \ {}^{w}\boldsymbol{\omega}^{10}\mathbf{J}_1^w\ {}^{w}\boldsymbol{\omega}^{10}\right) \end{aligned} $$

where $\mathbf{J}_1^s \triangleq \mathbf{A}^{s1}\mathbf{J}_1\mathbf{A}^{1s}$ and $\mathbf{J}_1^w \triangleq \mathbf{A}^{w1}\mathbf{J}_1\mathbf{A}^{1w}$. Combining these results the general form of the equations of motion, given by Eq. (3.5), can be restated in the stability axis

$$ \begin{aligned} \begin{bmatrix} \mathbf{M}\left(\dot{\boldsymbol{v}}_r^s + \tilde{\boldsymbol{\omega}}^{s1}\boldsymbol{v}_r^s + \ {}^{s}\tilde{\boldsymbol{\omega}}^{10}\boldsymbol{v}_r^s\right) \\ \mathbf{J}_1^s\left(\ {}^{s}\dot{\boldsymbol{\omega}}^{10} + \tilde{\boldsymbol{\omega}}^{s1}\ {}^{s}\boldsymbol{\omega}^{10}\right) + \ {}^{s}\tilde{\boldsymbol{\omega}}^{10}\mathbf{J}_1^s\ {}^{s}\boldsymbol{\omega}^{10} \end{bmatrix} &= \begin{bmatrix} \mathbf{A}^{s1}\boldsymbol{h}_v \\ \mathbf{A}^{s1}\boldsymbol{h}_\omega \end{bmatrix} \\ &+ \begin{bmatrix} \mathbf{A}^{s1}\mathbf{f}^1 + gm_T\mathbf{A}^{s0}\mathbf{e}_z^0 \\ \mathbf{A}^{s1}\mathbf{m}^1 + g\mathbf{A}^{s0}\hat{\mathbf{S}}\mathbf{e}_z^0 \end{bmatrix} \end{aligned} \tag{3.8} $$

and in the wind-axis

$$ \begin{aligned} \begin{bmatrix} \mathbf{M}\left(\dot{\boldsymbol{v}}_r^w + \tilde{\boldsymbol{\omega}}^{w1}\boldsymbol{v}_r^w + \ {}^{w}\tilde{\boldsymbol{\omega}}^{10}\boldsymbol{v}_r^w\right) \\ \mathbf{J}_1^w\left(\ {}^{w}\dot{\boldsymbol{\omega}}^{10} + \tilde{\boldsymbol{\omega}}^{w1}\ {}^{w}\boldsymbol{\omega}^{10}\right) + \ {}^{w}\tilde{\boldsymbol{\omega}}^{10}\mathbf{J}_1^w\ {}^{w}\boldsymbol{\omega}^{10} \end{bmatrix} &= \begin{bmatrix} \mathbf{A}^{w1}\boldsymbol{h}_v \\ \mathbf{A}^{w1}\boldsymbol{h}_\omega \end{bmatrix} \\ &+ \begin{bmatrix} \mathbf{A}^{w1}\mathbf{f}^1 + gm_T\mathbf{A}^{w0}\mathbf{e}_z^0 \\ \mathbf{A}^{w1}\mathbf{m}^1 + g\mathbf{A}^{w0}\hat{\mathbf{S}}\mathbf{e}_z^0 \end{bmatrix} \end{aligned} \tag{3.9} $$

Equations (3.8) and (3.9) give the general form of the dynamic equations of motion for a variable planform aircraft–with specific reference to the origin of the aircraft's main body (i.e., $O^1$ of $B_x$)–where the dynamics are formulated in the coordinates of both the stability and wind axes. Therefore, we have three moving frame representations of the dynamical equations: body-fixed frame, stability frame, and the wind frame. For convenience, the full equations have been included in the appendix.

Note that, we are not restricted to choosing any one frame description; any combination of these may be employed. For example, it is common to express the translational dynamics in the wind-axis and the rotational dynamics in the stability axis [88]. However, this practice is difficult for non-rigid aircraft due to the coupling of the translational and rotational dynamics. When this coupling is present the most convenient reference frame, in terms of

the length of the equations, is the body-fixed frame.

## 3.2 Longitudinal Dynamics

One of the most fundamental tasks of an autopilot system is to maintain a desired pitch and attitude (termed a *pitch-attitude-hold* autopilot). For a rigid aircraft the goal is simply to maintain steady and level flight in the presence of unknown disturbances such as wind gusts and turbulence. For a an aircraft that changes shape, the disturbances are both extraneous (i.e. unknown aerodynamic effects) and induced. The induced disturbances come from altering the structural geometry of the aircraft, thus altering the aerodynamics behavior. It is almost certain that these induced aerodynamic effects can not be accurately predicted and thus a portion must be considered as an unknown disturbance. Nonetheless, the equations required for this type of autopilot are the longitudinal dynamics.

Referring to the coordinates of the main body the attitude is represented by the 3-2-1 set of Euler angles $(\phi, \theta, \psi)$, where $\phi$ is a rotation about $\mathbf{e}_x^0$, $\theta$ denotes rotation about $\mathbf{e}_y^0$, and $\psi$ denotes rotation about $\mathbf{e}_z^0$. By convention $\mathbf{e}_x^0$ is directed along the horizontal length of the fuselage, $\mathbf{e}_y^0$ is directed along the right wing, and $\mathbf{e}_z^0$ is directed downward. The orientation angles are termed the *roll* ($\phi$), *pitch* ($\theta$), and *yaw* ($\psi$) angles. The longitudinal equations are arrived at by restricting the aircraft's motion so that $\phi, \dot{\psi}, V \equiv 0$. From Euler's kinematical equation, Eq. (2.22), this means that $P = R = 0$ and $\dot{\theta} = Q$. For this particular set of Eulerian angles, the vector transformation matrix is

$$\mathbf{A}^{10} = \begin{bmatrix} c\theta\ c\psi & c\theta\ s\psi & -s\theta \\ (-c\phi\ s\psi + s\phi\ s\theta\ c\psi) & (c\phi\ c\psi + s\phi\ s\theta\ s\psi) & s\phi\ c\theta \\ (s\phi\ s\psi + c\phi\ s\theta\ c\psi) & (-s\phi\ c\psi + c\phi\ s\theta\ s\psi) & c\phi\ c\theta \end{bmatrix} \tag{3.10}$$

The components of $\hat{\mathbf{S}}$ are taken to be $(\hat{S}_x, \hat{S}_y, \hat{S}_z)$, and the applied aerodynamic force and moment are $\mathbf{f}^1 = (F_x, F_y, F_z)$ and $\mathbf{m}^1 = (\mathscr{L}, \mathscr{M}, \mathscr{N})$. The longitudinal equations are derived from Eqs. (3.5) and are given as

$$\begin{bmatrix} m_T(\dot{U} + QW) \\ m_T(\dot{W} - QU) \\ J_y\ddot{\theta} \end{bmatrix} = \begin{bmatrix} h_x \\ h_z \\ h_m \end{bmatrix} + \begin{bmatrix} F_x - gm_T s\theta \\ F_z - gm_T c\theta \\ \mathscr{M} - g(\hat{S}_x c\theta + \hat{S}_z s\theta) \end{bmatrix} \tag{3.11}$$

where the function $\boldsymbol{h}_{lon}$ denotes the longitudinal reduction of $\boldsymbol{h}$. Now turning to the wind/stability axis equations, since $P = R = 0$ then from Eq. (3.6), $P_s = R_s = 0$ and $Q_s = Q = \dot{\theta}$. Also, since $V \equiv 0$ then from Eq. (3.2) we have $\beta = 0$. Carrying out the algebra from Eq. (3.8) with the appropriate assumptions, the corresponding longitudinal equations, in the stability axis, are

$$\begin{bmatrix} m_T\dot{V}_T \\ m_T V_T(\dot{\alpha} - \dot{\theta}) \\ J_y^s\ddot{\theta} \end{bmatrix} = \begin{bmatrix} h_x^s \\ h_z^s \\ h_m^s \end{bmatrix} + \begin{bmatrix} F_x^s - gm_T(c\theta s\alpha - s\theta c\alpha) \\ F_z^s - gm_T(c\theta c\alpha + s\theta s\alpha) \\ \mathscr{M}^s - g(\hat{S}_x c\theta + \hat{S}_z s\theta) \end{bmatrix} \tag{3.12}$$

Finally, the wind-axis equations are

$$\begin{bmatrix} m_T\dot{V}_T \\ m_T V_T(\dot{\alpha} - \dot{\theta}) \\ J_y^w\ddot{\theta} \end{bmatrix} = \begin{bmatrix} h_x^w \\ h_z^w \\ h_m^w \end{bmatrix} + \begin{bmatrix} F_x^w - gm_T(c\theta s\alpha - s\theta c\alpha) \\ F_z^w - gm_T(c\theta c\alpha + s\theta s\alpha) \\ \mathscr{M}^w - g(\hat{S}_x c\theta + \hat{S}_z s\theta) \end{bmatrix} \tag{3.13}$$

As a final addition, the longitudinal equations require that the altitude state be included. This requirement necessary for an accurate representation of the *phugoid mode* [88, 112]. The altitude is a component of the *navigation equations* and is determined by

$$\dot{h} = s\theta U - s\phi c\theta V - c\phi c\theta W$$

Application of the longitudinal assumption gives

$$\begin{aligned} \dot{h} &= s\theta U - c\theta W \\ &= (s\theta c\alpha - c\theta s\alpha)V_T \end{aligned} \tag{3.14}$$

## 3.3 Lateral Dynamics

The lateral dynamic equations are derived by specifying the behavior of the longitudinal variables–the longitudinal variables are $(\theta, Q, U, W)$ or $(\theta, Q, V_T, \alpha)$ depending on the chosen reference frame. Likewise, the longitudinal equations were derived in the previous section specifying the lateral variables were zero–these variables are $(\phi, \psi, P, Q, V)$ or $(\phi, \psi, P_s, R_s, \beta)$. As such, for the body axis equations it is assumed that $\theta, Q, W, \dot{U}, \dot{\alpha}, \dot{V}_T \equiv 0$, and also that $\beta$ is small such that $\sin\beta \approx \beta$. The constant forward speed of the aircraft is

$U_0$ in the body axis and $V_M$ in the wind axis. From Eq. (3.5), the lateral equations in the body axis are

$$\begin{bmatrix} m_T(\dot{V} + U_0 R) \\ J_x\dot{P} - J_{xz}\dot{R} + J_{xy}PR \\ -J_{xy}\dot{P} + (J_x - J_z)PR + J_{xz}(P+R)(P-R) \\ J_z\dot{R} - J_{xz}\dot{P} \end{bmatrix} = \begin{bmatrix} h_y \\ h_l \\ h_m \\ h_n \end{bmatrix} + \begin{bmatrix} F_y - m_T g s\phi \\ \mathscr{L} + g(c\phi\ \hat{S}_y - s\phi\ \hat{S}_z) \\ \mathscr{M} - gc\phi\ \hat{S}_x \\ \mathscr{N} + gs\phi\ \hat{S}_x \end{bmatrix} \tag{3.15}$$

Excluding the stability axis equations for brevity, from Eq. (3.9), the lateral equations in the wind axis are

$$\begin{bmatrix} m_T V_M(\dot{\beta} + R_s) \\ J_x^w\dot{P}_s - J_{xz}^w\dot{R}_s \\ (J_x^w - J_z^w)P_sR_s + J_{xz}^w(P_s - R_s)(P_s + R_s) \\ -J_{xz}^w\dot{P}_s + J_z^w\dot{R}_s \end{bmatrix} = \begin{bmatrix} h_y^w \\ h_l^w \\ h_m^w \\ h_n^w \end{bmatrix} + \begin{bmatrix} F_y^w - m_T g\sin\phi \\ \mathscr{L}^w + g[c\alpha(c\psi\hat{S}_y - s\psi\hat{S}_x) + s\alpha s\phi(c\psi\hat{S}_x + s\psi\hat{S}_y)] \\ \mathscr{M}^w - gc\phi(c\psi\ \hat{S}_x + s\psi\ \hat{S}_y) \\ \mathscr{N}^w + g[s\alpha(s\psi\hat{S}_x - c\psi\hat{S}_y) + c\alpha s\phi(c\psi\hat{S}_x + s\psi\hat{S}_y)] \end{bmatrix} \tag{3.16}$$

Comparing these results with the longitudinal equations, it is apparent that complexity of the lateral equations has been increased. Furthermore, there are four differential equations opposed to the three longitudinal equations. Generally, some additional assumptions are made to reduce the complexity. For example the third equation describing the pitching dynamics may be ignored with the assumption of small perturbations (i.e. the products of small perturbations are ignorable).

## 3.4 Inertial Contributions

The atmospheric flight equations have thus far been presented in the same manner as would be done for a rigid aircraft. In fact, without the terms of $\boldsymbol{h}(\ddot{\boldsymbol{y}}, \dot{\boldsymbol{y}}, t)$ (and $\hat{\mathbf{S}}$), Eqs. (3.5 - 3.9) are the standard rigid-body flight equations. The rigid body equations can be thought of as a subset of non-rigid body equations–both are subsets of the non-rigid body, non-constant mass equations. The aim of this section, is to develop the inertial forces due to morphing. These forces are contained within the function $\boldsymbol{h}(\ddot{\boldsymbol{y}}, \dot{\boldsymbol{y}}, t)$ and, as previously mentioned, the precise form depends on the particular representation.

### Nonrigid Body Terms

Starting with the non-rigid body approach of Eq. (2.70), where the quasi-coordinates were chosen as $\dot{\boldsymbol{y}} = (\boldsymbol{v}^1, \boldsymbol{\omega}^{10})$, the inertial forces are

$$\begin{aligned} \boldsymbol{h}_v &= \mathbf{S}\dot{\boldsymbol{\omega}}^{10} + \tilde{\boldsymbol{\omega}}^{10}\mathbf{S}\boldsymbol{\omega}^{10} + 2\dot{\mathbf{S}}\boldsymbol{\omega}^{10} - \sum m_k \ddot{\boldsymbol{\rho}}_k \\ \boldsymbol{h}_\omega &= -\mathbf{S}(\dot{\boldsymbol{v}}^1 + \tilde{\boldsymbol{\omega}}^{10}\boldsymbol{v}^1) + 2(\sum m_k \tilde{\boldsymbol{\rho}}_k \dot{\tilde{\boldsymbol{\rho}}}_k)\boldsymbol{\omega}^{10} - \sum m_k \tilde{\boldsymbol{\rho}}_k \ddot{\boldsymbol{\rho}}_k \end{aligned} \tag{3.17}$$

Given the definitions from the previous section, this can also be expressed as

$$\begin{aligned} \boldsymbol{h}_v &= \mathbf{S}\mathbf{A}^{1s}(\dot{\boldsymbol{\omega}}^s + \tilde{\boldsymbol{\omega}}^{s1}\tilde{\boldsymbol{\omega}}^s) + \mathbf{A}^{1s}\tilde{\boldsymbol{\omega}}^s\mathbf{A}^{s1}\mathbf{S}\mathbf{A}^{1s}\boldsymbol{\omega}^s + 2\dot{\mathbf{S}}\mathbf{A}^{1s}\boldsymbol{\omega}^s - \sum m_k \ddot{\boldsymbol{\rho}}_k \\ \boldsymbol{h}_\omega &= -\mathbf{S}\mathbf{A}^{1s}(\dot{\boldsymbol{v}}_r^s + \tilde{\boldsymbol{\omega}}^{s1}\boldsymbol{v}_r^s + \tilde{\boldsymbol{\omega}}^s\boldsymbol{v}_r^s) + 2(\sum \tilde{\boldsymbol{\rho}}_k \dot{\tilde{\boldsymbol{\rho}}}_k)\mathbf{A}^{1s}\boldsymbol{\omega}^s - \sum m_k \tilde{\boldsymbol{\rho}}_k \ddot{\boldsymbol{\rho}}_k \end{aligned} \tag{3.18}$$

or

$$\begin{aligned} \boldsymbol{h}_v &= \mathbf{S}\mathbf{A}^{1w}(\dot{\boldsymbol{\omega}}^w + \tilde{\boldsymbol{\omega}}^{w1}\tilde{\boldsymbol{\omega}}^w) + \mathbf{A}^{1w}\tilde{\boldsymbol{\omega}}^w\mathbf{A}^{w1}\mathbf{S}\mathbf{A}^{1w}\boldsymbol{\omega}^w + 2\dot{\mathbf{S}}\mathbf{A}^{1w}\boldsymbol{\omega}^w - \sum m_k \ddot{\boldsymbol{\rho}}_k \\ \boldsymbol{h}_\omega &= -\mathbf{S}\mathbf{A}^{1w}(\dot{\boldsymbol{v}}_r^w + \tilde{\boldsymbol{\omega}}^{w1}\boldsymbol{v}_r^w + \tilde{\boldsymbol{\omega}}^w\boldsymbol{v}_r^w) + 2(\sum \tilde{\boldsymbol{\rho}}_k \dot{\tilde{\boldsymbol{\rho}}}_k)\mathbf{A}^{1w}\boldsymbol{\omega}^w - \sum m_k \tilde{\boldsymbol{\rho}}_k \ddot{\boldsymbol{\rho}}_k \end{aligned} \tag{3.19}$$

Therefore, we have

$$\begin{aligned} \boldsymbol{h}_v^s &= \mathbf{S}^s(\dot{\boldsymbol{\omega}}^s + \tilde{\boldsymbol{\omega}}^{s1}\boldsymbol{\omega}^s) + \tilde{\boldsymbol{\omega}}^s\mathbf{S}^s\boldsymbol{\omega}^s + 2\dot{\mathbf{S}}^s\boldsymbol{\omega}^s - \mathbf{A}^{s1}\sum m_k \ddot{\boldsymbol{\rho}}_k \\ \boldsymbol{h}_\omega^s &= -\mathbf{S}^s(\dot{\boldsymbol{v}}_r^s + \tilde{\boldsymbol{\omega}}^{s1}\boldsymbol{v}_r^s + \tilde{\boldsymbol{\omega}}^s\boldsymbol{v}_r^s) + 2\mathbf{A}^{s1}(\sum \tilde{\boldsymbol{\rho}}_k \dot{\tilde{\boldsymbol{\rho}}}_k)\mathbf{A}^{1s}\boldsymbol{\omega}^s - \mathbf{A}^{s1}\sum m_k \tilde{\boldsymbol{\rho}}_k \ddot{\boldsymbol{\rho}}_k \end{aligned} \tag{3.20}$$

and

$$\begin{aligned}
\boldsymbol{h}_v^w &= \mathbf{S}^w(\dot{\boldsymbol{\omega}}^w + \tilde{\boldsymbol{\omega}}^{w1}\boldsymbol{\omega}^w) + \tilde{\boldsymbol{\omega}}^w\mathbf{S}^w\boldsymbol{\omega}^w + 2\dot{\mathbf{S}}^w\boldsymbol{\omega}^w - \mathbf{A}^{w1}\sum m_k\ddot{\boldsymbol{\rho}}_k \\
\boldsymbol{h}_\omega^w &= -\mathbf{S}^w(\dot{\boldsymbol{v}}_r^w + \tilde{\boldsymbol{\omega}}^{w1}\boldsymbol{v}_r^w + \tilde{\boldsymbol{\omega}}^w\boldsymbol{v}_r^w) + 2\mathbf{A}^{w1}(\sum\tilde{\boldsymbol{\rho}}_k\dot{\tilde{\boldsymbol{\rho}}}_k)\mathbf{A}^{1w}\boldsymbol{\omega}^w \\
&- \mathbf{A}^{w1}\sum m_k\tilde{\boldsymbol{\rho}}_k\ddot{\boldsymbol{\rho}}_k
\end{aligned} \tag{3.21}$$

where $\mathbf{S}^s = \mathbf{A}^{s1}\mathbf{S}\mathbf{A}^{1s}$ and $\mathbf{S}^w = \mathbf{A}^{w1}\mathbf{S}\mathbf{A}^{1w}$. It would be beneficial if some of the terms of $\boldsymbol{h}$ could be ignored, however at this point there are no such candidates. The appearance of ignorable terms will be apparent when the dynamics are decoupled into the longitudinal and lateral equations.

For the multibody representation, the inertial contribution can be expressed as

$$\begin{aligned}
\boldsymbol{h}_v &= (\mathbf{S}_x + \hat{\mathbf{S}})\dot{\boldsymbol{\omega}}^{10} - \sum\mathbf{M}_i\ddot{\boldsymbol{b}}^{1i} - \sum\mathbf{M}_i\tilde{\boldsymbol{b}}^{1i}\dot{\boldsymbol{\omega}}^{1i} + \tilde{\boldsymbol{\omega}}^{10}(\mathbf{S}_x + \hat{\mathbf{S}})\boldsymbol{\omega}^{10} \\
&- 2\sum\mathbf{M}_i\tilde{\boldsymbol{\omega}}^{10}\dot{\boldsymbol{b}}^{1i} \\
\boldsymbol{h}_\omega &= -(\mathbf{S}_x + \hat{\mathbf{S}})\dot{\boldsymbol{v}}^1 - \hat{\mathbf{J}}\dot{\boldsymbol{\omega}}^{10} + \sum\mathbf{A}^{1i}\mathbf{J}_i\dot{\boldsymbol{\omega}}^{i1} - (\mathbf{S}_x + \hat{\mathbf{S}})\tilde{\boldsymbol{\omega}}^{10}\boldsymbol{v}^1 - \tilde{\boldsymbol{\omega}}^{10}\hat{\mathbf{J}}\boldsymbol{\omega}^{10} \\
&- \sum\hat{\mathbf{S}}\tilde{\boldsymbol{\omega}}^{10}\dot{\boldsymbol{b}}^{1i} - (2\mathbf{I}_i - \mathbf{A}^{1i}\tilde{\boldsymbol{\omega}}^{i1}\mathbf{J}_i)\boldsymbol{\omega}^{i1}
\end{aligned} \tag{3.22}$$

where the sum is taken to be from 2 to $\mu$. The transformation to the stability and wind-axis is the same process as previously identified.

## 3.5 Summary

This chapter develops the equations of motion in the form of atmospheric flight equations. The representations of Chapter 2 are reduced to a set of equations describing the motion of the main body. The remaining terms resulting from aircraft structural changes are grouped into a single term. Stability axis and wind axis equations for the entire aircraft are derived expressly. Furthermore, the longitudinal and lateral equations are derived by standard approximations. The longitudinal equations consist of a group of three equations and the longitudinal consist of four. Once again, the reduced equations are expressed in the stability and wind axes.

# Chapter 4

# Aerodynamic Modeling

In the previous section the dynamic equations of motion were developed for a morphing aircraft. They are, of course incomplete because the applied aerodynamic forces and moments were not defined. In general, the aerodynamic contributions are complex functions of the kinematic state of the aircraft and also the flight conditions (i.e., altitude, Reynold's number, etc.). For an aircraft that is undergoing shape changes, these contributions are evidently much more complex as they will necessarily involve a time-dependent component. This chapter demonstrates approximate methods by which these aerodynamic forces and moments are incorporated into the dynamic flight equations for morphing aircraft.

## 4.1 Aerodynamic Derivatives

The method of introducing the aerodynamic forces and moments into the equations of motion is by the *aerodynamic derivative*, first introduced by Bryan [35]–this method is in contrast to solving the complex differential equations that are produced from fluid mechanics. The aerodynamic derivatives can be explained by considering an aircraft flying in steady state, such that the aerodynamic reactions are balanced with the inertial and gravitational forces. A change in the aerodynamic reaction takes place due to a changes in the aircraft configuration relative to the airflow. Letting $\boldsymbol{x}$ be the state vector, a single aerodynamic reaction, represented by $A$ (this could be $F_x$, $F_y$, $M_x$, etc.), is assumed to be a continuous function of the instantaneous state values; $A = A(\boldsymbol{x})$. This is known as the *quasi-steady* approximation.

The function, which is not really known, can be approximated by a Taylor series expansion:

$$A(\boldsymbol{x}) \approx A(\boldsymbol{x}_r) + \nabla A(\boldsymbol{x}_r) \cdot \Delta \boldsymbol{x} + \text{h.o.t}$$

where $\Delta \boldsymbol{x}$ denotes a variation from a given reference state, $\boldsymbol{x}_r$, such that $\Delta \boldsymbol{x} = \boldsymbol{x} - \boldsymbol{x}_r$. Disregarding the higher order terms, the components of $\nabla A(\boldsymbol{x}_r)$ are the aerodynamic derivatives which are divided into two categories: *damping derivatives* and *acceleration derivatives*. The damping derivatives are the components of $\nabla A(\boldsymbol{x}_r)$ that result from differentiating with respect $(P, Q, R)$ and the acceleration derivatives are those components associated with $(\dot{\alpha}, \dot{\beta})$. If the reference state is also a stationary point ($\boldsymbol{x}_r = \boldsymbol{x}_0$) then the resulting derivatives are termed *trimmed coefficients*; otherwise they are *untrimmed coefficients*. In either case the aerodynamic forces and moments show up in the equations of motion in the form

$$\Delta A(\boldsymbol{x}) = \nabla A(\boldsymbol{x}_r) \cdot \Delta \boldsymbol{x}$$

For an aircraft that has a large operating range, several reference points (or "operating regions") are identified and the untrimmed coefficients are evaluated at each of these points. A "lookup-table" combined with a interpolation algorithm may then be constructed for simulation purposes.

For an aircraft that changes configuration, it is apparent that an evaluation of the aerodynamic reactions becomes much more involved. Specifically, one must determine the aerodynamic derivatives for various operating regions as well as for various planform configurations. This process is the equivalent of evaluating multiple aircraft, the number being equal to the number of planform configurations. In addition there is also the task of evaluating the transient stage of morphing in which the aircraft is in the process of changing shape. One option of incorporating the resulting aerodynamic effects is to simply create the aforementioned lookup table. However, once again, unsteady aerodynamic effects will have been ignored and the uncertainty is further increased. Accurate simulation–a neccessary tool for flight control design–would require extensive wind-tunnel testing for each aircraft configuration as well as for the transition between shapes. As an example, data for the Lockheed F-22 Raptor, a rigid aircraft, consists of thousands of aerodynamic tables [88].

For analytical evaluation, it would be beneficial to incorporate the structural changes into the state vector. As an example, if $\delta_s$ is an input controlling the wing sweep angle, the

associated aerodynamic reaction due to a change in sweep angle might be approximated by

$$\Delta A(\delta_s) = \frac{\partial A}{\partial \delta_s}\ \delta_s$$

Although extremely convenient, the ability to accommodate such a representation may prove difficult depending on the complexity of the shape change and the corresponding aerodynamic behavior.

The following sections are devoted to determining an adequate representation of the aerodynamic forces and moments of a morphing aircraft. For simplicity, it is desirable to maintain the quasi-steady approximation; hence, aerodynamic derivatives will be determined for a specific aircraft design. Datcom is used to calculate these derivatives for the aircraft when symmetric planform changes are implemented. For the case of non-symmetric changes, Datcom is no longer useful, and alternative methods must be used.

## 4.2 Morphing Aircraft Model

The Teledyne Ryan BQM-34 "Firebee", depicted in Fig. (4.1), was chosen as the platform for investigating morphing aircraft flight control. This choice is based on the work of Joshi *et al*, in which both the wing shape and camber were optimized for various flight mission requirements [77]. Using basic aircraft performance equations, as might be found in standard design texts [113, 114], the wings for the Firebee were optimized for operating regimes which can be divided into loiter, maneuvering, take-off, and dash.

The Firebee, first flown in 1985, is an unmanned remotely controlled aircraft originally constructed as a target drone for use by the military for training intercept pilots and for missile targeting practice. Many variants of this aircraft have been constructed, utilizing various planform designs, to accommodate mission requirements such as subsonic targeting, supersonic targeting, reconnaissance, and attack configurations. The baseline configuration chosen for evaluation is the BQM-34C. Some important specifications are listed in Table 4.1.

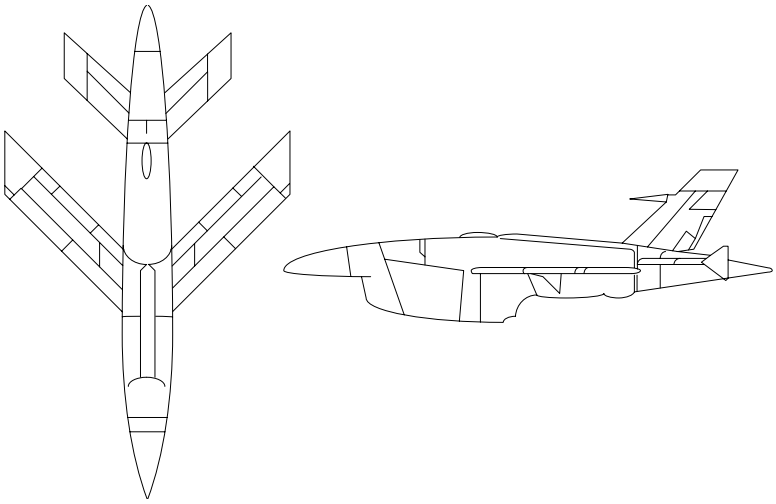


Figure 4.1: Teledyne Ryan BQM-34 Firebee

Table 4.1: BQM-34C Baseline Specifications

| | |
|---|---|
| Span | 12 ft. 11 in. |
| Length | 22 ft. 11 in. |
| Weight | 2000 lbs. |
| Maximum Speed | 580 mph |
| Range | 600 miles |
| Service Ceiling | 60,000 ft. |

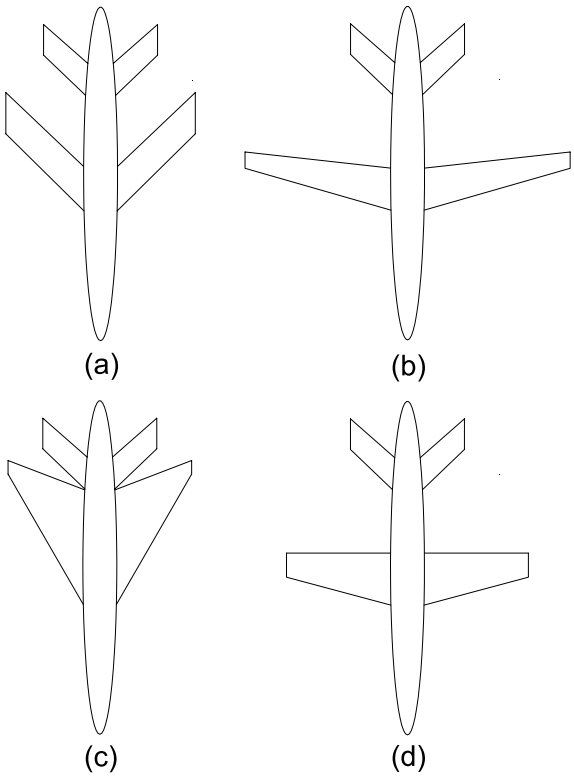



Figure 4.2: Morphing Planform Configurations; (a) Standard, (b) Loiter, (c) Dash, (d) Maneuver

## Planform Configurations

To refrain from performing an exercise in aircraft planform optimization, four distinct wing shapes were chosen based on the design of NextGen Aeronautics–this design was depicted in Fig. (1.2). The planform configurations include designs for loiter, maneuver, dash, as well as the standard configuration of the Firebee. These four basic configurations are shown in Fig. (4.2); more detailed design specifications are given in Appendix B. It is important to note that none of the configurations were analyzed for mission optimality, and in fact, such matters are of less importance in the current investigation. In contrast, the configurations were chosen as to provide large changes in aerodynamic behavior and mass distribution. Such models will provide the necessary complexity and uncertainty for flight control studies.

To determine the applied aerodynamic forces and moments for each aircraft configuration Missile Datcom was employed. Missile Datcom provides methods for calculating the stability derivatives previously discussed for subsonic, transonic, and supersonic conditions. A similar

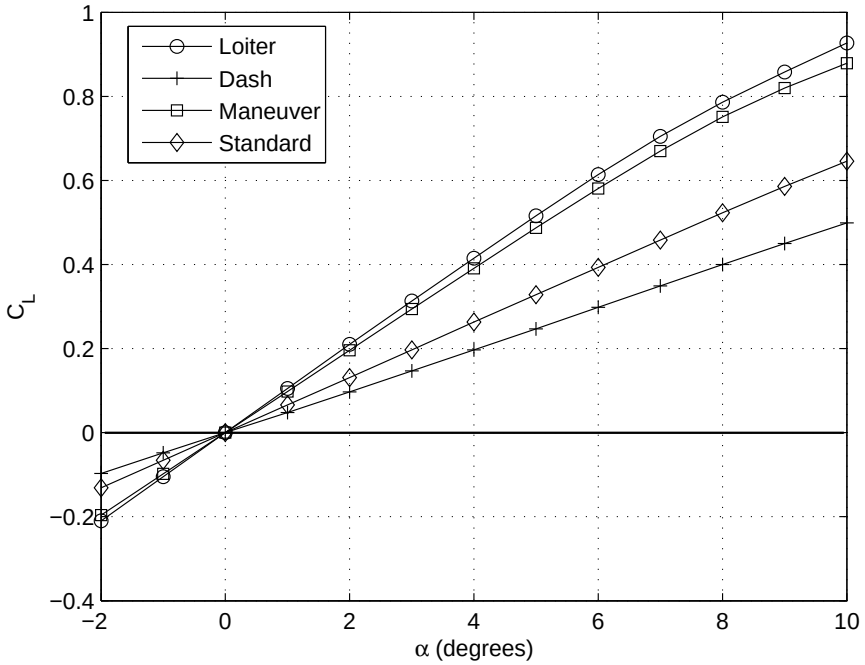



Figure 4.3: Variation in Lift Coefficient for Morphing Configurations

program available for such purposes is Stability and Control Datcom [115], the functionality of which exceeds the demands of modeling the given aircraft design. Moreover, many of the methods that are applied in Missile Datcom are derived from Stability and Control Datcom [116].

Some basic differences in the aerodynamic properties of each planform configuration, as calculated by Datcom, are demonstrated by the lift and pitching moment coefficients, shown in Figs. (4.3) and (4.4) over range of angle of attack ($\alpha$). For the pitching moment, it was assumed that the center of gravity (c.g.) could be located, through morphing control, at any desired position. The c.g. position was chosen such that each configuration was statically stable (i.e., a negative value of $C_{m_\alpha}$), but with a very small static margin at low angles of attack. A high static margin leads to both increased drag and reduced maneuverability– aircraft such as the F-16 and SR-71 are designed to be statically unstable for these reasons, and are made dynamically stable through feedback control. Active location of the aircraft c.g. requires an additional method of control other than what is provided solely by the change in wing geometry. This is because the weight of the wings is typically not large enough to move the center of gravity in proportion with the aerodynamic center (a.c.). For

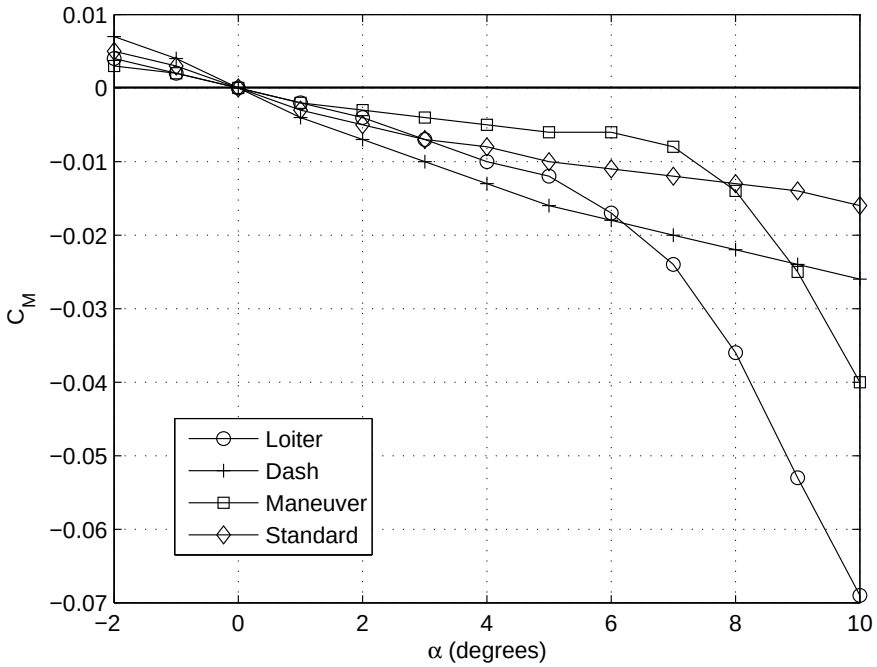



Figure 4.4: Variation in Moment Coefficient for Morphing Configurations

instance, a reconfiguration from loiter to dash produces a shift in the aerodynamic center that is larger than that of the center of gravity. This causes the aircraft to be more stable which may not be beneficial. Designers of the variable sweep F-14 remedied this problem moving the pivot point further outboard causing the static margin to initially rise and then fall with increasing wing sweep angle [117].

The position of the a.c. can be located at will by proper design of the tail, specifically by design of the *horizontal tail volume ratio*. For morphing applications, Neal *et al* investigated a variable position and camber fuselage effector for actively controlling both the a.c. and c.g. locations [34]. Another method of redistributing mass that has been used previously is to pump fuel from a forward fuel tank to an aft tank.

Here, we assume that the a.c. location is fixed by the planform design and the c.g. location is determined by both the planform distribution and an additional mass that may be located through structural control. The additional mass, denoted $m_A$, is calculated based on a desired c.g. location taking into account the mass distribution of the shape-changing wings and the rigid feuselage. Further details of these assumptions are given in Chapter 5.

## Aerodynamic Buildup

The aerodynamic derivatives calculated by Datcom are given in Table (4.2). These derivatives are calculated in the body-fixed frame and follow conventionally accepted standards with regards to nomenclature and non-dimensionality [111, 118]. Basic familiarity of aircraft nomenclature is assumed in this section (see [88], for example).

Table 4.2: Datcom Aerodynamic Derivatives

| | |
|---|---|
| $C_X$ | Axial force |
| $C_Y$ | Side force |
| $C_Z$ | Normal force |
| $C_l$ | Rolling moment |
| $C_m$ | Pitching moment |
| $C_n$ | Yawing Moment |
| $C_{n_q}$ | Normal force due to pitch rate |
| $C_{m_q}$ | Pitching moment due to pitch rate |
| $C_{X_q}$ | Axial force due to pitch rate |
| $C_{Z_{\dot{\alpha}}}$ | Normal force due to angle of attack rate |
| $C_{m_{\dot{\alpha}}}$ | Pitching moment due to angle of attack rate |
| $C_{Y_r}$ | Side force due to yaw rate |
| $C_{n_r}$ | Yawing moment due to yaw rate |
| $C_{l_r}$ | Rolling moment due to yaw rate |
| $C_{Y_p}$ | Side force due to roll rate |
| $C_{n_p}$ | Yawing moment due to roll rate |
| $C_{l_p}$ | Rolling moment due to roll rate |

In general, the aerodynamic forces involve complex interactions and are a function of a very large number of parameters. Therefore, approximate modeling methods are typically constructed via *component buildup*. Using practices presented by Stevens and Lewis [88], for each configuration the aerodynamic forces are calculated by

$$\begin{aligned} C_Y &= C_{Y_\beta}(\alpha, M)\ \beta + C_{Y_{\delta_r}}(\alpha, \beta, M)\ \delta_r + C_{Y_{\delta_a}}(\alpha, \beta, M)\ \delta_a \\ &+ \frac{b}{2V_T}[C_{Y_p}(\alpha, M)\ P + C_{Y_r}(\alpha, M)\ R] \\ C_Z &= C_Z(\alpha, \beta, M) + C_{Z_{\delta_e}}(\alpha, \beta, M)\ \delta_e \end{aligned} \tag{4.1}$$

and the aerodyamic moments by

$$\begin{aligned}
C_l &= C_{l_\beta}(\alpha, M)\ \beta + C_{l_{\delta_a}}(\alpha, \beta, M)\ \delta_a + C_{l_{\delta_r}}(\alpha, \beta, M)\ \delta_r \\
&+ \frac{b}{2V_T}[C_{l_p}(\alpha, M)\ P + C_{l_r}(\alpha, M)\ R] \\
C_m &= C_m(\alpha, M, h) + C_{m_{\delta_e}}(\alpha, M, h)\ \delta_e + \frac{c}{2V_T}[C_{m_q}\ Q + C_{m_{\dot\alpha}}\ \dot\alpha] \\
C_n &= C_{n_\beta}(\alpha, M)\ \beta + C_{n_{\delta_r}}(\alpha, \beta, M)\ \delta_r + C_{n_{\delta_a}}(\alpha, \beta, M)\ \delta_a \\
&+ \frac{b}{2V_T}[C_{n_p}(\alpha, M)\ P + C_{n_r}(\alpha, M)\ R] \qquad (4.2)
\end{aligned}$$

Eqs. (4.1) and (4.2) constitute the aerodynamic contributions utilized in nonlinear flight simulations. Lookup tables were constructed based on the Datcom aerodynamic data for each configuration. Transition from one configuration to another was accommodated adding aircraft planform as an additional dimension in the lookup tables; interpolation was used to construct the aerodynamic data during transition. The detailed aerodynamic data used for simulations is included in Appendix B.

## 4.3 Variable Span Morphing

The structural changes discussed so far have been limited to those that preserve symmetry. This, however, is somewhat of a limitation since assymmetry may be quite useful. For example, a bird will exhibit significant assymmetry in various stages of flight for control authority while maneuvering. An example of assymmetry, one which is investigated in this section, is variable span morphing–span change may also be symmetric. Symmetric span changes, such as depicted in Fig. (4.5), are considered to be particularly well suited for the highly varying mission requirements. Variable span morphing has been previously investigated for application in cruise missiles with the specific goal of increasing range and endurance [119, 32, 31].

The following investigates the aerodynamics of variable span morphing, first with regards to symmetric and then for the asymmetric case. Particular focus is given to the calculation of the roll producing and roll damping moments resulting from asymmetric wing extension.

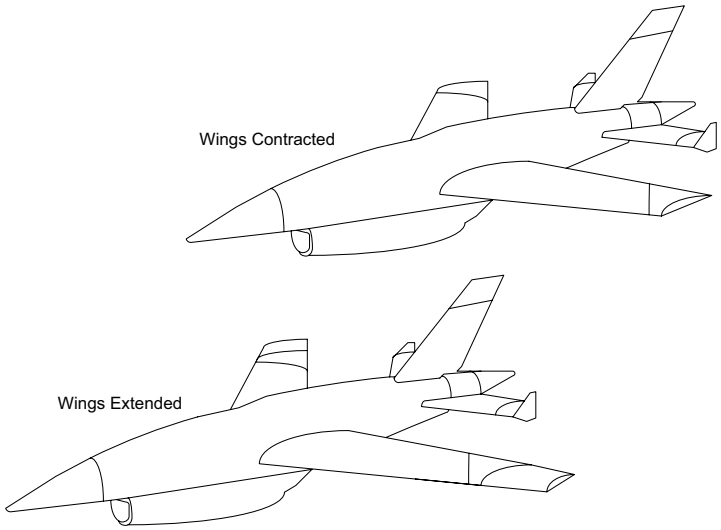



Figure 4.5: Aircraft with Variable Span Morphing

## Spanwise Circulation

The *lifting line theory* used in this section is based on Prandtl's assertion that an unswept wing of finite span acts as a collection of isolated two-dimensional wing sections [120, 121]. General spanwise circulation distribution is approximated by the Fourier series

$$\Gamma(y) = 4sU_\infty \sum_{n=1}^{N} A_n \sin(n\varphi) \tag{4.3}$$

where $s$ is the half span, $U_\infty$ is the free-stream airspeed, $\rho_\infty$ is the air density, and $\varphi$ is defined by the coordinate transformation

$$y = -s\cos(\varphi) \tag{4.4}$$

The sectional lift force is given by

$$l(\varphi) = \rho_\infty U_\infty \Gamma(\varphi) = 4\rho_\infty U_\infty^2 s \sum_{n=1}^{N} A_n \sin(n\varphi) \tag{4.5}$$

Respectively, the lift and moment can be expressed as

$$L = \int_{-s}^{s} \rho_\infty U_\infty \Gamma(\varphi)\ dy \tag{4.6}$$

and

$$\mathscr{L} = \int_{-s}^{s} \rho_\infty U_\infty \Gamma(\varphi) y\ dy \tag{4.7}$$

The sectional lift coefficient is

$$c_L(\varphi) = \frac{2l(\varphi)}{\rho_\infty U_\infty^2 s} = \frac{2\Gamma(\varphi)}{U_\infty s} \tag{4.8}$$

The boundary condition at each section can be expressed as

$$c_L = \left(\frac{dC_l}{d\alpha}\right)(\alpha - \alpha_i) = a_0(\alpha_0 + \alpha_p + \alpha_{0l} - \alpha_i) \tag{4.9}$$

where $\alpha_0$, $\alpha_{0l}$, $\alpha_i$ are, respectively, the initial angle of attack, zero-lift angle of attack, and induced angle of attack. Also, $\alpha_p$ is the angle of attack due to roll rate $P$ and can be written as

$$\alpha_p(y) = -\frac{Py}{U_\infty} \tag{4.10}$$

The induced angle of attack can be expressed by

$$\alpha_i = -\frac{w}{U_\infty} \tag{4.11}$$

where $w$ is a downwash, which can be expressed as

$$-w = \frac{1}{4\pi}\int_{-s}^{s} \frac{d\Gamma/dy}{y - dy_1} = U_\infty \frac{\sum nA_n \sin(n\varphi)}{\sin(\varphi)} \tag{4.12}$$

From Eqs. (4.8), (4.9), and (4.12) we have

$$\frac{8s}{ca_0}\sum A_n \sin n\varphi = (\alpha_0 + \alpha_p - \alpha_{0l}) - \frac{\sum nA_n \sin(n\varphi)}{\sin(\varphi)} \tag{4.13}$$

Defining $\mu = ca_0/8s$, the final governing equation is

$$\mu(\alpha_0 + \alpha_p - \alpha_{0l}) \sin\varphi = \sum A_n \sin n\varphi(\mu n + \sin\varphi) \tag{4.14}$$

which is known as the *monoplane equation*. Applying Eq. (4.14) to $N$ span locations, we can obtain $A_i$ $(n = 1, ..., N)$, and from this the circulation can be established.

## Symmetric Span Extension

The lift distribution along the wingspan is symmetric about the wing root, therefore the even terms of the series representation given by Eq. (4.3) can be eliminated; that is $A_{2k} = 0$ $(k = 1, 2, ...)$. Therefore, the circulation $\Gamma(\varphi)$ becomes

$$\Gamma(y) = 4sU_\infty \sum_{n=1}^{N} A_{2n-1} \sin[(2n-1)\varphi] \tag{4.15}$$

The resulting wing lift is

$$\begin{aligned} L &= \int_{-s}^{s} \rho_\infty U_\infty \Gamma(y)\, dy = \int_0^\pi \rho_\infty U_\infty s\Gamma(\varphi) \sin\varphi\, d\varphi \\ &= 4\rho_\infty U_\infty^2 s^2 \int_0^\pi \sum_{n=1}^{N} A_{2n-1} \sin[(2n-1)\varphi] \sin\varphi\, d\varphi \end{aligned} \tag{4.16}$$

where all terms $n \neq 1$ are zero. Therefore, the lift coefficient becomes

$$C_L = A_1 \pi AR \tag{4.17}$$

where $AR = 4s^2/2S$ is the aspect ratio and $S$ is the wing area. The spanwise lift coefficient of Eq. (4.8) can now be written

$$c_L(\varphi) = \frac{2AR(1+\lambda)}{1 + (\lambda - 1)\cos\varphi} \sum_{n=1}^{N} A_{2n-1} \sin[(2n-1)\varphi] \tag{4.18}$$

where $\lambda$ is the taper ratio. Substituting Eq. (4.3) into (4.7), the total moment expression becomes

$$\mathscr{L} = -2\rho_\infty U_\infty^2 s^3 \int_0^\pi \sum A_{2n-1} \sin n\varphi \ \sin 2\varphi \ d\varphi = 0 \tag{4.19}$$

The moment generated by, for instance, the left wing is

$$\begin{aligned} \mathscr{L}_{left} &= 2\rho_\infty U_\infty^2 s^3 \int_0^\pi \sum A_{2n-1} \sin n\varphi \ \sin 2\varphi \ d\varphi \\ &= 2\rho_\infty U_\infty^2 s^3 \left[\frac{2}{3}A_1 + \frac{2}{5}A_3 - \frac{2}{21}A_5 + \frac{2}{45}A_7 - \frac{2}{77}A_9 + ...\right] \\ &= 2\rho_\infty U_\infty^2 s^3 A_s \end{aligned} \tag{4.20}$$

where $A_s$ can be deduced by observation. The moment is expressed in terms of the moment coefficient, $C_l$, by

$$\mathscr{L} = \frac{1}{2}\rho_\infty U_\infty^2 S s C_l$$

From Eq. (4.20), the moment coefficient for a single wing–in this case the right one–is therefore

$$C_l = 2A_s AR$$

## Asymmetric Span Extension

The lift distribution due to roll speed $P$ is asymmetric about the wing root axis. As such, the odd terms of the series given by Eq. (4.3) can be eliminated. The spanwise circulation can be written

$$\Gamma(y) = 4sU_\infty \sum_{n=1}^{N} A_{2n} \sin(2n\varphi) \tag{4.21}$$

The sectional lift becomes

$$c_L(\varphi) = \frac{2AR(1+\lambda)}{1+(\lambda-1)\cos\varphi} \sum_{n=1}^{N} A_{2n} \sin(2n\varphi) \tag{4.22}$$

The lift on the left wing is

$$\begin{aligned} L &= \int_0^{\pi/2} \rho_\infty U_\infty s\Gamma(\varphi)\sin\varphi \; d\varphi = 4\rho_\infty U_\infty^2 s^2 \int_0^{\pi} \sum_{n=1}^{N} A_{2n}\sin(2n\varphi)d\varphi \\ &= 2\rho_\infty U_\infty^2 s^2 \left[\frac{4}{3}A_2 - \frac{8}{15}A_4 + \frac{12}{35}A_6 + \frac{18}{99}A_{10} - \ldots\right] \\ &= 2\rho_\infty U_\infty^2 s^2 A_a \end{aligned} \tag{4.23}$$

The lift coefficient on the left wing is

$$C_L = 2A_a AR \tag{4.24}$$

Similarly, the moment is calculated as

$$\begin{aligned} \mathscr{L} &= 2\rho_\infty U_\infty^2 s^3 \int_0^{\pi} \sum A_{2n}\sin(2n\varphi)\sin(2\varphi) \; d\varphi \\ &= \pi\rho_\infty U_\infty^2 s^3 A_a = \rho_\infty U_\infty^2 SsC_M \end{aligned} \tag{4.25}$$

and the moment coefficient is

$$C_l = \frac{\pi}{2}A_a AR \tag{4.26}$$

## Drag and Range

The main benefit of symmetric wing extension is an increase in the lift to drag ratio, which results in an increase in range and endurance. The total drag of the aircraft wing is a combination of the induced drag and the profile drag:

$$C_D = C_{D_0} + C_{D_i} \tag{4.27}$$

The profile drag can be approximated based on an empirical database and can be defined as

$$C_{D0} = a_0 + a_1 C_L + a_2 C_L^2 \tag{4.28}$$

where $a_0$, $a_1$, and $a_2$ are constants which are obtained by curve-fitting the profile drag. As an example, consider a wing with the physical dimensions given in Table (4.3). As shown

Table 4.3: Baseline Wing Properties

| | |
|---|---|
| Root Chord | 0.5 m |
| Wing Span | 1.0 m |
| Sweep Angle | 5.7 deg |
| Taper Ratio | 0.6 |
| Wing Area | 0.413 $m^2$ |
| Aspect Ratio | 5 |
| Airfoil | NACA-0010 |

by Fig. (4.6), the wing has the ability of increasing its span by up to %50 in which case the aspect ratio is increased to 8.18 and the wing area increases to 0.568$m^2$–the area ratio is 1.38. The increase in range can be calculated using the following equation [114]:

$$\text{Range} = 2\sqrt{\frac{2}{\rho_\infty}}\frac{1}{c_t}\frac{(C_L S)^{1/2}}{C_D S}(W_0^{1/2} - W_1^{1/2}) \tag{4.29}$$

where $c_t$, $W_0$, and $W_1$ are the fuel consumption rate, gross vehicle weight with full tank, and gross weight with empty tank, respectively. As shown in Fig. (4.7), as the wingspan increases, the induced drag decreases, whereas the profile drag increases linearly; the increase of the profile drag is due to the increase of the wing area. The total drag is decreased by approximately 25%, and therefore the range is increased by approximately 30%.

## Roll Producing and Damping Moments

Let $S_0$, $s_0$, and $AR_0$ be, respectively, the area, half-span length, and aspect ratio of the wing before changing shape. Using these definitions, the relative moment coefficient, $C'_M$, is expressed as

$$C'_l = C_l \frac{Ss}{S_0 s_0}$$

As demonstrated by Fig. (4.6), let $y_e$ be the initial wing extension and $\Delta y_e$ be the additional extension. Furthermore, let the wings be coupled such that an extension of one wing results in a retraction of the other by the same amount. The half span is then given by $s = s_0 + y_e + \Delta y_e$

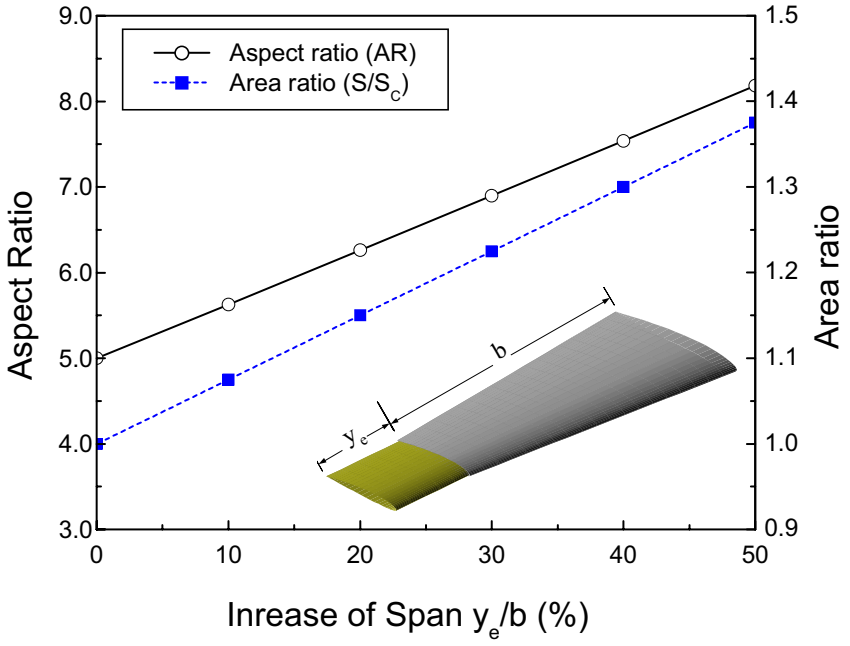



Figure 4.6: Changes of Aspect Ratio and Wing Area

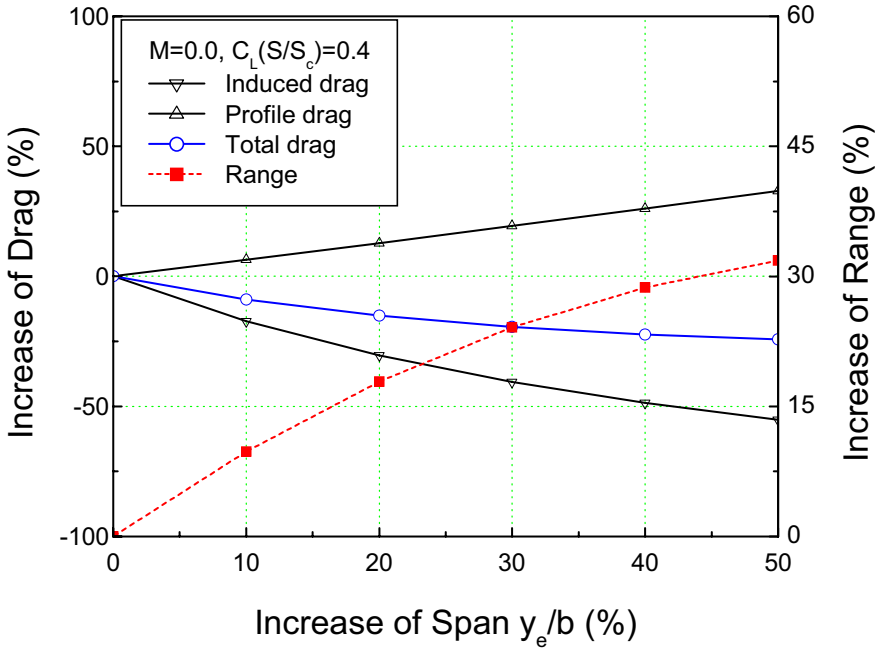



Figure 4.7: Effects of Wingspan on Drag and Range

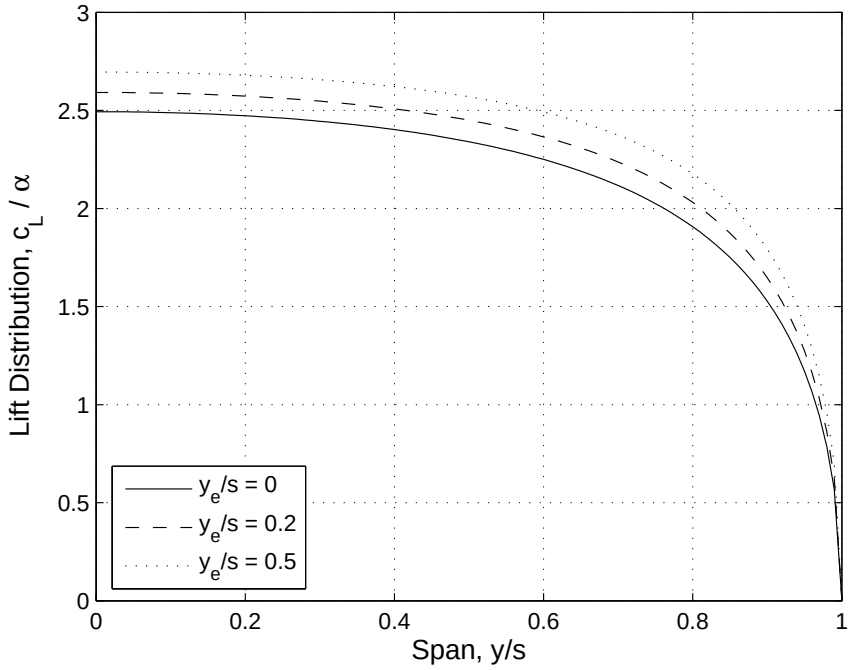



Figure 4.8: Spanwise Lift Distribution

and the moment coefficient can be written

$$C_l' = C_l(1+\bar{y}_e)^2 = 2A_sAR_0(1+\bar{y}_e)^3 \tag{4.30}$$

where $\bar{y}_e = y_e/s_0$. When the wing span of the right wing is increased by $\delta_{y_e} = \Delta y_e/s_0$–and subsequently the left wing is reduced by this amount–the total moment coefficient can be expressed by

$$\begin{aligned} \Delta C_l' &= 2A_sAR_0\left[(1+\bar{y}_e+\delta_{y_e})^3-(1+\bar{y}_e-\delta_{y_e})^3\right] \\ &= 2A_s\frac{AR}{1+\bar{y}_e}\left[(1+\bar{y}_e+\delta_{y_e})^3-(1+\bar{y}_e-\delta_{y_e})^3\right] \end{aligned} \tag{4.31}$$

The spanwise lift distribution for varying wing extensions is shown in Fig. (4.8). The moment produced by each wing is shown by Fig. (4.9) and the total roll producing moment due to wing extension is shown by Fig. (4.10).

For the roll damping moment, let the initial angle $\alpha_0$ be equal to zero. Following the same

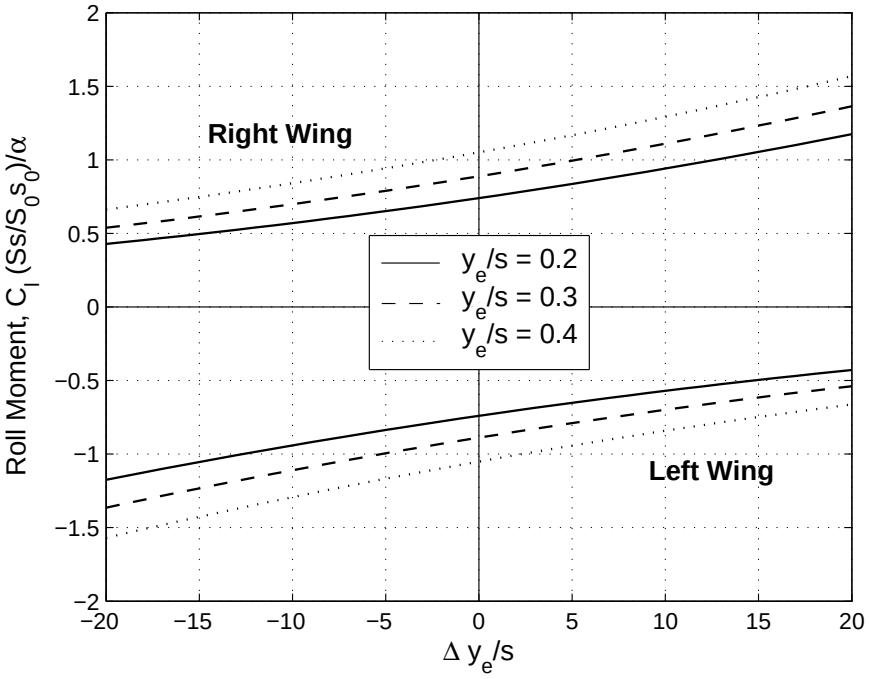



Figure 4.9: Moment due to Left and Right Wing (right wing extended)

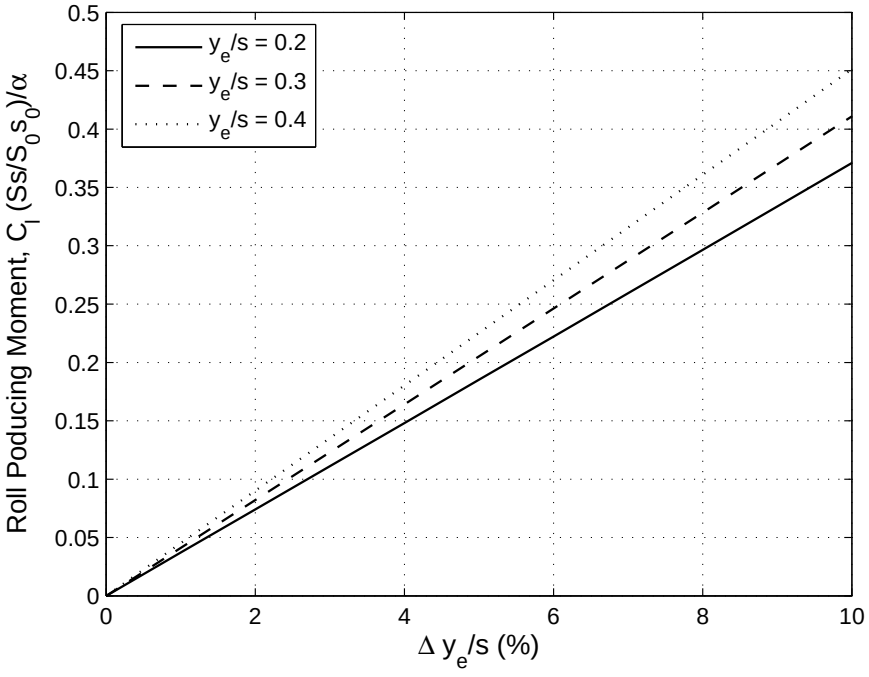



Figure 4.10: Roll Producing Moment due to Wing Extension

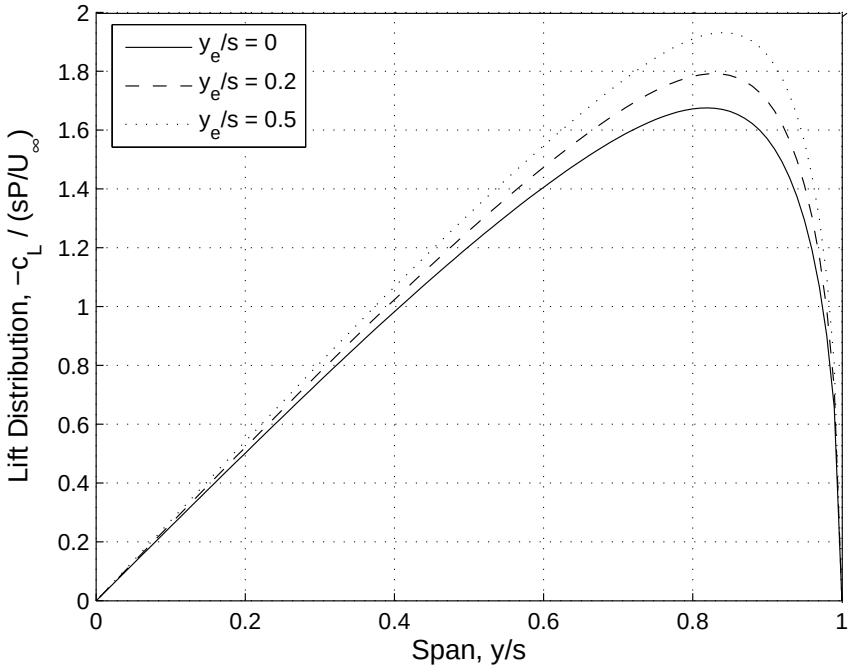



Figure 4.11: Spanwise Lift Distribution Due to Roll Speed $P$

procedure as before, the roll damping moment of the right wing is

$$C_l' = C_l(1+\bar{y}_e)^2 = -\frac{\pi}{8}A_a AR_0(1+\bar{y}_e)^3 \tag{4.32}$$

Therefore, the roll damping moment due to a small wing extension $\Delta y_e$ is

$$\begin{aligned}\Delta C_l' &= -\frac{\pi}{8}A_a AR_0\left[(1+\bar{y}_e+\delta_{y_e})^3+(1+\bar{y}_e-\delta_{y_e})^3\right] \\ &= \frac{\pi A_a AR}{8(1+\bar{y}_e)}\left[(1+\bar{y}_e+\delta_{y_e})^3+(1+\bar{y}_e-\delta_{y_e})^3\right]\end{aligned} \tag{4.33}$$

The spanwise lift distribution while the wing is rotating at constant angular velocity is shown in Fig. (4.11), the roll damping moment supplied by each wing is shown in Fig. (4.12), and the total roll damping moment is demonstrated by Fig. (4.13).

The roll producing moment due to asymmetric wing extension is a function of the Mach number, angle of attack, altitude, and sideslip angle. The explicit dependence on sideslip was not demonstrated with the assumption that this parameters remained very small. The dependence on Mach number and altitude is indirectly implied through the free-stream air

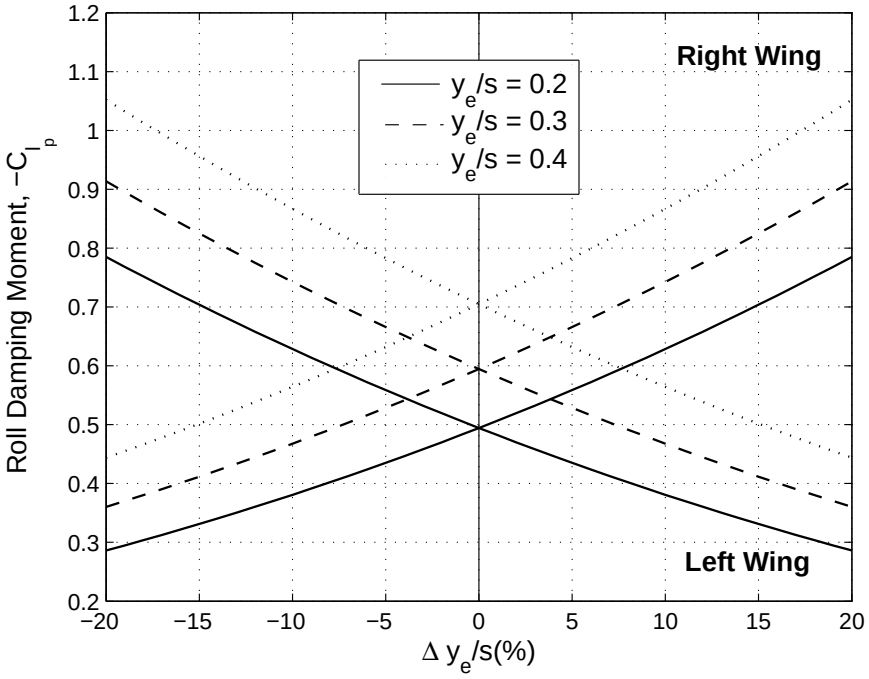



Figure 4.12: Roll Damping Moment of Left and Right Wings (right wing extended)

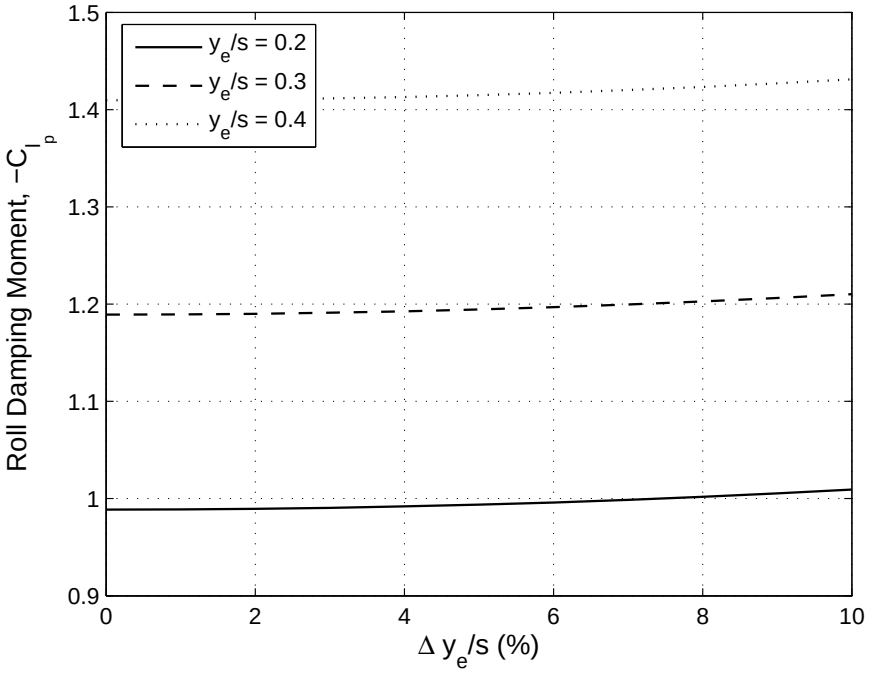



Figure 4.13: Total Roll Damping Moment due to Wing Extension

density. Treating the wing extension and an actuation device, similar to an aileron, the change in the roll producing moment coefficient is approximated by

$$\Delta C_{l_{\delta_{y_e}}}(\alpha, \beta, h, M, \bar{y}_e) \approx C_{l_{\delta_{y_e}}}(\alpha, h, M, \bar{y}_e)\ \delta_{y_e} \tag{4.34}$$

The total roll damping moment due to wing extension, as shown by Fig. (4.12), is approximately constant throughout a range of $0 \leq \delta_{y_e} \leq 0.1$. Hence, the derivative $C_{l_p}$ is considered to be unaffected by a small increase in wing extension.

Replacing the function of the aileron $\delta_a$ by the wing extension parameter $\delta_{y_e}$, the rolling moment coefficient of Eq. (4.2) becomes

$$\begin{aligned} C_l &= C_l(\alpha, M)\ \beta + C_{l_{\delta_{y_e}}}(\alpha, \beta, M, \bar{y}_e)\ \delta_{y_e} + C_{l_{\delta_r}}(\alpha, \beta, M)\ \delta_r \\ &+ \frac{b}{2V_T}[C_{l_p}(\alpha, M, \bar{y}_e)\ P + C_{l_r}(\alpha, M)\ R] \end{aligned} \tag{4.35}$$

which may be linearized for control design purposes.

## 4.4 Summary

In this chapter, representations for the aerodynamic forces and moments were developed. Four aircraft configurations–three of these are used in later analysis–were considered as a platform for studying the dynamic effects of morphing aircraft. Based on the work performed by NextGen Aeronautics, the Teledyne Ryan Firebee was used as a baseline aircraft. The specific configurations considered were dash, where the aircraft wings are swept back at 60 degrees, a loiter design with a large wing-span and a maneuver configuration. Methods of developing aerodynamic models were discussed based on widely accepted methods. Datcom was introduced as the method used in determining the aerodynamic derivatives used in flight analysis.

Specific to morphing control, an aerodynamic representation for a variable span aircraft was developed. In particular, it was shown that a asymmetric wing extension could be used to generate a large moment that may be suitable for control authority in maneuvering flight. Based on Prandtle's lifting line theory, an expression for the both the roll producing and damping moments were calculated. It was further shown, that for wing deflections of

less than 10% of half span, the roll producing moment remains constant thus allowing the standard linear roll damping derivative approximation.

# Chapter 5

# Flight Control Design and Analysis

There are multiple types of automated flight control systems that are designed to accommodate various flight demands. One of the first of these was the pitch attitude hold system in which the goal was to maintain a desired pitch angle. These "pilot relief" control systems are more commonly known as simply *autopilot*. Over the years, the autopilot systems have become more sophisticated and have grown to aid the pilot in such tasks as altitude hold, speed/Mach hold, automatic landing, roll-angle hold, turn coordination, and heading hold.

An autonomous aircraft, which is the subject of current interest, must have the capability of handling each of the aforementioned flight regimes in addition to those accounted for by a pilot. In the following sections a subset of these autopilot control systems will be examined. In particular, we will investigate the stabilization of an aircraft undergoing large structural changes and also some tracking and guidance systems. For the latter, we will examine flight systems suitable for control morphing, in which the structural changes are used for control authority.

The following sections on control design and analysis will focus on two particular autonomous design problems. The first is a stabilization autopilot in which the goal is to maintain a desired trimmed flight condition in the presence of large variations in both inertial and aerodynamic forces–this is generally referred to as the standard *regulator* problem. The second is a navigation problem in which the aircraft controller attempts to achieve a desired spatial location formulated by a guidance system.

## 5.1 General Considerations

The equations of motion for a morphing aircraft can be expressed in the state space by the general form

$$\dot{\boldsymbol{x}} = \boldsymbol{f}\left(\boldsymbol{x}, t\right) + \boldsymbol{f}_a(\boldsymbol{x}, \boldsymbol{u}, t) \tag{5.1}$$

where $\boldsymbol{x} \in \mathbb{R}^p$ is the state vector (comprising both the configuration and kinematic coordinates), and $\boldsymbol{u} \in \mathbb{R}^m$ is the control input (comprising the aerodynamic and planform controls). The first term in Eq. (5.1) includes the kinematics and dynamics states of the system and the second term denotes the applied forces and moments due to aerodynamic and gravitational effects. As discussed in the previous section, the aerodynamic forces and moments are a complicated function of the aircraft's dynamic state and the external atmospheric flight conditions. The manner in which they are incorporated into the flight dynamic equations is via the quasi-steady assumption; this assumption results in the linear aerodynamic derivatives.

Since it is difficult to work with the full nonlinear equations directly, it is sometimes convenient to approximate Eq. (5.1) by a reduced set of equations. There are at least two ways to accomplish this task. The first is to linearize the dynamic equations directly about some specific $(\boldsymbol{x}_0, \boldsymbol{u}_0, t_0)$, resulting in the linear equations

$$\dot{\boldsymbol{x}} = (\mathbf{A} + \mathbf{A}_a)\boldsymbol{x} + \mathbf{G}\boldsymbol{u} \tag{5.2}$$

where the constant matrices are determined by

$$\mathbf{A} = \left.\frac{\partial \boldsymbol{f}}{\partial \boldsymbol{x}}\right|_{\boldsymbol{x}_0,\ t_0}, \quad \mathbf{A}_a = \left.\frac{\partial \boldsymbol{f}_a}{\partial \boldsymbol{x}}\right|_{\boldsymbol{x}_0,\ t_0}, \quad \mathbf{G} = \left.\frac{\partial \boldsymbol{f}_a}{\partial \boldsymbol{u}}\right|_{\boldsymbol{u}_0,\ t_0}$$

A particular set $(\boldsymbol{x}_0, \boldsymbol{u}_0, t_0)$ is said to be an *equilibrium point* (or *stationary point*) of the Eq. (5.1) if

$$\boldsymbol{f}(\boldsymbol{x}_0, t_0) + \boldsymbol{f}_a(\boldsymbol{x}_0, \boldsymbol{u}_0, t_0) = \mathbf{0}$$

The determination of these equilibrium points typically results in solving a complex nonlinear algebra problem which can be evaluated by numerical iteration techniques. This technique of linearization, although the predominant method, is dependent on a specific aircraft design

and, therefore, does not allow a general analysis.

Equation (5.2) is extremely convenient for evaluating stability and designing control laws for rigid aircraft due to the numerous methods of analysis provided by linear system theory. However, this linearized form is only suitable for small perturbations about the stationary point. Often times it is desired to work equations that are accurate for much larger perturbations. For this reason, another approach used is to decouple Eq. (5.2) into *longitudinal* and *lateral* equations. To decouple the equations a steady-state flight condition is chosen, such as steady wings-level or steady turning flight, so that some of the states go to zero. Furthemore, the aerodynamics are divided into longitudinal and lateral components and the resulting equations of motion are of the form

$$\dot{\boldsymbol{x}} = \boldsymbol{f}(\boldsymbol{x}) + \mathbf{A}_a\boldsymbol{x} + \mathbf{G}\boldsymbol{u} \tag{5.3}$$

where the second term, $\mathbf{A}_a\boldsymbol{x}$, consists of the state-dependent aerodynamic forces and moments. Note that the matrices $\mathbf{A}_a$ and $\mathbf{G}$ result from the quasi-steady aerodynamic approximation. For a symmetrical rigid aircraft, Eq. (5.3) produces nine equations which are divided into four longitudinal and five lateral equations; the longitudinal equations are naturally decoupled from the lateral, but not vice-versa. Supposing that the aerodynamic parameters are valid for the desired perturbations (the operating range), each nonlinear set of equations may be evaluated independently, although the lateral equations require some additional assumptions.

For a non-rigid aircraft these dynamics are more complex. The general form of the equations of motion for a morphing aircraft is given by Eq. (5.1). For the rigid aircraft the next step in the process was to approximate the aerodynamics in a quasi-steady manner, thus eliminating the time dependence of the state equations. For an aircraft that is changing shape, however, the time dependence will invariably appear in the aerodynamics and also in the inertial forces, even if they are not accounted for explicitly. The equations of motion may still be linearized into the form of Eq. (5.2). However, this form is only suitable for a single instant in time and does not extend to the necessary perturbations of large planform alterations. If the equations are linearized at several intermittent steps as the aircraft changes shape, then Eq. (5.2) becomes

$$\dot{\boldsymbol{x}} = [\mathbf{A}(t) + \mathbf{A}_a(t)]\boldsymbol{x} + \mathbf{G}(t)\boldsymbol{u} \tag{5.4}$$

This process can be thought of as a quasi-steady dynamic approach, analogous to the quasi-steady aerodynamic approach previously described. The difficulty of Eq. (5.4) is that it is nonautonomous. In general, evaluating the stability of and designing control laws for nonautonomous systems is more difficult than time-invariant systems. The process of removing the time-dependence, if desired, involves relating the structural changes to a control input and constructing the aerodynamics as solely state-dependent functions.

To explain further, consider the particular case in which the aircraft is at a steady-state wings-level trimmed flight condition. For simplicity of expression, let the morphing portion of the aircraft be approximated by only 2 particles of total mass $\bar{m} = m_1 + m_2$–these may represent the aircraft wings. The longitudinal dynamics of this representation may be expressed as

$$\begin{aligned}
&\begin{bmatrix} mV_T & -\bar{m}b_x & 0 & \bar{m} \\ -\bar{m}V_T b_x & J_y + \bar{m}(b_x^2 + b_z^2) & \bar{m}b_z & -\bar{m}b_x \\ 0 & 0 & 1 & 0 \\ 0 & 0 & 0 & 1 \end{bmatrix} \begin{bmatrix} \dot{\alpha} \\ \ddot{\theta} \\ \ddot{b}_x \\ \ddot{b}_z \end{bmatrix} \\
&\quad = \begin{bmatrix} \bar{m}\dot{b}_x\dot{\theta} + \bar{m}b_z\dot{\theta}^2 + mV_T\dot{\theta} \\ -\bar{m}b_x\dot{b}_x\dot{\theta} - \bar{m}b_z\dot{b}_z\dot{\theta} - \bar{m}V_T b_x\dot{\theta} - \bar{m}V_T b_z\dot{\theta} \\ 0 \\ 0 \end{bmatrix} + \begin{bmatrix} F_z \\ \mathscr{M} \\ u_x \\ u_z \end{bmatrix}
\end{aligned} \tag{5.5}$$

where symmetry has been assumed ($b_x^{12} = b_x^{13} = b_x$, $b_z^{12} = b_z^{13} = b_z$, and $b_y^{12} = -b_y^{13}$). With the goal of linearizing Eq. (5.5), the state vector representation is chosen as

$$\boldsymbol{x} = \begin{bmatrix} \alpha & \theta & \dot{\theta} & e_x & \dot{e}_x & e_z & \dot{e}_z \end{bmatrix}^T$$

where $e_x = b_x - b_x^c$ and $e_x = b_z - b_z^c$ are the position errors and $b_x^c$ and $b_z^c$ are the commanded positions–both assumed to be constant. The mass positions are then controlled by defining $u_x = f(e_x, \dot{e}_x)$ and $u_z = f(e_z, \dot{e}_z)$. Given the state definition of Eq. (5.6), the state representation of Eq. (5.5) thus be written in the form

$$\dot{\boldsymbol{x}} = \boldsymbol{f}\left(\boldsymbol{x}, F_z, \mathscr{M}\right) \tag{5.6}$$

For a rigid aircraft the longitudinal aerodynamic forces and moments are typically taken

to be a function of $\alpha$, $\dot{\alpha}$, $\dot{\theta}$, and $\delta_e$–the longitudinal aerodynamic control. For morphing flight, there will be additional dependencies on $b_x$, $b_z$, and also time. To maintain the state dependence and avoid time-varying forcing functions it would be helpful if the forces and moments could be expressed as

$$F_z = F_z\left(\boldsymbol{x}, \delta_e\right)$$
$$\mathscr{M} = \mathscr{M}\left(\boldsymbol{x}, \delta_e\right)$$

such that the changes in normal force and pitching moment contributed by planform variations may be approximated in a quasi-steady manner using constant aerodynamic derivatives. With this assumption Eq. (5.6) may be written as $\dot{\boldsymbol{x}} = f(\boldsymbol{x}, \delta_e)$ and then upon linearization about an equilibrium point $\dot{\boldsymbol{x}} = \mathbf{A}\boldsymbol{x} + \mathbf{G}\delta_e$. Subsequently, the linearized equations can be used for longitudinal control design and stability analysis via conventional time-invariant linear techniques.

Such an evaluation could be considered a *unified approach* to morphing flight control. The difficulty with this approach is that the aerodynamic effects involve highly complex dependencies on the aircraft structure. An accurate aerodynamic description typically relies on complex numerical routines involving both theory and interpolation methods such as used by Datcom; wind tunnel testing is also substantially important. One such attempt was made by Meirovitch for flexible aircraft [45]; to alleviate the complexity of aerodynamic effects basic *strip theory* was employed.

Instead of an attempt on the unified approach, the following sections are concerned with the control of a morphing aircraft using the standard aerodynamic approximations provided by Datcom. As such, the aerodynamic forces and moments can not be determined as an analytic function. Thus, a control design must either attempt to compensate for the changing aerodynamics on a discrete basis, such as relying on aerodynamic tables, or simply ignore the nonlinear variations.

## 5.2 Morphing Stabilization Analysis

We first consider the problem of stabilizing an aircraft during a configuration change. The aircraft is initially operating in steady, wings-level, trimmed flight. A configuration change

is then initiated in which the aircraft morphs into a different shape. Referring to Fig. (4.2), we will specifically consider a transformation from loiter to dash, since these configurations represent the largest variations in both mass center and aerodynamic properties.

## Longitudinal Dynamics

The longitudinal dynamics that describe this motion are given by Eqs. (3.11-3.13). The main body of the aircraft, of mass $m_f$ and inertia $J_y$, is assumed to be of uniform density and the aircraft wings, of mass $m_w$, are approximated by a concentrated mass located at 50% of the mean aerodynamic chord. The center of gravity is specified for each configuration, therefore, and additional mass ($m_a$) is positioned accordingly to accommodate the required c.g. location. As previously discussed, the additional mass could be an extending tail section as developed by Neal *et al* [34].

The motion of both masses is confined to the $x$-direction; the position of $m_a$ with respect to the origin of the body-fixed reference frame is defined as $x_a$ and the position of $m_w$ as $x_w$ where $x_a = f(x_w, x_{cg})$. Note that the total mass of the aircraft is

$$m_T = m_f + m_w + m_a \tag{5.7}$$

With the additional assumption that the aircraft is throttled such that it maintains a constant velocity $V_T$ (i.e., $\dot{V}_T = 0$), the equations of motion, in the wind axis, are

$$\begin{aligned} m_T V_T(\dot{\alpha} - Q) &= h_z^w + F_z^w + g m_T(c\theta c\alpha + s\theta s\alpha) \\ J_y \dot{Q} &= h_m^w + \mathscr{M}^w - g\cos\theta(m_w x_w + m_a x_a) \end{aligned} \tag{5.8}$$

where

$$\begin{aligned} h_z^w &= \cos\alpha(m_w x_w + m_a x_a)\dot{Q} + 2\cos\alpha(m_w \dot{x}_w + m_a \dot{x}_a)Q \\ &- 2\sin\alpha(m_w x_w + m_a x_a)Q\dot{\alpha} \\ h_m^w &= -V_T(m_w x_w + m_a x_a)(\dot{\alpha} - Q) - 2(m_w x_w \dot{x}_w + m_a x_a \dot{x}_a)Q \\ &- (m_w x_w^2 + m_a x_a^2)\dot{Q} \end{aligned} \tag{5.9}$$

The applied aerodynamic normal force and pitching moment are

$$\begin{aligned} \frac{1}{Sq}F_z^w &= (\cos\alpha)\ C_z \\ \frac{1}{Sqc}\mathscr{M}_y^w &= C_m \end{aligned}$$

where $C_z$ and $C_m$ were previously defined by Eqs. (4.1) and (4.2). Furthermore, the elevator dynamics are modeled as a first-order lag with gain $K_{\delta_e}$; that is

$$\dot{\delta}_e = K_{\delta_e}(-\delta_e + u_{\delta_e})$$

where $u_{\delta_e}$ is the commanded elevator input. For numerical simulations, both rate and saturation limits are enforced. Choosing the state vector as

$$\boldsymbol{x} = \begin{bmatrix} h & \alpha & \theta & Q & \delta_e \end{bmatrix}^T$$

where $h$ is the altitude from Eq. (3.14), the equations of motion may be expressed in state-space form as

$$\begin{aligned} \dot{\boldsymbol{x}} &= \begin{bmatrix} 1 & 0 & 0 & 0 & 0 \\ 0 & \frac{m_T V_T}{Sq} + \frac{2}{Sq}\hat{S}_x s\alpha Q & 0 & -\frac{1}{Sq}\hat{S}_x c\alpha & 0 \\ 0 & 0 & 1 & 0 & 0 \\ 0 & -\frac{V_T}{Sqc}\hat{S}_x & 0 & \frac{1}{Sqc}(J_y + m_a x_a^2 + m_w x_w^2) & 0 \\ 0 & 0 & 0 & 0 & 1 \end{bmatrix}^{-1} \\ &\quad * \begin{bmatrix} V_T(s\theta c\alpha - c\theta s\alpha) \\ \frac{V_T}{Sq}Q + \frac{2}{Sq}(m_a\dot{x}_a + m_w\dot{x}_w)c\alpha Q + \frac{gm_T}{Sq}(c\theta c\alpha + s\theta s\alpha) + c\alpha C_z \\ Q \\ -\frac{V_T}{Sqc}\hat{S}_x Q - \frac{2}{Sqc}(m_a x_a\dot{x}_a + m_w x_w\dot{x}_w)Q - \frac{g}{Sqc}c\theta\hat{S}_x + C_m \\ -K_{\delta_e}\delta_e + K_{\delta_e}u_{\delta_e} \end{bmatrix} \end{aligned} \tag{5.10}$$

where $\hat{S}_x = (m_w x_w + m_a x_a)$.

## Linear Control Design

The current task is to design a pitch-attitude hold autopilot control design that will achieve a desired pitch reference command during transition from loiter to dash. The form of Eq. (5.10) is the standard nonlinear form given by Eq. (5.1). To perform a classical control design we wish to linearize these equations about a given operating point–not necessarily an equilibrium value–with the assumption that the states will remain "close" to the given operating values. Performing the operation of linearization, however, will result in non-constant coefficients since both $x_w$ and $x_a$ will vary with the commanded configuration changes. Another option would be to include $x_w$ and $x_a$ as components of the state vector, and then linearize. This assumes that the aircraft is rigid and is equivalent to defining the dynamics about the body-fixed origin.

We will proceed by designing a control law for both the loiter and dash configurations separately, using the rigid aircraft equations. Assuming that the control structure is the same for each configuration, the gains can be scheduled (i.e., gain scheduling) during transition based on the the c.g. location. Both before and after the aircraft changes shape, the short-period steady state dynamics are given by

$$\begin{aligned} \dot{h} &= V_T(s\theta c\alpha - c\theta s\alpha) \\ m_T V_T \dot{\alpha} &= V_T Q + (\cos\alpha) Sqc\, C_z \\ J_y^c \dot{Q} &= Sqc\, C_m \end{aligned} \tag{5.11}$$

where $J_y^c$ is the second inertial moment measured about the center of gravity. Upon linearizing the aerodynamic forces the small perturbation values are

$$\begin{aligned} C_z &= C_{z_\alpha}\alpha + C_{z_{\delta_e}}\delta_e \\ C_m &= C_{m_\alpha}\alpha + \frac{c}{2U}(C_{m_{\dot{\alpha}}}\dot{\alpha} + C_{m_q}Q) + C_{m_{\delta_e}}\delta_e \end{aligned} \tag{5.12}$$

where the steady-state conditions are chosen as $\alpha = 2$ deg, $M = 0.5$, $h = 30,000$ ft, and $V_T = 500$ ft/s. The parameters for both configurations are listed in Table (5.1). The reference quantities are those of the loiter configuration. Linearizing Eq. (5.11) results in the linear state-space representation

$$\dot{\boldsymbol{x}} = \mathbf{A}\boldsymbol{x} + \mathbf{B}u_{\delta_e}$$

Table 5.1: Morphing Aircraft Parameters

| | Loiter | Dash |
|---|---|---|
| $x_{cg}$ | 10.8 ft | 13.2 ft |
| $C_{m_\alpha}$ | -0.1373 | -0.7269 |
| $\frac{J_y}{Sqc}$ | 0.2537 | 0.3088 |
| $\frac{c}{2U}C_{m_q}$ | -0.0508 | -0.02875 |
| $\frac{c}{2U}C_{m_{\dot{\alpha}}}$ | -0.0253 | -0.0302 |
| $C_{z_{\delta_e}}$ | 0.8136 | 0.8193 |
| $C_{m_{\delta_e}}$ | 2.8533 | 1.9940 |

where

$$\text{Loiter} \quad : \quad \mathbf{A} = \begin{bmatrix} 0 & -499.7 & 499.7 & 0 & 0 \\ 0 & -0.9913 & 0 & 1 & 0.1351 \\ 0 & 0 & 0 & 1 & 0 \\ 0 & -0.5736 & 0 & -0.3899 & 14.58 \\ 0 & 0 & 0 & 0 & -20.2 \end{bmatrix}, \quad \mathbf{B} = \begin{bmatrix} 0 \\ 0 \\ 0 \\ 0 \\ 20.2 \end{bmatrix}$$

$$\text{Dash} \quad : \quad \mathbf{A} = \begin{bmatrix} 0 & -499.7 & 499.7 & 0 & 0 \\ 0 & -0.6567 & 0 & 1 & 0.1361 \\ 0 & 0 & 0 & 1 & 0 \\ 0 & -2.029 & 0 & -0.1659 & 5.71 \\ 0 & 0 & 0 & 0 & -20.2 \end{bmatrix}, \quad \mathbf{B} = \begin{bmatrix} 0 \\ 0 \\ 0 \\ 0 \\ 20.2 \end{bmatrix} \tag{5.13}$$

The root locus of both configurations is shown in Fig. (5.2)–note that there is a real pole at $-25.2$ due the actuator time constant that is not shown. Both systems have a pole at the origin resulting in a Type 1 system. Since the dynamics were linearized about the initial pitch angle $\theta = 0$, gravity does not appear in the linearized equations. For non-zero pitch angle the zero pole will be moved away from the origin to the left resulting in a Type 0 system.

The procedure for designing the pitch attitude autopilot is to first design the inner-loop pitch rate feedback, analyze this subsystem and the design the outer-loop compensation based on pitch attitude feedback. The block diagram for this design is shown in Fig. (5.1). The inner-loop control is a gain feedback, $K_q$, is used to increase the damping of the short-period oscillation. A proportional-integral (PI) compensator–$K_\theta$ and $K_I$ are respectively the

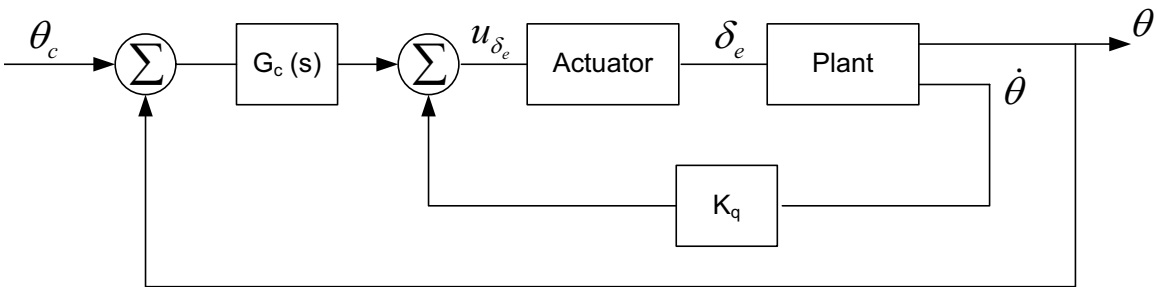



Figure 5.1: Pitch Attitude Hold with Dynamic Compensation

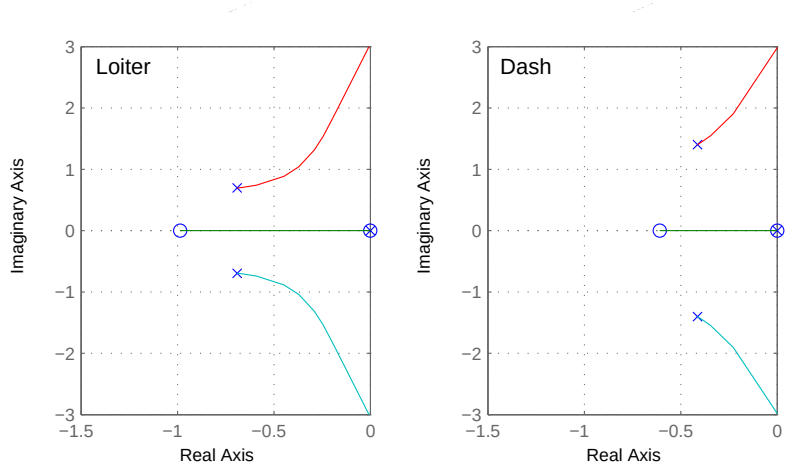



Figure 5.2: Root Locus for Loiter and Dash Configurations, $\theta(s)/u_{\delta_e}(s)$

proportional and integral gains–based on pitch feedback is used to move the zero-value poles away from the right-half plane. Additional lead compensation is then designed to fine-tune the dynamic performance via the gain and phase margins. The two control designs are

$$\begin{aligned} \text{Loiter} \quad &: \quad K_q = 0.3, \quad G_c(s) = 21\frac{(s+0.3)(s+2.5)}{s(s+25)} \\ \text{Dash} \quad &: \quad K_q = 0.7, \quad G_c(s) = 40\frac{(s+0.3)(s+2.5)}{s(s+25)} \end{aligned} \tag{5.14}$$

The resulting open-loop Bode plots are shown in Fig. (5.3). The stability margins were designed to be sufficiently large to accommodate model uncertainty. Typical desired values are a phase margin of 30 to 60 degrees and a gain margin of 6 to 15 dB [88]. The respective step responses are shown in Fig. (5.4).

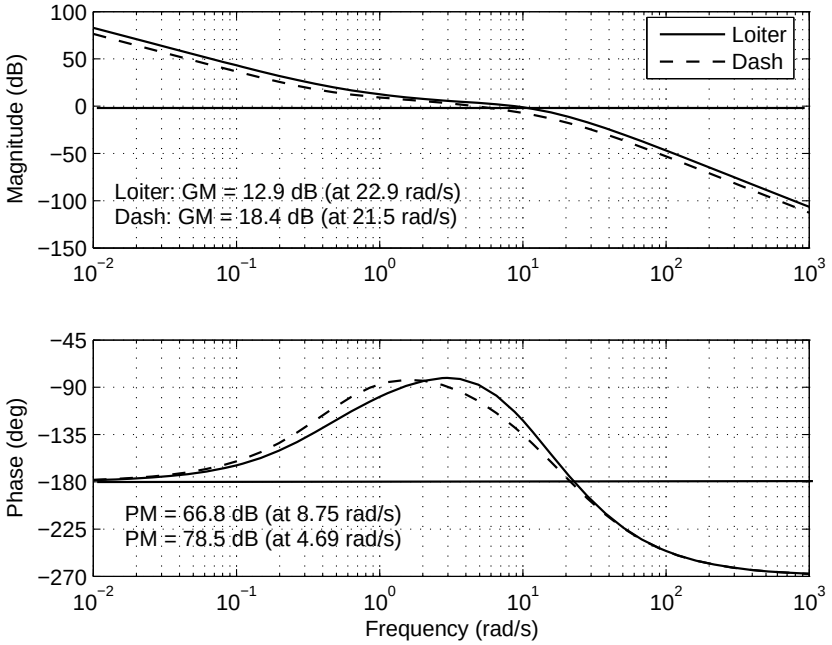



Figure 5.3: Open-Loop Bode for Pitch-Attitude Compensators

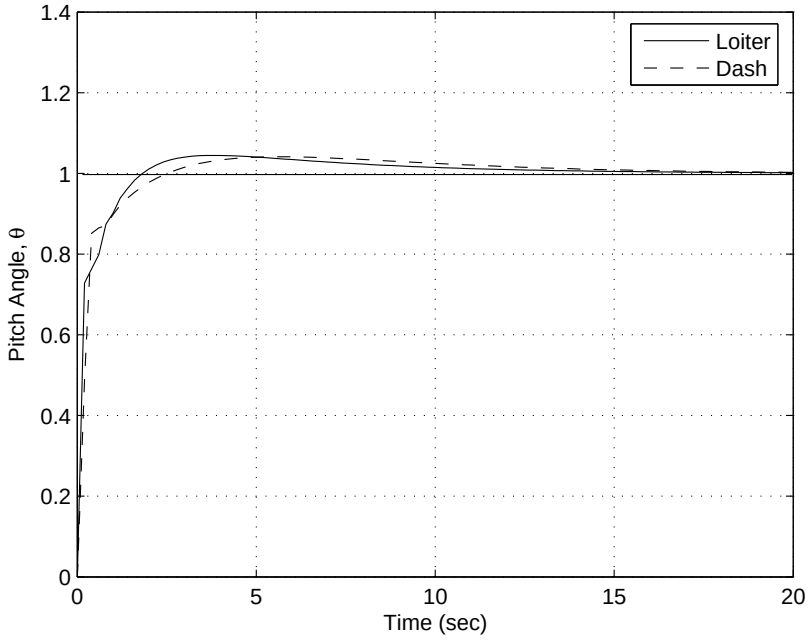



Figure 5.4: Step Response for Closed-Loop Pitch-Attitude Control

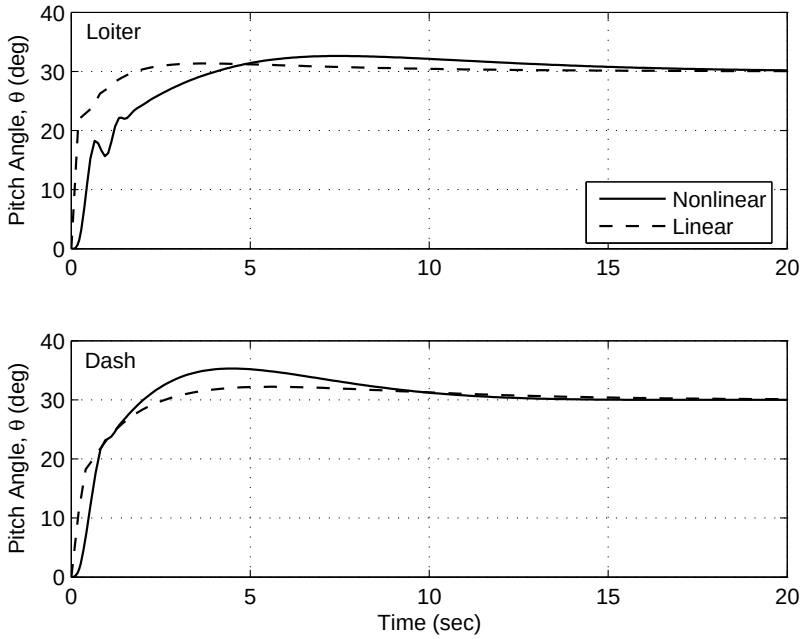



Figure 5.5: Comparison of Linear and Nonlinear Simulations for Pitch-Attitude Control Design

## Numerical Simulations

The numerical simulations are based on the nonlinear dynamics given by Eq. (5.8), thus accounting for the changes in mass distribution and changing aerodynamic effects. As discussed previously Chapter 4, the aerodynamics forces and moments were constructed in the form of look-up tables to account for variations due to both orientation, altitude, and aircraft configuration.

The control laws given by Eq. (5.14) were simulated for both configurations to test the performance of the compensator designs. A comparison of both the linear and nonlinear simulations for both cases is shown if Fig. (5.5). In general, the nonlinear results exhibit an increases in both in overshoot and settling time; this is an expected result due to the ignored nonlinear effects. Nonetheless, the designs exhibit adequate performance for each configuration.

Having designed suitable controllers for both loiter and dash, we now consider the dynamics of a configuration change. This consideration introduces some complexity in the control

design. Although it is not demonstrated, the control design for loiter does not provide a stable response for the dash configuration. In an attempt to alleviate this difficulty the control gains are scheduled linearly as a function of the center of gravity position. It is noted that typical pitch control gain scheduling for a rigid aircraft with constant mass center is performed by attempting to maintain a constant ratio, $-K_\theta C_{m_{\delta_e}}/C_{m_\alpha}$, by updating the proportional gain [122]. This, however, relies on the assumption that the aerodynamic derivatives do not alter substantially. Stability analysis for a gain-scheduled control design is inherently difficult due to the time-varying nature of resulting closed-loop dynamics. Furthermore, even if the dynamics are stable at each discrete transition point, this does not imply dynamic stability. In general, the rate of transition must be sufficiently small to ensure stability [123].

To begin, we consider a transitioning from loiter to dash while attempting to maintain a zero pitch angle. The transition rate is controlled by a first order time lag $\tau_{cg}$. As demonstrated by Fig. (5.6), for slow transition rates the response exhibits small angle deviations with a maximum of approximately 2 degrees. As the transition rate is increased the overshoot becomes much larger and with greater oscillation. A transition rate of $\tau_{cg} = 5$ sec appears to be a limiting value in that the maximum overshoot demonstrates no further increase. The main reason for this behavior is the lack of sophistication in the aerodynamic model. The aircraft quickly transitions into the dash configuration with the corresponding steady-state aerodynamics. Although not investigated here, it is probable that transient aerodynamic effects will have a significant effect.

We next consider a configuration change while maneuvering. As shown in Fig. (5.7), a transition takes place while the aircraft attempts to achieve a pitch angle of 30 degrees. Compared to Fig. (5.5) the response shows a large increase in both overshoot and settling time. Note that aft moving mass promotes a greater rise time, but also the undesirable overshoot effects. Also, the compensator proves to be incapable of providing stability for rate transitions of more than approximately $\tau_{cg} = 2$ sec.

Now considering a reverse transformation–from dash to loiter–Fig. (5.8) shows an opposite effect of rate transition. That is, the rate of structural transition provides a stabilizing effect on the regulated response. This result is, in part, caused by the forward moving mass which provides a negative stabilizing moment. Another contribution is that the loiter configuration is inherently more stable with larger valued aerodynamic damping derivatives. The maneuvering case is considered in Fig. (5.9). Once again the stabilizing rate transition effects are apparent; the stable compensation range is shown to be for values $\tau_{cg} > 0.5$ sec

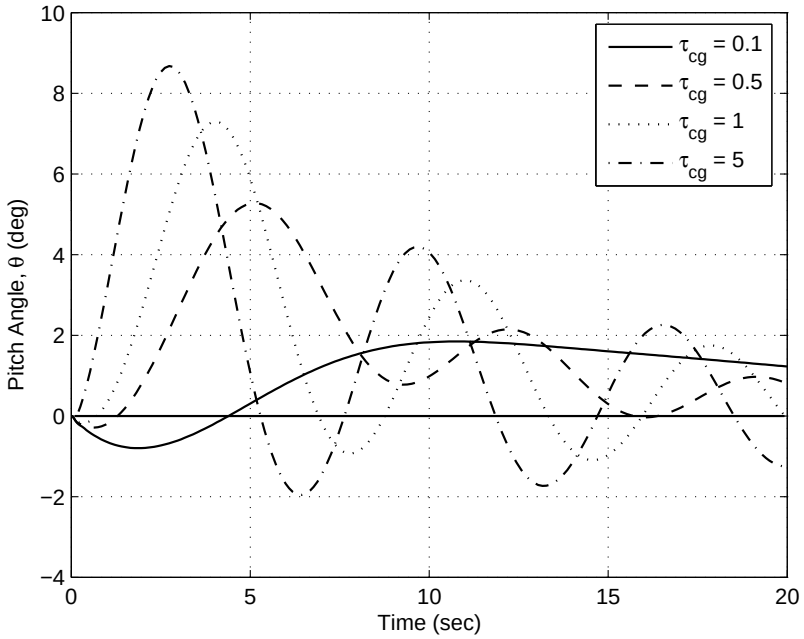



Figure 5.6: Configuration Change from Loiter to Dash Using Gain Scheduled Compensator; The Results Demonstrate the Effects of Transition Rate

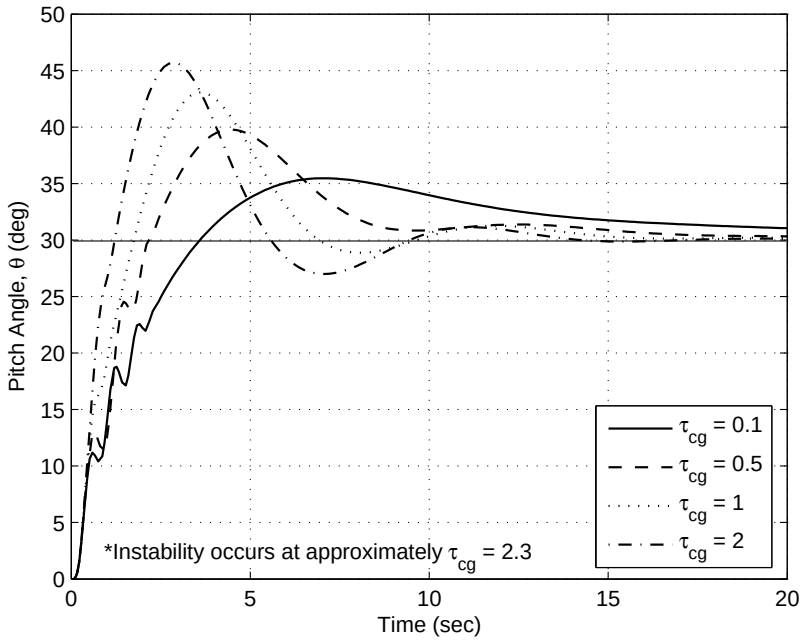



Figure 5.7: Configuration Change from Loiter to Dash While Maneuvering

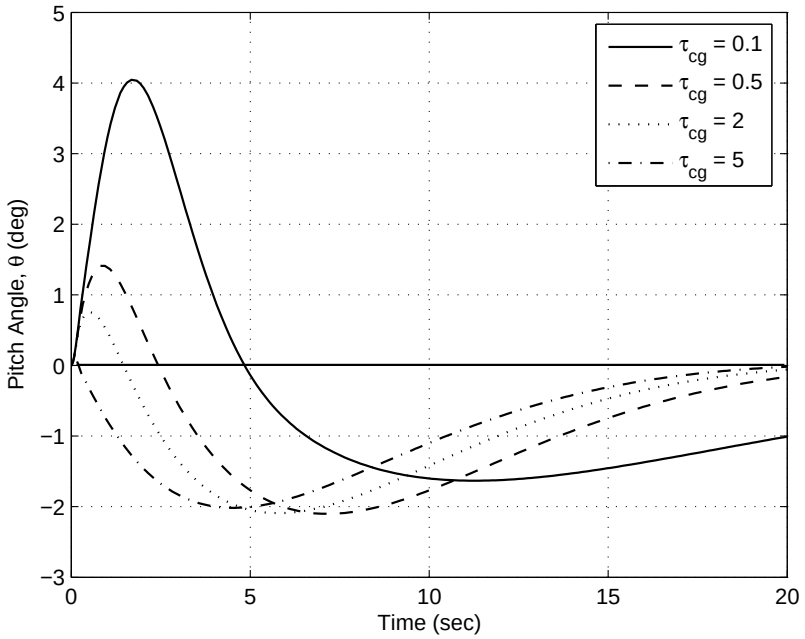



Figure 5.8: Configuration Change from Dash to Loiter Using Gain Scheduled Compensator; The Results Demonstrate the Effects of Transition Rate

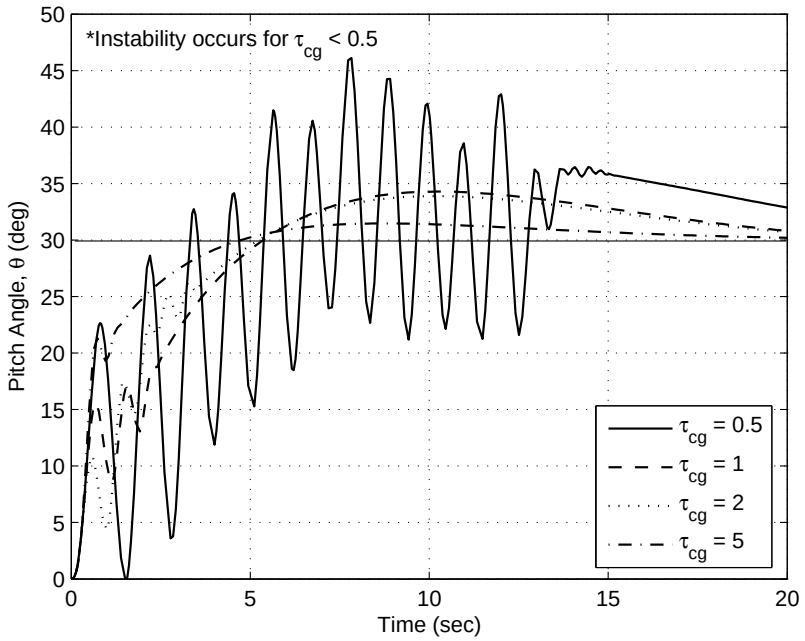



Figure 5.9: Configuration Change from Dash to Loiter While Maneuvering

## 5.3 Nonlinear Navigation Control

Linear control methods are used in the overwhelming majority of aircraft flight control systems. This is due to the vast amount of knowledge available in the field of linear system theory. Linear control methods, however, are all built upon the assumption that the dynamic model behaves linearly within some perturbation of a stationary point–there is also the underlying assumption that the system is indeed linearizable. Once the bounds of this perturbation are exceeded, the dynamic system is likely to behave poorly or even possibly be unstable. Therefore, the design of a flight control system will necessarily require the design of multiple controllers, one for each operating region. For a morphing aircraft, the complexity is compounded since a flight control law must be designed for each operating region and for each planform configuration.

In this section, some alternative concepts are discussed. Particularly, nonlinear methods of flight control are investigated as a means of overcoming some of the restrictions of linear systems. Nonlinear control design relies on Lyapunov's second method in which a Lyapunov function is used to derive a stabilizing control law. In general, finding the required Lyapunov function is a non-trivial task. One way of getting around this problem is to employ a method of differential geometry termed *feedback linearization* in which the dynamical equations are placed in a form where finding the required Lyapunov function is trivial.

In the following sections feedback linearization is presented as a candidate method for controlling the motions of a variable planform aircraft. Unfortunately, the robustness properties of this control design are shown to be less than adequate. The main focus of this section will be to investigate the possible benefits of variable span morphing for maneuvering control.

### Bank-to-Turn Flight

The necessity of BTT guidance is due to the air-breathing propulsion system that requires direct access to the relative wind motion for power. There are two major aspects that must be addressed in designing an autopilot system for bank-to-turn (BTT) aircraft. The first involves the inherent nonlinearities involved in flight dynamics. That is, there exists a significant cross-coupling of the rotational dynamics whose effect is especially influential for BTT aircraft due to the high roll rates required for achieving high performance. As opposed to skid-to-turn guidance where the acceleration commands are in the form of a yaw and

pitch angle, BTT guidance commands are ultimately given as a roll angle and and pitch acceleration. The difference in these guidance schemes stems from the associated propulsion system involved. For an air-breathing propulsion system, the angle between the total velocity vector and the longitudinal axis (i.e., the sideslip angle $\beta$) of the aircraft must be kept small to ensure proper air intake–this is the second aspect of importance. STT guidance is not sufficient for meeting such requirements and hence the development of BTT guidance and control has been a significant topic of research.

One method for dealing with the nonlinearities that has been studied as applied to missile guidance is to treat the roll rate as a constant at each instant in time. This is termed as an *adiabatic approximation* by Williams and Friedland [124] and in their work, the familiar method of gain scheduling is implemented. The missile dynamics are linearized at multiple operating points and optimal linear techniques are used to schedule the control gains as a function of dynamic pressure.

The commands for BTT guidance come from navigation commands in the form of body-axis accelerations. The target location is modeled as a point mass and is located with respect to $\mathcal{F}^0$ by the vector $\boldsymbol{r}_T^0 \in \mathcal{F}^0$, and with respect to $\mathcal{F}^1$ by $\boldsymbol{r}_{T,M}^1 \in \mathcal{F}^1$ with the relationship

$$\boldsymbol{r}_T^0 = \boldsymbol{b}^{01} + \mathbf{A}^{10}\boldsymbol{r}_{T,M}^1 \tag{5.15}$$

The relative velocity between the aircraft and target is

$$\dot{\boldsymbol{r}}_{T,M}^1 = \dot{\boldsymbol{r}}_T^0 - \boldsymbol{v}^1 + \tilde{\boldsymbol{r}}_{T,M}^1\boldsymbol{\omega}^{10} \tag{5.16}$$

The guidance scheme used in subsequent simulations is the classical proportional navigation. Mathematically, the guidance law known as *proportional navigation* is stated as

$$\boldsymbol{a}_c^1 = NV_c\dot{\lambda} \tag{5.17}$$

where $\boldsymbol{a}_c^1$ is the acceleration command, $N$ is the effective navigation ratio, $V_c$ is the closing velocity and $\lambda$ is the line of sight angle [125]. It can be shown that this guidance law can be reduced into acceleration commands in $\mathcal{F}^1$ [125]. The acceleration commands are given as

$$\mathbf{a}_c^1 = \frac{\boldsymbol{r}_{T,M}^1 + (\dot{\boldsymbol{r}}_{T,M}^1)t_{go}}{t_{go}^2} \tag{5.18}$$

where $t_{go}$ is time-to-go until intercept and is defined as

$$t_{go} = \frac{|\boldsymbol{r}^1_{T,M}|}{V_c} \tag{5.19}$$

Referring to Fig. (5.10) the roll angle error is determined as

$$\phi_e = \tan^{-1}(\boldsymbol{a}^1_c \cdot \mathbf{e}^1_y / \boldsymbol{a}^1_c \cdot \mathbf{e}^1_z) \tag{5.20}$$

The roll angle command can then be calculated by

$$\phi_c = \phi + \phi_e \tag{5.21}$$

The angle of attack is limited to positive values thus requiring a 180 degree roll angle to perform a pitch-down maneuver. Therefore, the angle of attack command is given as

$$\alpha_c = K_\alpha \sqrt{(\boldsymbol{a}^1_c \cdot \mathbf{e}^1_y)^2 + \boldsymbol{a}^1_c \cdot \mathbf{e}^1_z} \tag{5.22}$$

where $K_\alpha$ is a control gain. Qualitatively, Equations (5.21) and (5.22) state that the direction of acceleration is determined by $\phi_c$ and the acceleration magnitude by $\alpha_c$. Here it is assumed that the acceleration is proportional to the angle of attack; it is actually proportional to $\dot{\alpha}$. Angle of attack tracking will be shown as an adequate method.

## Input-Output Linearization

In this section, we consider a complete dynamic model and attempt to control only a subset the state vector via linearization; this process known as *input-output linearization* or sometimes *input-output decoupling*. The development that follows may be found in many references, some of these are [126, 127, 123, 128], for example.

To begin, it is assumed that the dynamics of interest can be expressed as a nonlinear, time-

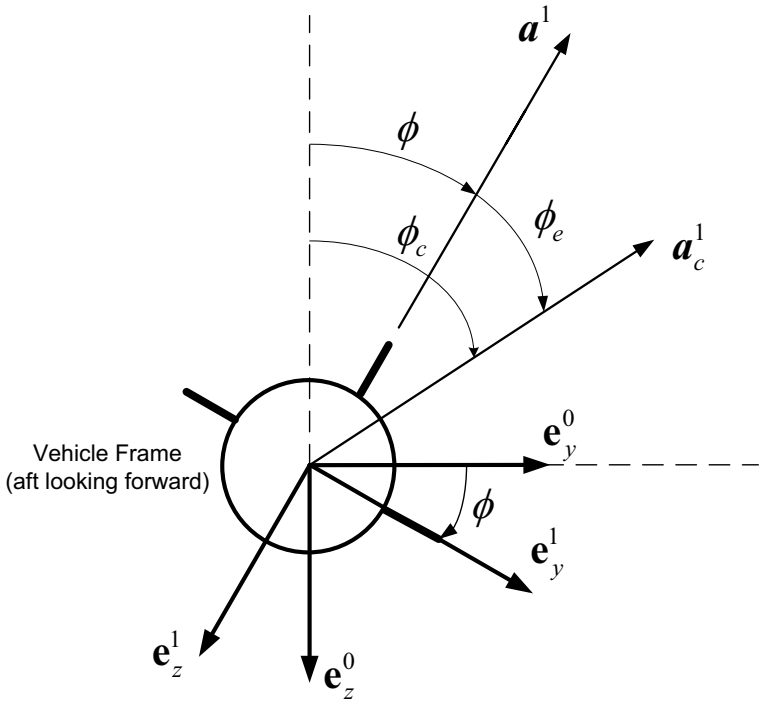



Figure 5.10: Geometry of Bank-to-turn Guidance

invariant, multi-input, multi-output square system of the general form

$$\begin{aligned} \dot{\boldsymbol{x}} &= \boldsymbol{f}(\boldsymbol{x}) + \Delta\boldsymbol{f}(\boldsymbol{x}) + \sum_{k=1}^{m}[\boldsymbol{g}_k(\boldsymbol{x}) + \Delta\boldsymbol{g}_k(\boldsymbol{x})]u_k \\ &= \boldsymbol{f}(\boldsymbol{x}) + \Delta\boldsymbol{f}(\boldsymbol{x}) + [\mathbf{G}(\boldsymbol{x}) + \Delta\mathbf{G}(\boldsymbol{x})]\boldsymbol{u} \\ \boldsymbol{y} &= \boldsymbol{h}(\boldsymbol{x}) \end{aligned} \tag{5.23}$$

where $\boldsymbol{x} \in \mathbb{R}^n$, $\boldsymbol{y} \in \mathbb{R}^p$, and $\boldsymbol{u} \in \mathbb{R}^m$. The terms $\Delta\boldsymbol{f}(\boldsymbol{x})$ and $\Delta\mathbf{G}(\boldsymbol{x})$ account for model uncertainty. Note that when $\Delta\boldsymbol{f}(\boldsymbol{x}) \neq 0$ the so-called *matching condition* is not satisfied. That is, the uncertain terms are not directly attached to the control inputs. This will be a topic of interest in later discussion.

The nominal dynamics are taken to be those of Eq. 5.23 where $\Delta\boldsymbol{f}(\boldsymbol{x}) = \mathbf{0}$ and $\Delta\mathbf{G} = \mathbb{0}$. The nominal system can be input-output decoupled provided that

- $p = m$,

- there exists finite non-negative integers $r_1, ..., r_m$ such that

$$\begin{cases} L_{g_i} L_f^{k-1} h_i(\boldsymbol{x}) = 0, & k = 1, ..., r_i, \\ L_{g_i} L_f^{r_i} h_i(\boldsymbol{x}) \neq 0, & i = 1, ..., m \end{cases}$$

The second condition states that $y$ has *vector relative degree* $r = \sum r_i \leq n$. Note that if $r = n$, then the system can be fully decoupled. Taking the $\rho_j$-th derivative of the $j$-th output of $y_j$ with respect to time results in

$$y_j^{\rho_j} = L_f^{\rho_j} h_j + \sum_{i=1}^{m} (L_{g_i} L_f^{\rho_j - 1} h_j) u_i \tag{5.24}$$

where, in general

$$L_f \boldsymbol{h}(\boldsymbol{x}) = \frac{\partial \boldsymbol{h}}{\partial \boldsymbol{x}} \boldsymbol{f}(\boldsymbol{x})$$

is the Lie Derivative of the function $\boldsymbol{h}(\boldsymbol{x})$ along the smooth vector field $\boldsymbol{f}(\boldsymbol{x})$. The vector relative degree $r_j$ of $y_j$ is the derivative order $\rho_j$ for which $\sum_{i=1}^{m} (L_{g_i} L_f^{\rho_j - 1} h_j) u_i \neq 0$. From the previous conditions, if the total relative degree $r = \sum_{j=1}^{m} r_j \leq n$, then the output state equation can be constructed as

$$\begin{bmatrix} y_1^{(r_1)} \\ \vdots \\ y_m^{(r_m)} \end{bmatrix} = \begin{bmatrix} L_f^{r_1} h_1 \\ \vdots \\ L_f^{r_m} h_m \end{bmatrix} + \begin{bmatrix} L_{g_1} L_f^{r_1 - 1} h_1 & \cdots & L_{g_m} L_f^{r_1 - 1} h_1 \\ \vdots & \ddots & \vdots \\ L_{g_1} L_f^{r_m - 1} h_m & \cdots & L_{g_m} L_g^{r_m - 1} h_m \end{bmatrix} \begin{bmatrix} u_1 \\ \vdots \\ u_m \end{bmatrix} \tag{5.25}$$

The input-output decoupled system is obtained by defining the control law

$$\begin{bmatrix} u_1 \\ \vdots \\ u_m \end{bmatrix} = - \begin{bmatrix} L_{g_1} L_f^{r_1 - 1} h_1 & \cdots & L_{g_m} L_f^{r_1 - 1} h_1 \\ \vdots & \ddots & \vdots \\ L_{g_1} L_f^{r_m - 1} h_m & \cdots & L_{g_m} L_g^{r_m - 1} h_m \end{bmatrix}^{-1} \left( \begin{bmatrix} L_f^{r_1} h_1 \\ \vdots \\ L_f^{r_m} h_m \end{bmatrix} - \begin{bmatrix} v_i \\ \vdots \\ v_m \end{bmatrix} \right) \tag{5.26}$$

so that

$$\begin{bmatrix} y_1^{(r_1)} \\ \vdots \\ y_m^{(r_m)} \end{bmatrix} = \begin{bmatrix} v_i \\ \vdots \\ v_m \end{bmatrix} \tag{5.27}$$

The dynamics are then defined by the new inputs $v_i$ which may be chosen in any convenient manner.

A complete dynamical description may be presented by assuming the existence of a smoothly differentiable map (i.e., a *diffeomorphism*), $\boldsymbol{T}(\cdot) : \mathbb{R}^n \rightarrow \mathbb{R}^n$ such that

$$\nabla \boldsymbol{T}(\boldsymbol{x})\mathbf{G}(\boldsymbol{x}) = \mathbb{0}$$

where $\nabla \boldsymbol{T}(\boldsymbol{x})$ denotes the gradient of $\boldsymbol{T}(\boldsymbol{x})$–the conditions under which such a diffeomorphism exists can be found in the literature [123, 126]. Given the change of coordinates

$$\left[ \begin{array}{c} \boldsymbol{\eta} \\ \boldsymbol{\xi} \end{array} \right] = \boldsymbol{T}(\boldsymbol{x}), \quad \boldsymbol{\eta} \in \mathbb{R}^{n-m},\ \boldsymbol{\xi} \in \mathbb{R}^m$$

where

$$\begin{aligned} \boldsymbol{\eta} &= \left[ \begin{array}{ccc} T_1(\boldsymbol{x}) & \cdots & T_{n-r}(\boldsymbol{x}) \end{array} \right]^T \\ \boldsymbol{\xi} &= \left[ \begin{array}{ccccccc} h_1 & \cdots & L_f^{r_1-1}h_1 & \cdots & h_m & \cdots & L_f^{r_m-1}h_m \end{array} \right]^T \\ &= \left[ \begin{array}{ccccccc} y_1 & \cdots & y_1^{r_1-1} & \cdots & y_m & \cdots & y_m^{r_m-1} \end{array} \right]^T \end{aligned}$$

With this coordinate change the dynamics of Eq. (5.23) are transformed into the system of Eq. (5.25) plus the system

$$\dot{\boldsymbol{\eta}} = \boldsymbol{f}_0(\boldsymbol{\eta}, \boldsymbol{\xi}) \tag{5.28}$$

Equation (5.28) represents the internal dynamics the system which are unobservable from the output $\boldsymbol{y}(t)$. Evaluated at the stationary point $\boldsymbol{\xi} = \boldsymbol{\xi}_0$ this becomes

$$\dot{\boldsymbol{\eta}} = \boldsymbol{f}_0(\boldsymbol{\eta}, \boldsymbol{\xi}_0) \tag{5.29}$$

which are the *zero dynamics* of the system. The system is *minimum phase* if the origin the zero dynamics are asymptotically stable–this ensures that $\boldsymbol{\eta}(t)$ will be bounded for all possible $\boldsymbol{y}(t)$ and all intitial conditions $\boldsymbol{\eta}(\mathbf{0})$.

The method of feedback linearization, as applied to missile systems, has been previously suggested by [73, 129, 130, 131, 132]–first derived about 20 years before the author's discovery–

and some of the derivation that follows is included in these works. In applying input-output linearization to control the BTT aircraft previous section, the state vector is defined as

$$\boldsymbol{x} = \begin{bmatrix} \phi & \theta & \psi & \alpha & \beta & P & Q & R \end{bmatrix}^T \tag{5.30}$$

and the input vector is defined as $\mathbf{u} = (\delta_r, \delta_e, \delta_a)^T$. Assuming a principle axis, the equations of motion may be expressed as

$$\boldsymbol{f}(\boldsymbol{x}) = \begin{bmatrix} P + Q\sin\phi\tan\theta + R\cos\phi\tan\theta \\ Q\cos\phi - R\sin\phi \\ Q\sin\phi\sec\theta + R\cos\phi\sec\theta \\ \frac{Z_\alpha}{V_T}\alpha + g_{zw} + Q - P\beta \\ \frac{Y_\beta}{V_T}\beta + g_{yw} + P\alpha - R \\ L_pP + L_rR + L_\beta\beta \\ I_qPR + M_\alpha\alpha + M_qQ \\ I_rPQ + N_pP + N_rR + N_\beta\beta \end{bmatrix} \tag{5.31}$$

and

$$\mathbf{G} = \begin{bmatrix} 0 & 0 & 0 & 0 & Y_{\delta_r}/V_T & 0 & 0 & N_{\delta_r} \\ 0 & 0 & 0 & Z_{\delta_e}/V_T & 0 & 0 & M_{\delta_e} & 0 \\ 0 & 0 & 0 & 0 & 0 & L_{\delta_a} & 0 & N_{\delta_a} \end{bmatrix}^T \tag{5.32}$$

The principle axis assumption is not a required assumption and is employed for simplicity. The output state vector is chosen to be

$$\boldsymbol{y} = \boldsymbol{h}(\boldsymbol{x}) = [\phi, \alpha, \beta]^T \tag{5.33}$$

Differentiating the outputs defined by Eqn. (5.33) according to Eqn. (5.24) we find that

$$\begin{aligned} \dot{y_1} &= \dot{\phi} \\ \dot{y_2} &= \dot{\alpha} \\ \dot{y_3} &= \dot{\beta} \end{aligned} \tag{5.34}$$

where it is apparent that $r_2 = r_3 = 1$. To determine the total relative degree the output

$h_1(\boldsymbol{x})$ is differentiated once again

$$\begin{aligned} \ddot{y}_1 &= L_f^2 h_1 + (N_{\delta_r} \cos\phi \tan\theta)\delta_r + (M_{\delta_e} \sin\phi \tan\theta)\delta_e \\ &+ (L_{\delta_a} + N_{\delta_w} \cos\phi \tan\theta)\delta_a \end{aligned} \tag{5.35}$$

In Eqn. (5.35) an input appears in the second derivative of $h_1(\boldsymbol{x})$ and therefore $y_1$ has vector relative degree $r_1 = 2$. The system has total relative degree $r = 4$, and therefore meets the first requirement for I/O linearization. The second requirement comes from constructing the output state equation. Referring to Eq. (5.25) we have

$$\mathbf{A}(\boldsymbol{x}) = \begin{bmatrix} L_f^2 h_1 \\ \frac{Z_\alpha}{V_T}\alpha + Q - P\beta + \frac{g_{zw}}{V_T} \\ \frac{Y_\beta}{V_T}\beta + P\alpha - R + \frac{g_{yw}}{V_T} \end{bmatrix} \tag{5.36}$$

and

$$\mathbf{B}(\boldsymbol{x}) = \begin{bmatrix} N_{\delta_r} c\phi\ t\theta & M_{\delta_e} s\phi\ t\theta & L_{\delta_a} + N_{\delta_a} c\phi\ t\theta \\ 0 & Z_{\delta_e}/V_T & 0 \\ Y_{\delta_r}/V_T & 0 & 0 \end{bmatrix} \tag{5.37}$$

The matrix $\mathbf{B}(\boldsymbol{x})$ is well-defined and nonsingular for all $\theta \in (-\frac{\pi}{2}, \frac{\pi}{2})$, which is also a stipulation for the inversion of $\mathbf{A}^{01}$ when implementing the 3-2-1 Euler angle representation. The input-output linearized equations of motion are

$$\begin{bmatrix} \ddot{\phi} & \dot{\alpha} & \dot{\beta} \end{bmatrix}^T = \mathbf{A}(\boldsymbol{x}) + \mathbf{B}(\boldsymbol{x})\boldsymbol{u} \tag{5.38}$$

We can then define the state control feedback law as

$$\mathbf{u} = -\mathbf{B}^{-1}(\boldsymbol{x})\mathbf{A}(\boldsymbol{x}) + \mathbf{B}^{-1}(\boldsymbol{x})\boldsymbol{v} \tag{5.39}$$

resulting in the linear system

$$\begin{bmatrix} \ddot{\phi} & \dot{\alpha} & \dot{\beta} \end{bmatrix}^T = \boldsymbol{v} \tag{5.40}$$

The input to this linear system is then chosen to be

$$\boldsymbol{v} = \begin{bmatrix} \ddot{\phi}_c - K_{\phi_1}(\dot{\phi} - \dot{\phi}_c) - K_{\phi_2}(\phi - \phi_c) \\ \dot{\alpha}_c - K_\alpha(\alpha - \alpha_c) \\ \dot{\beta}_c - K_\beta(\beta - \beta_c) \end{bmatrix} \tag{5.41}$$

where the $K$ values are control gains and $\phi_c$, $\alpha_c$, and $\beta_c$ are the commanded state values. Note that $\boldsymbol{v}$ may be defined in any manner and can be cast in the form of, for example, optimal control or robust control. For simplicity we consider solely the PD control. Substituting (5.41) into (5.40) gives the linear system

$$\begin{aligned} \ddot{\phi}_e + K_{\phi_1}\dot{\phi}_e + K_{\phi_2}\phi_e &= 0 \\ \dot{\alpha}_e + K_\alpha \alpha_e &= 0 \\ \dot{\beta}_e + K_\beta \beta_e &= 0 \end{aligned} \tag{5.42}$$

where the $e$ subscript denotes the signal error. Note that for every $K > 0$ the error is assured to converge to zero.

There are three actuators that control the 3 desired state trajectories. The actuator blending is defined as follows:

$$\begin{aligned} \delta_r &= \delta_1 \\ \delta_a &= \delta_2 + \delta_3 \\ \delta_e &= -\delta_2 + \delta_3 \end{aligned} \tag{5.43}$$

where $\delta_1$ is the vertical tail fin, $\delta_2$ is the right tail fin (aft looking forward), and $\delta_3$ is the left tail fin.

To demonstrate the effectiveness of the ($\phi,\ \alpha,\ \beta$) controller, numerical simulations of the nominal dynamics were constructed using the Maneuver planform design described in Chapter 4 (see Fig. (4.2))–the complete aerodynamic data tables are given in Appendix B. The aircraft is considered to be tail-controlled with all-moving vertical and horizontal fins. As before, actuator constraints were imposed in the form of both rate and saturation limits. Fixed input tracking control is demonstrated in Fig. (5.11). Using proportional guidance, a fixed spatial command is tracked to within a small distance as shown by Fig. (5.13). The time-varying input commands and the resulting aircraft orientation associated with this

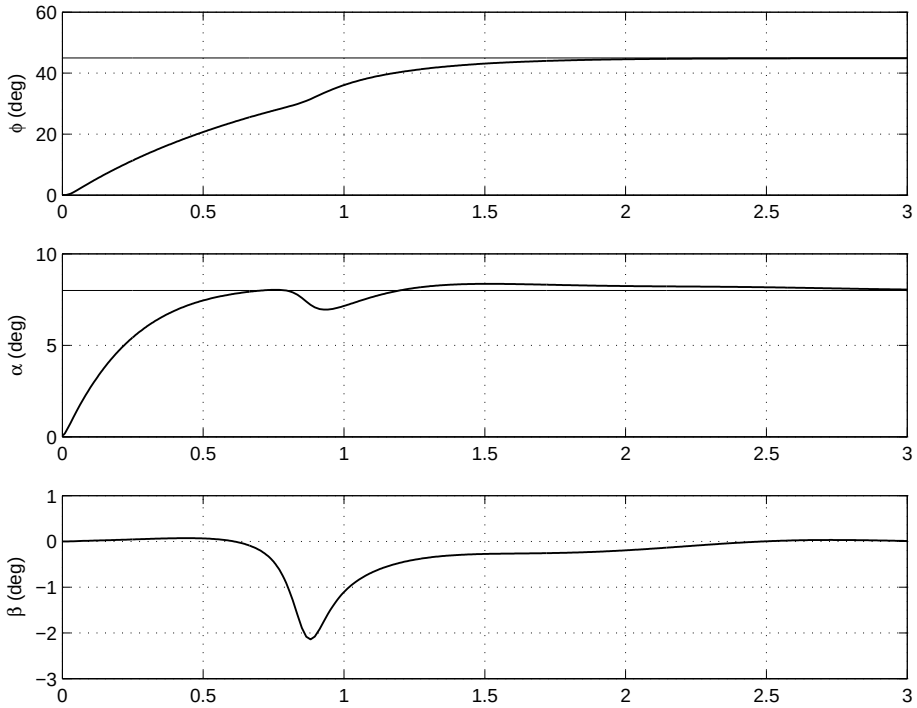



Figure 5.11: Nominal I/O Linearization Control Tracking Stationary Commands

simulation are shown in Fig. (5.13).

## Variable Span Roll Control

The nonlinear controller presented in the previous section is implemented here to evaluate the flight performance improvements of variable span morphing. Again considering the maneuver planform, we implement the existing design with wings that are capable of extending asymmetrically up to 10% of the half span length. As discussed in Chapter 4, the wings are considered to be coupled such that an extension of one wing results in a retraction of the other. The coupled deflection is given by the input ratio $\delta_{y_e}$. With the tail control fins there are a total of 4 actuators controlling only 3 states. The actuator blending of Eq. (5.43) is now not so easily expressed. Furthermore, the input-output linearization design was developed under the assumption of a square system. Consider the yawing and rolling moments

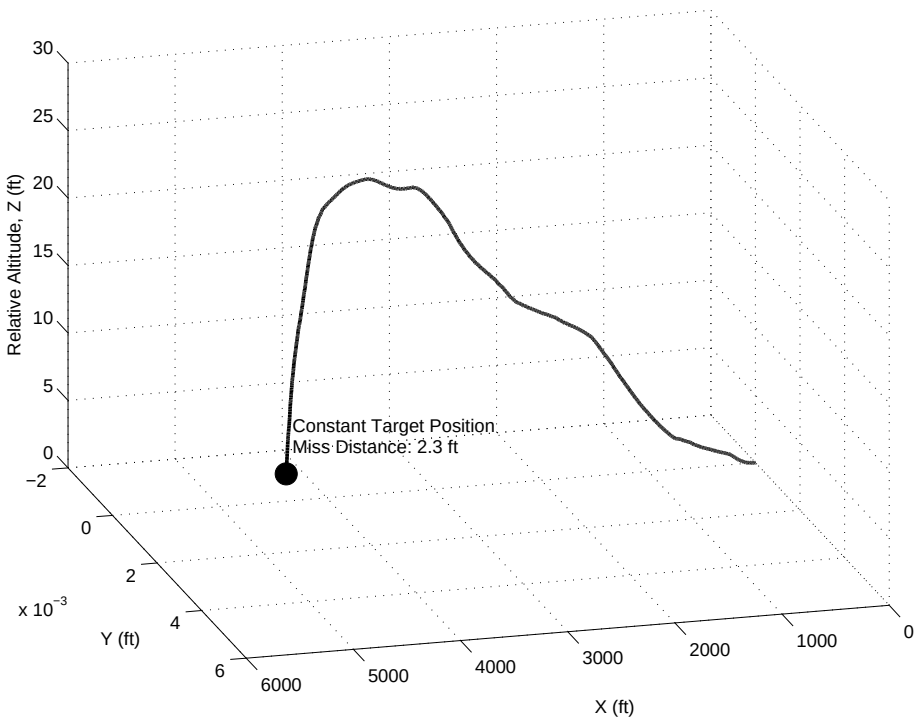



Figure 5.12: Set-Point Guidance with Nominal I/O Linearization Control

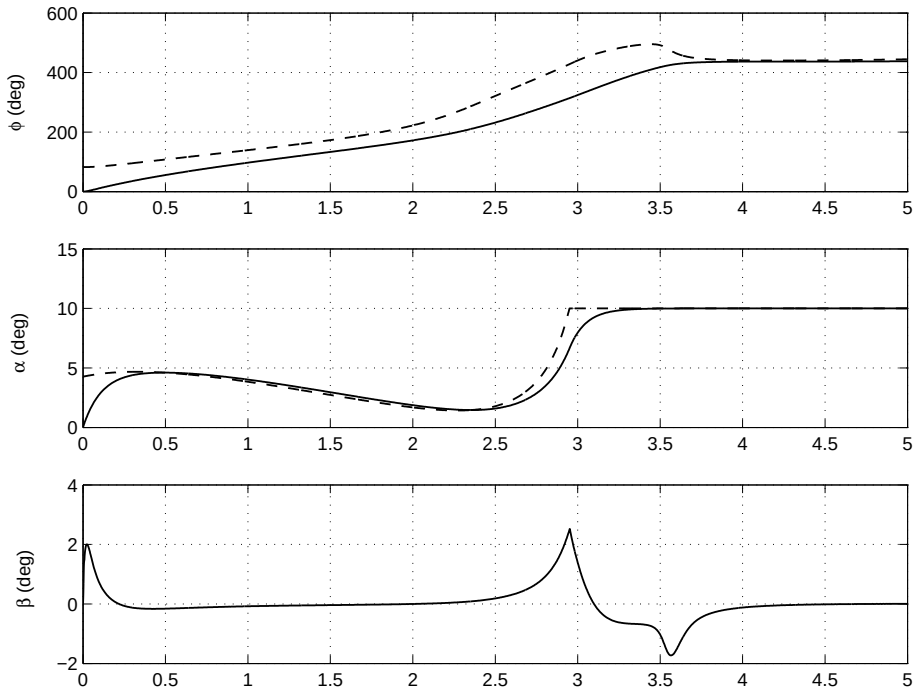



Figure 5.13: Nominal I/O Linearization Control Tracking Time-Varying Commands from Guidance System

due to actuation where the aileron-like controls are displayed;

$$L_{\delta_a}\delta_a \quad + \quad L_{\delta_{y_e}}\delta_{y_e} = L_{\delta_a}(\delta_2+\delta_3) + L_{\delta_{y_e}}\delta_4 \tag{5.44}$$

$$N_{\delta_a}\delta_a \quad + \quad N_{\delta_{y_e}}\delta_{y_e} = N_{\delta_a}(\delta_2+\delta_3) + N_{\delta_{y_e}}\delta_4 \tag{5.45}$$

It is apparent that $\delta_a \neq (\delta_2+\delta_3+\delta_4)$ which would be required for a square system. To proceed define $\delta_4^1 = (L_{\delta_4}/L_{\delta_a})\delta_4$ and $\delta_4^2 = (N_{\delta_4}/N_{\delta_a})\delta_4$ so that

$$\begin{aligned} L_{\delta_a}\delta_a \quad &+ \quad L_{\delta_a}(\delta_2+\delta_3+\delta_4^1) \\ N_{\delta_a}\delta_a \quad &+ \quad N_{\delta_a}(\delta_2+\delta_3+\delta_4^2) \end{aligned} \tag{5.46}$$

Noting that the yawing moment due to small aileron extension can be considered negligible in comparison with the fin deflections (i.e., $N_{\delta_{y_e}} = 0$), the aileron input can be defined as $\delta_a = (\delta_2+\delta_3+\delta_4^1+\delta_4^2)$. Both $\delta_e$ and $\delta_r$ are as previously defined and the system is once again square. Now, however, determining the actuator commands is a non-unique (non-invertible) problem given by

$$\begin{bmatrix} \delta_a \\ \delta_e \\ \delta_r \end{bmatrix} = \begin{bmatrix} 0 & 1 & 1 & 1 \\ 0 & -1 & 1 & 0 \\ 1 & 0 & 0 & 0 \end{bmatrix} \begin{bmatrix} \delta_1 \\ \delta_2 \\ \delta_3 \\ \delta_4^1 \end{bmatrix} \tag{5.47}$$

This dilemma is referred to a the *control allocation* problem [133, 134]. To solve this problem we consider an optimal approach. Let $\boldsymbol{\delta} = (\delta_1,\ \delta_2,\ \delta_3, \delta_4^1)$ and the dynamics associated with these actuators be described by the first-order system

$$\begin{aligned} \dot{\boldsymbol{\delta}} &= \mathbf{A}_\delta\boldsymbol{\delta} + \mathbf{G}_\delta\boldsymbol{u}_\delta \\ \boldsymbol{y}_\delta &= \mathbf{C}\boldsymbol{\delta} \end{aligned} \tag{5.48}$$

where $\mathbf{A}_\delta$ and $\mathbf{G}_\delta$ are diagonal matrices containing the actuator time constants. The span extension is given a rate limit of 0.2 seconds; in comparison, the tail controls were given a 0.0495 second time constant.

The method of inversion is only slightly different in that we assume modal control; that is,

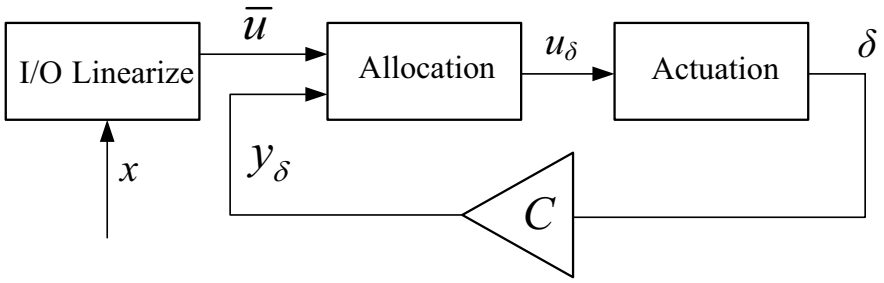



Figure 5.14: Optimal Allocation Scheme

$\bar{\boldsymbol{u}} \triangleq \mathbf{B}\boldsymbol{u}$ and define the linearizing control law

$$\bar{\boldsymbol{u}} = -\mathbf{A}(\boldsymbol{x}) + \boldsymbol{v} \tag{5.49}$$

The control inputs are then determined by minimizing the cost function

$$J = \int_0^{t_f} (\boldsymbol{e}_I \cdot \boldsymbol{e}_I + \boldsymbol{u}_\delta^T \mathbf{R} \boldsymbol{u}_\delta) dt \tag{5.50}$$

subject to the previously defined actuator state equations where

$$\dot{\boldsymbol{e}}_I = \bar{\boldsymbol{u}} - \boldsymbol{y}_\delta = \bar{\boldsymbol{u}} - \mathbf{C}\boldsymbol{u}_\delta \tag{5.51}$$

is the error between the desired and actual modal force vector. This is the standard *linear quadratic regulator* problem (LQR) and allows for consideration of the varying time constants associated with the individual actuators.

Before continuing, it was previously stated that $\mathbf{B}$ of Eq. (5.37) is invertible for all suitable values of $\theta$. The assumption with this statement was that $L_{\delta_a}$ is a constant value. If the value is zero, then invertibility can not be assumed. For less than zero angles of attack the lift of an aircraft wing goes to a zero value; for a un-cambered wing this this angle of attack value is zero. This means that the the differential lift (i.e., the rolling moment) created by one wing compared to another becomes negligible at small angles of attack. This is also true for a tail fins at high angles of attack where the control authority reduces drastically.

Referring to Fig. (5.19), a comparison is shown for the maneuvering performance for the conventional and variable span aircraft configurations. For this simulation a random excitation applied to the aerodynamic coefficients was applied with a maximum of 5% error. In

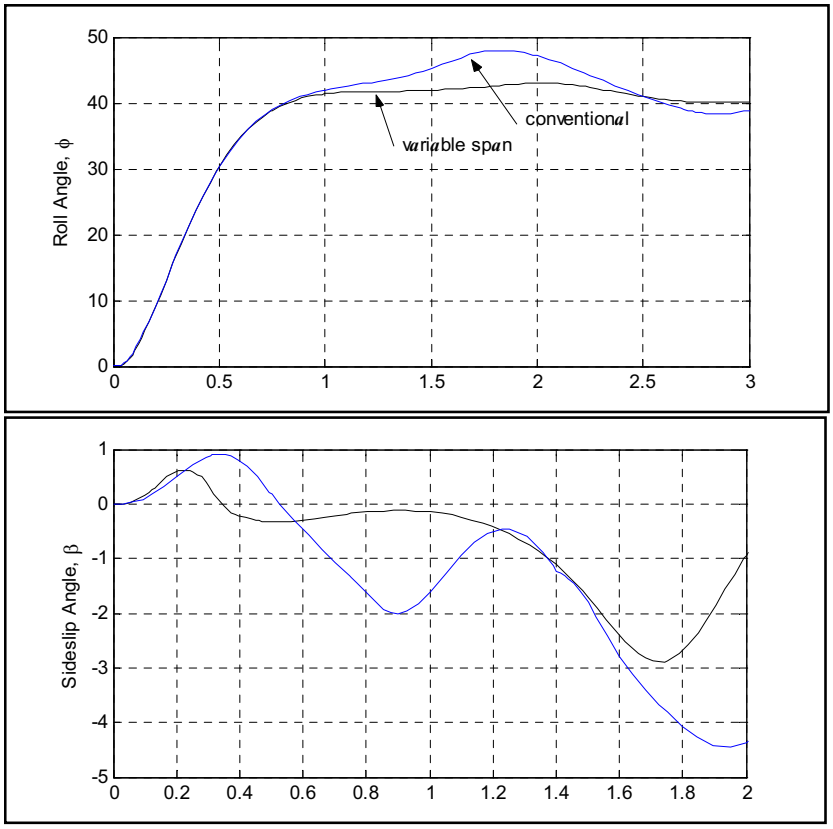



Figure 5.15: Comparison of Variable Span Control and Conventionally Actuated Designs Simulated 5% Error Applied to the Aerodynamic Coefficients

Fig. (5.19) the error was increased to 10%. The angle of attack tracking for both cases was approximately equivalent and thus is not shown.

We now implement the proportional navigation as before to track a fixed-point spatial reference. In Fig. (5.17), the conventional design is subjected to commanded inputs from the guidance system. Given the same conditions Fig. (5.18) demonstrates the improved performance of the variable span design. The ultimate result is demonstrated by Fig. (5.19) in which both designs are subjected to the same guidance location.

## Discussion

In applying the input-output control design it was assumed that the zero dynamics of the system are stable. In many cases this assumption is necessary due to nonlinearity of the resulting equations. Furthermore, determining the required diffeomorphism is often non-trivial. Lin-

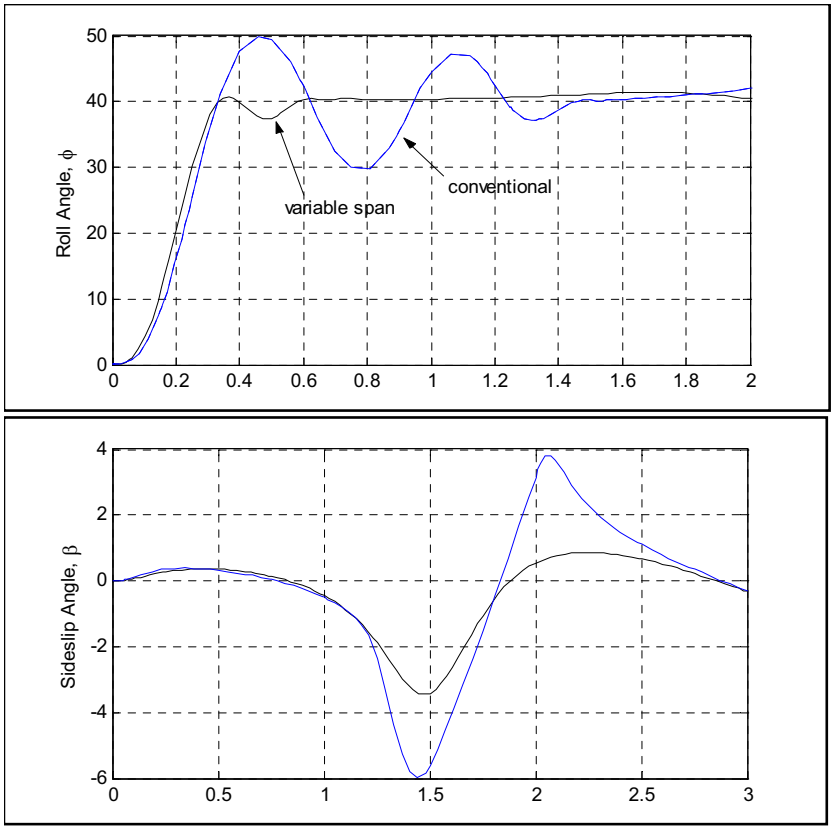



Figure 5.16: Comparison of Variable Span Control and Conventionally Actuated Designs Simulated 10% Error Applied to the Aerodynamic Coefficients

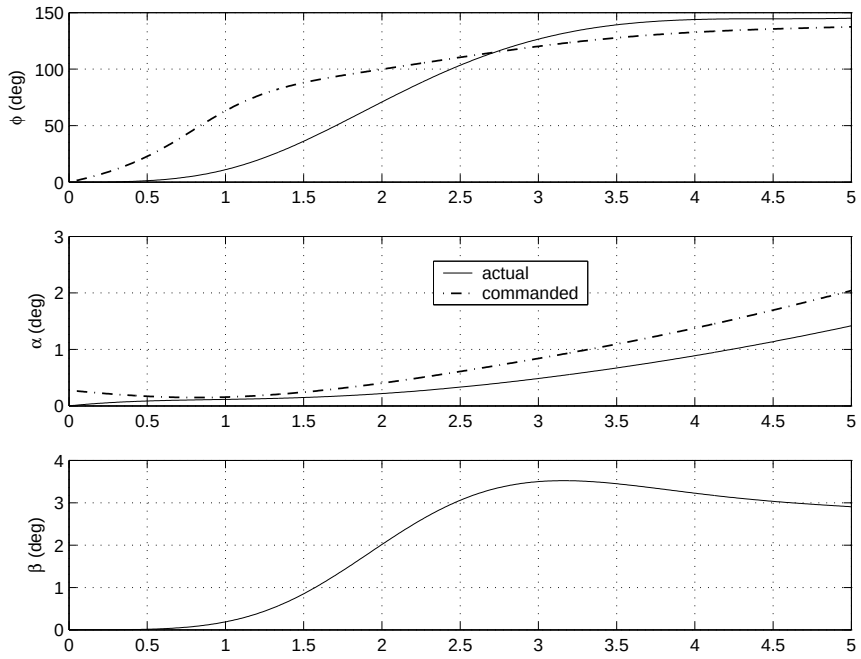



Figure 5.17: Conventional Aircraft Design Tracking ($\phi,\ \alpha\ \beta$) Commands from Proportional Navigation

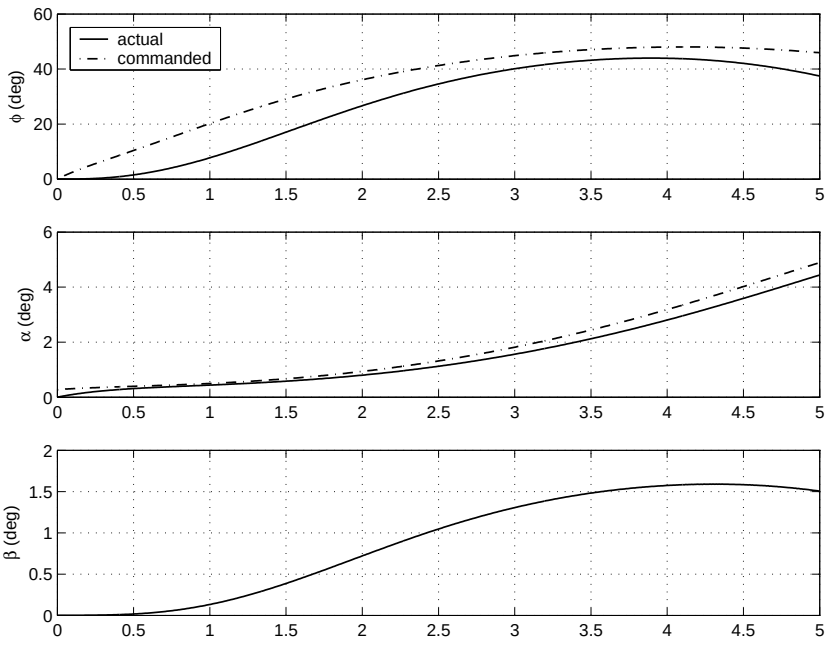



Figure 5.18: Variable Span Aircraft Design Tracking ($\phi,\ \alpha\ \beta$) Commands from Proportional Navigation

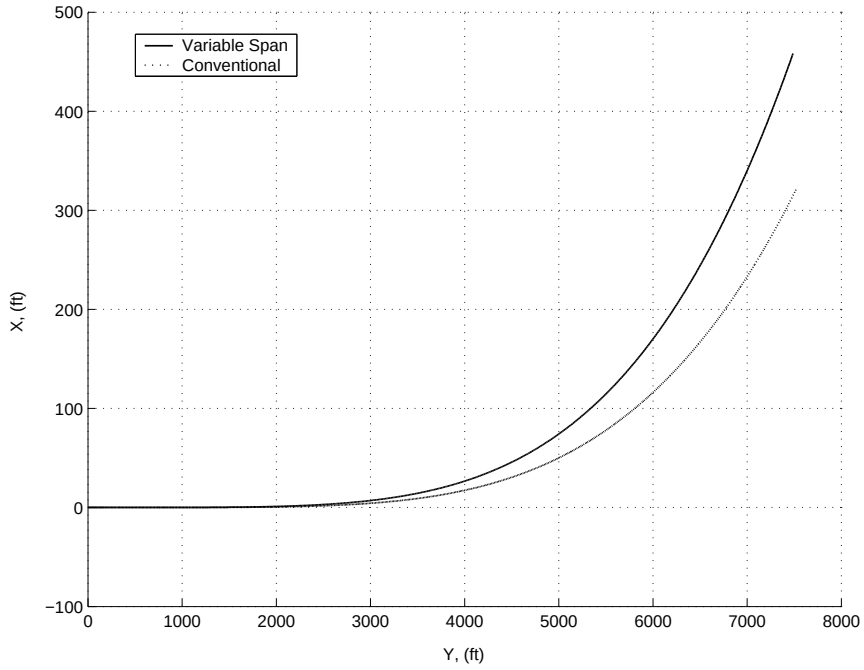



Figure 5.19: X-Y Spacial Position of Aircraft Subjected to Proportional Navigation Tracking Commands

earization and numerical simulations are both methods of investigating the stability of the zero dynamics. Also, it was noted that the dynamic equations do not satisfy the matching condition, which stipulates that parametric uncertainty in the model appears at the same order of differentiation as the control input. There are several methods of guaranteed stability given that the system meets the matching condition. For an ideal case, when the physical model is in controller canonical form, robust techniques such as as sliding mode control can be easily implemented. Methods such as the *Lyapunov redesign* attempt to add additional control input to the system based on bounds of the matched error. Matching conditions have been relaxed for certain limited classes of systems. Of particular interest, Qu and Dawson demonstrated robust linearization given a system that does not meet the matching condition, but can be represented as a cascaded system where each subsystem individually satisfies the condition [127]. The current system does not fall under any of these requirements.

Although used solely for the purpose of investigating control morphing, given the desirable attributes of the ($\phi,\ \alpha,\ \beta$) nominal control design presented in the previous section, a means of providing robustness would be beneficial. As a final topic of discussion, we consider augmenting the I/O linearization control design with variable structure control.

Consider the nonlinear nonautonomous system of the form

$$\dot{\boldsymbol{z}} = \boldsymbol{f}(\boldsymbol{z}, t) + \boldsymbol{v} \tag{5.52}$$

where $\boldsymbol{z}$ is the state vector, $\boldsymbol{f}(\cdot)$ is an unknown function and $\boldsymbol{v}$ is the control input. The dynamical system given by Eq. (5.52) corresponds to Eq. (5.40) when dynamics have not been canceled completely due considering only the nominal system of Eq. (5.23). Letting $\boldsymbol{z}_e = \boldsymbol{z}_e - \boldsymbol{z}_d$ be the error vector we define the sliding surface $s = \boldsymbol{\Lambda} \cdot \boldsymbol{z}_e$ where $\boldsymbol{\Lambda}$ is a vector whose components are contained in the expression

$$s = (d/dt + \lambda)\boldsymbol{z}_e \tag{5.53}$$

where $\lambda$ is a positive constant. Suppose that the control input is selected as

$$\boldsymbol{v} = -\boldsymbol{f}(\boldsymbol{z}, t) + \dot{\boldsymbol{z}}_d - \boldsymbol{\Lambda}^{-1}\xi \ \mathrm{sgn}(s) \tag{5.54}$$

for some $\xi > 0$. Substituting this control into Eq. (5.52) gives

$$\dot{s} = -\xi \ \mathrm{sgn}(s) \tag{5.55}$$

stating that $s$ converge to zero in finite time; consequently so must the error vector $\boldsymbol{z}_e$. The error dynamics are said to exhibit *sliding mode* behavior if confined to this manifold. Of course, it is obvious that $\boldsymbol{f}(\cdot)$ is not a known function. Otherwise we would have canceled the term in the inversion process. This, however, does not prevent us from applying the control design via trial and error parameter design. Although it is of no significance to the current investigation, it can be demonstrated through simulation that the variable structure control design provides some robustness to the nominal I/O design. Such a "proof by simulation", however, would add very little to the content.

## 5.4 Summary

In this chapter we studied the dynamic behavior of an aircraft while undergoing planform changes. A commonly implemented robust pitch-attitude-hold compensator design was developed for analysis. Specifically, the control design was proportional-integral (PI) controller

with pitch rate feedback and additional lead compensation for robustness. To accommodate for configuration changes, the gains were scheduled according to the center of mass location of the aircraft. Nonlinear numerical simulations were conducted for a transformation from a loiter aircraft configuration to dash; the reverse transformation was also considered. When regulating a zero pitch angle it was shown that the compensator was capable of maintaining stability for various structural transformation rates. However, while attempting to maneuver a critical transformation speed was observed for both cases in which the pitch attitude became divergent. In general, if the transformation was sufficiently slow then adequate stabilization could be obtained.

A nonlinear control design was implemented to demonstrate its usefulness for morphing aircraft designs. Opposed to designing several control laws for each morphing configuration and for a range of flight conditions a single controller was developed. The input-output linearized model was shown to be adequate in tracking a fixed spacial point such as would be employed in waypoint navigation. The design was used as basis for investigating a variable span missile design. Using asymmetric wing extension bank-angle maneuvers could be achieved at higher accuracy as compared with the conventional tail-controlled aircraft. Navigation results were included to demonstrate the resulting improvements with regards to guidance tracking.

Although a very useful means of compensation, the I/O control design is inadequate in accounting for model uncertainty. Furthermore, due to not meeting the matching condition, there are very few tools that are helpful to ensure robustness. As a means of overcoming the difficulties with the nominal I/O nominal control design, a variable structure control addition was discussed as a means to add a measure of robustness.

# Chapter 6

# Conclusions and Recommendations

## 6.1 Conclusions

This thesis was concerned with examining the flight performance of morphing aircraft. The two distinct topics covered were the stabilization of an aircraft undergoing large changes in aerodynamic and inertial properties, and the flight performance improvements of morphing control actuation. In leading to these investigations, a complete dynamic description was constructed for aircraft undergoing large structural changes. Using Kane's method two different models were derived. The first is a nonrigid body model in which only one body-fixed basis is defined and the motion of the aircraft is defined about this point. The nonlinear model leads to terms that are difficult to define explicitly, particularly for complex structural changes. The resulting model is considered to be time-varying, including the first and second inertial moments, in that the structure of the aircraft is assumed to be a known function of time. Development of a autonomous model was peformed by considering the aircraft structure to be composed of a finite number of rigid bodies. Explicit state equations were developed to identify the motion of the total aircraft relative the main body-fixed frame. Finally, as a compromise between the time-varying nonrigid equations and the complex multibody expression, a point mass approximation was presented. The resulting form produced time-invariant equations of significantly reduced form relative to the multibody approach.

Three aircraft configurations were considered as platforms for studying the dynamic effects of morphing aircraft. The Teledyne Ryan Firebee was used as a baseline aircraft; the specific

configurations considered were dash, a loiter design and a maneuver configuration. Methods of developing aerodynamic models were discussed based on widely accepted methods. Datcom was introduced as the method used in determining the aerodynamic derivatives used in flight analysis. Specific to morphing control, an aerodynamic representation for a variable span aircraft was developed. In particular, it was shown that a asymmetric wing extension could be used to generate a large moment that may be suitable for control authority in maneuvering flight. Based on Prandtle's lifting line theory, an expression for the both the roll producing and damping moments were calculated. It was further shown, that for wing deflections of less than 10% of half span, the roll producing moment remains constant thus allowing the standard linear roll damping derivative approximation.

In the final chapter a numerical study was conducted on the dynamic behavior of an aircraft while undergoing planform changes. A commonly implemented robust pitch-attitude-hold compensator design was developed for analysis. Specifically, the control design was gain-scheduled proportional-integral (PI) controller with pitch rate feedback and additional lead compensation for robustness. Nonlinear numerical simulations were conducted for a transformation from a loiter aircraft configuration to dash; the reverse transformation was also considered. When regulating a zero pitch angle it was shown that the compensator was capable of maintaining stability for various structural transformation rates. However, while attempting to maneuver a critical transformation speed was observed for both cases in which the pitch attitude became divergent. In general, if the transformation was sufficiently slow then adequate stabilization could be obtained.

A nonlinear control design was implemented to demonstrate it usefulness for morphing aircraft designs. Opposed to designing several control laws for each morphing configuration and for a range of flight conditions a single controller was developed. The input-output linearized model was shown to be adequate in tracking a fixed spacial point such as would be employed in waypoint navigation. The design was used as basis for investigating a variable span aircraft design. Using asymmetric wing extension bank-angle maneuvers could be achieved at higher accuracy as compared with the conventional tail-controlled aircraft. Navigation results were included to demonstrate the resulting improvements with regards to guidance tracking.

## 6.2 Recommendations

As all currently designed aircraft are centered round a fixed planform arrangement, the consideration of morphing aircraft opens up several new research areas. In fact, the prospect calls for a complete reinvestigation of the theory of aircraft dynamics and control. Morphing aircraft research contains within its bounds a large variety of topics including material and actuation design, aerodynamics, dynamics, and flight control. Futhermore, any one of these individual topics contains vast opportunity for investigation.

The current trend is the design of aircraft that are capable of significant geometry alterations with the goal of optimality in any given flight regime. As such, a main topic of consideration is flight control design. A morphing aircraft requires flight control laws capable of high performance while maintaining stability in the presence of large variations in aerodynamic forces, moments of inertia, and mass center. These requirements lead to underlying research aspects involving the interaction between the environment, aircraft structure, and flight control system. Current methods of flight control rely on small perturbation linear models about a given operating points. For a single configuration aircraft the implementation of a flight control system involves an extensive process of aerodynamic testing, analytical design, numerical simulation, and flight testing. For a multi-configuration aircraft it is apparent that the task of control design becomes exceedingly more involved. A significant contribution if the field of autonomous morphing flight control would be the development of stable, robust controllers to accommodate the required trajectory tracking for the highly nonlinear present in variable configuration aircraft. In general, the dynamics of flight are not amenable to robust nonlinear designs. The matching condition is of significant consequence in that it remains a large obstacle for robust design. In flight dynamics, uncertainties are included in almost every aspect of the dynamical equations. As such, the highly desirable controller canonical form is difficult to obtain.

Recommendations for future work are experimental investigations into the flight behavior through extensive wind-tunnel testing. Specifically, the issues of immediate concern are the identification and approximation of the transient aerodynamic forces and moments of significant consequence, and methods of dynamic/aerodynamic modeling that are suitable for analysis and control design.

# Bibliography


[1] J. Birkler, A. G. Bower, J. A. Drezner, G. Lee, M. Lorell, G. Smith, F. Timson, W. P. G. Trimble, and O. Younossi. *Competition and Innovation in the US Fixed-Wing Military Aircraft Industry.* RAND National Defense Research Institute, Prepared for the Office of the Secretary of Defense, 2003.

[2] Lazarus K. B. Crawley, E. F. and D. J. Warkentin. Embedded actuation and processing in intelligent materials. *2nd International Workshop on Composite Materials and Structures, Troy, NY 1989.*

[3] T. A. Weisshaar. *Structural Tailoring for Aircraft Performance - Recent Trends in Aeroelasticitiy, Structures, and Structural Dynamics, Ed. P. Hajela.* Florida University Press, 1987.

[4] R. L. Spangler and S. R. Hall. Piezoelectric actuators for helicopter rotor control. *31st Structures, Structural Dynamics and Materials Conference, Long Beach, CA, 1990.*

[5] D. K. Samak and I. Chopra. Feasibility study to build a smart rotor trailing edge flap actuation. *Proceedings of the North American Conference on Smart Materials and Structures*, pages 225–237, 1993.

[6] P. Chen and I. Chopra. Feasibility study to build a smart rotor: Induced strain actuation of airfoil twist. *North American Conference on Smart Materials and Structures, Albuquerque, NM, 1993.*

[7] R. Barrett. All moving active aerodynamic surface research. *Smart Materials and Structures*, 4:65–74, 1995.

[8] R. Barrett, S. R. Gross, and F. Brozoski. Missile flight control using active flexspar actuators. *Smart Materials and Structures*, 5:121–128, 1996.

[9] L. B. Scherer, C. A. Martin, K. Appa, J. N. Kudva, and M. N. West. Smart wing test results. *SPIE Proceedings*, 3044(2), 1997.

[10] J. N. Kudva. Overview of DARPA/AFRL/NASA Smart Wing program. *SPIE Proceedings, March 1-4, Newport Beach, CA*, 3674(26), 1999.

[11] C. A. Martin, J. Bartley-Cho, and B. F. Carpenter. Design and fabrication of smart wing model and SMA control surfaces. *SPIE Proceedings, March 1-4, Newport Beach, CA*, 3674(27), 1999.

[12] J. N. Kudva. Overview of the DARPA Smart Wing project. *Journal of Intelligent Material Systems and Structures*, 15(4):261–268, 2004.

[13] B. Sanders, F. E. Eastep, and E. Foster. Aerodynamic and aeroelastic considerations of wings with conformal control surfaces for morphing aircraft. *Journal of Aircraft*, 40(1):94–99, 2003.

[14] E. Pendleton, K. Griffin, M. Kehoe, and B. Perry. The Active Aeroelastic Wing Flight Research program. *Proceedings of the 37th AIAA Structures, Structural Dynamics, and Materials Conference, AIAA-98-1972, Long Beach, CA, 20-23 April 1998.*

[15] E. Pendleton, D. Bassette, P. Field, G. Miller, and K. Griffin. A flight research program for active aeroelastic wing technology. *Proceedings of the 37th AIAA Structures, Structural Dynamics, and Materials Conference, AIAA-96-1574, Salt Lake City, Utah 15-17 April 1996.*

[16] J. R. Wilson. Active aeroelastic wing: A new/old twist on flight. *Aerospace America*, 40(9):34–37, 2002.

[17] S. Kusmina. Review and outlook for active and passive aeroelastic design concepts for future aircraft. *Proceedings of 23rd International Congress of Aerospace Sciences*, 2002.

[18] M. Amprikidis and J. E. Cooper. Development of smart spars for active aeroelastic structures. *AIAA Paper 2003-1799*, 2002.

[19] M. Amprikidis, J. E. Cooper, C. Rogerson, and G. Vio. Experimental validation of wing twist control using adaptive internal structures. *45th AIAA/ASME/ASCE/AHS/ASC*

*Structures, Structural Dynamics & Materials Conference, AIAA Paper-2004-1884, Palm Springs, California, 19-22 April, 2004.*

[20] M. Amprikidis, J. E. Cooper, C. Rogerson, and G. Vio. On the use of adaptive internal structures for wing shape control. *46th AIAA/ASME/ASCE/AHS/ASC Structures, Structural Dynamics and Materials Conference, AIAA Paper 2005-2042, 18-21 April 2005.*

[21] F. H. Gern, D. J. Inman, and R. K. Kapania. Structural and aeroelastic modeling of general planform wings with morphing airfoils. *AIAA Journal*, 40(4):628–637, 2002.

[22] F. H. Gern, D. J. Inman, and R. K. Kapania. Computation of actuation power requirements for smart wings with morphing airfoils. *43rd AIAA/ASME/ASCE/AHS/ASC Structures, Structural Dynamics & Materials Conference, AIAA Paper-2002-1629, Denver, Colorado, 22-25 April, 2002.*

[23] G. W. Petit, H. H. Robertshaw, and D. J. Inman. Morphing wings for unmanned aircraft. *Smart Materials Bulletin*, ISSN 1471-3918, 2001.

[24] B. C. Prock, T. A. Weisshaar, and W. A. Crossley. Morphing airfoil shape change optimization with minimum actuator energy as an objective. *9th AIAA/ISSMO Symposium on Multidisciplinary Analysis and Optimization, AIAA Paper-2002-5401, Atlanta, Georgia, 4-6 September, 2002.*

[25] C. Johnston, D. Neal, L. Wiggins, H. R. Robertshaw, Mason W. H., and D. J. Inman. A model to compare the dynamic performance of flight control energy requirements of morphing and conventionally actuated wings. *44th AIAA/ASME/ASCE/AHS/ASC Structures, Structural Dynamics & Materials Conference, AIAA Paper-2004-1726, Norfolk, VA, 7-10 April, 2003.*

[26] S. E. Gano, J. E. Renaud, S. M. Batill, and A. Tovar. Shape optimization for conforming airfoils. *44th AIAA/ASME/ASCE/AHS/ASC Structures, Structural Dynamics & Materials Conference, AIAA Paper-2004-1579, Norfolk, VA, 7-10 April, 2003.*

[27] L. Saggere and S. Kota. Static shape control of smart structures using compliant mechanisms. *AIAA Journal*, 37(5):572–578, 2003.

[28] D. S. Ramrkahyani, G. A. Lesieutre, M. Frecker, and S. Bharti. Aircraft structural morphing using tendon actuated compliant cellular trusses. *45th*

*AIAA/ASME/ASCE/AHS/ASC Structures, Structural Dynamics & Materials Conference, AIAA Paper-2004-1728, Palm Springs, California, 19-22 April, 2004.*

[29] K. Manute and G. W. Reich. An aeroelastic topology optimization approach for adaptive wing design. *45th AIAA/ASME/ASCE/AHS/ASC Structures, Structural Dynamics & Materials Conference, AIAA Paper 2004-1805, Palm Springs, California, 19-22 April, 2004.*

[30] M. H. Love, P. S. Zink, R. L. Stroud, D. R. Bye, and C. Chase. Impact of actuation concepts on morphing aircraft structures. *45th AIAA/ASME/ASCE/AHS/ASC Structures, Structural Dynamics & Materials Conference, AIAA Paper-2004-1724, Palm Springs, California, 19-22 April, 2004.*

[31] J. S. Bae, T. M. Seigler, and D. J. Inman. Aerodynamic and aeroelastic considerations of a variable-span morphing wing. *45th AIAA/ASME/ASCE/AHS/ASC Structures, Structural Dynamics & Materials Conference, AIAA Paper-2004-1726, Palm Springs, California, 19-22 April, 2004.*

[32] J. S. Bae, T. M. Seigler, and Inman D. J. Aerodynamic and static aerolelastic characteristics of a variable-span morphing wing. *Journal of Aircraft*, 42(2):528–534, 2005.

[33] J. Blondeau, J. Richeson, and D. J. Pines. Development of smart spars for active aeroelastic structures. *AIAA Paper 2003-1718*, 2003.

[34] D. A. Neal, M. G. Good, C. O. Johnston, H. H. Robertshaw, W. H. Mason, and D. J. Inman. Design and wind tunnel analysis of a fully adaptive aircraft configuration. *45th AIAA/ASME/ASCE/AHS/ASC Structures, Structural Dynamics & Materials Conference, AIAA Paper-2004-1727, Palm Springs, California, 19-22 April, 2004.*

[35] G. H. Bryan. *Stability in Aviation.* London: Macmillan, 1911.

[36] M. J. Abzug and E. E. Larrabee. *Airplane Stability and Control - A History of the Technologies that Made Aviation Possible.* Cambridge Aerospace Series, 2002.

[37] V. Mukhopadhyay. Historical perspective on analysis and control of aeroelastic responses. *Journal of Guidance, Control, and Dynamics*, 26(5):673–684, 2003.

[38] A. R. Collar. The expanding domain of aeroelasticity. *Journal of the Royal Aeronautical Society*, 50:428, 1946.

[39] A. S. Taylor. The present status of aircraft stability problems in the aeroelastic domain. *Journal of the Royal Aeronautical Society*, 63:580, 1959.

[40] R. L. Bisplinghoff and H. Ashley. *Principles of Aeroelasticity*. Wiley, New York, 1962.

[41] R. D. Milne. *Dynamics of Deformable Aeroplane, Parts I and II*. Her Majesty's Stationary Office, Reports and Memoranda No. 3345, London, 1962.

[42] W. P. Rodden and J. R. Love. Equations of motion of a quasi-steady flight vehicle utilizing restrained static aeroelastic characteristics. *Journal of Aircraft*, 22(9):802–809, 1985.

[43] M. R. Waszak and D. K. Schmidt. Flight dynamics of aeroelastic vehicles. *Journal of Aircraft*, 25(6):167–177, 1988.

[44] D. K. Schmidt and D. L. Raney. Modeling and simulation of flexible flight vehicles. *Journal of Guidance, Control, and Dynamics*, 24(3):539–546, 2001.

[45] L. Meirovitch. A unified theory for the flight dynamics and aeroelasticity of whole aircraft. *Proceedings of the Eleventh Symposium on Structural Dynamics and Control, Blacksburg, VA, May 12-14*, pages 461–468, 1997.

[46] L. Meirovitch and I. Tuczu. Multidisciplinary approach to the modeling of flexible aircraft. *International Forum on Aeroelasticity and Structural Dynamics, Madrid, Spain, June 5-7*, pages 435–448, 2001.

[47] L. Meirovitch and I. Tuczu. Time simulations of the response of maneuvering flexible aircraft. *Journal of Guidance, Control, and Dynamics*, 27(5):814–828, 1965.

[48] W. W. Hooker and G. Margulies. The dynamic attitude equations for n-body satellite. *Journal of Astronomical Science*, 12:123–128, 1965.

[49] R. L. Huston. Multibody dynamics - modeling and analysis methods. *Applied Mechanics Review*, 44:109–117, 1991.

[50] A. A. Shabana. Flexible multibody dynamics: Review of past and recent developments. *Multibody System Dynamics*, 1:189–222, 1997.

[51] W. Schiehlen. Multibody system dynamics: Roots and perspectives. *Multibody System Dynamics*, 1:149–188, 1997.

[52] T. R. Kane and C. F. Wang. On the derivation of equations of motion. *Journal of the Society of Industrial and Applied Mathematics*, 13(2):487–492, 1965.

[53] J. W. Gibbs. On the fundamental formulas of dynamics. *American Journal of Mathematics*, 2:49–64, 1879.

[54] P. Appell. Sur les mouvements de roulment; equations du mouvement analougues a celles de Lagrange. *Comptes Rendus*, 129:317–320, 1899.

[55] T. R Kane. Formulation of the equations of motion for complex spacecraft. *Journal of Guidance, Control, and Dynamics*, 3(2):99–112, 1980.

[56] T. R. Kane and D. A. Levinson. The use of Kane's dynamical equations in robotics. *International Journal of Robotics Research*, 2:3–21, 1983.

[57] D. Rosenthal and M. Sherman. High performance multibody simulations via symbolic equation manipulation and Kane's method. *Journal of Astronautical Sciences*, 34(3):223–239, 1990.

[58] K. Anderson. An order-n formulation for the motion simulation of general multi-rigid-body constrained systems. *Computers and Structures*, 43(3):565–579, 1992.

[59] K. Anderson. An efficient formulation for the modeling of general multi-flexible-body constrained systems. *International Journal of Solids and Structures*, 30(7):921–945, 1993.

[60] D. Rosenthal. An order-n formulation for robotic systems. *Journal of Astronautical Sciences*, 38(4):511–529, 1990.

[61] L. Meirovitch and H. D. Nelson. On the high-spin motion of a satellite containing elastic parts. *Journal of Spacecraft and Rockets*, 3(11):1597–1602, 1966.

[62] L. Meirovitch. Hybrid state equations of motion for flexible bodies in terms of quasi-coordinates. *Journal of Guidance, Control, and Dynamics*, 14(5):1008–1013, 1991.

[63] L. Meirovitch. Derivation of equations of motion for flexible multibody systems in terms of quasi-coordinates for the extended Hamilton's principle. *Journal of Shock and Vibrations*, 1(2):107–119, 1993.

[64] L. Meirovitch and T. J. Stemple. Hybrid equations of motion for flexible multibody systems using quasi-coordinates. *Journal of Guidance, Control, and Dynamics*, 18(4):678–688, 1995.

[65] C. A. Woolsey. Reduced Hamiltonian dynamics for a rigid body/mass particle system. *Journal of Guidance, Control, and Dynamics*, 28(1):131–138, 2005.

[66] F. L. Lewis. *'Introduction to Modern Control Theory', Applied Optimal Control and Estimation*. Prentice Hall, Upper Saddle River, NJ, 1992.

[67] P. Dorato. A historical review of robust control. *IEEE Control Systems*, 7(2):44–47, 1987.

[68] R. Bellman. *Dynamic Programming*. Princeton University Press, New Jersey, 1957.

[69] L. S. Pontryagin, V. G. Boltyansky, R. V. Gamkrelidze, and E. F. Mishchenko. *The Mathematical Theory of Optimal Processes*. Wiley, New York, 1962.

[70] A. G. J. MacFarlane and I. Postlethwaite. The generalized Nyquist stability criterion and multivariable root loci. *International Journal of Control*, 25:81–127, 1977.

[71] J. C. Doyle and G. Stein. Multivariable feedback design: Concepts for a classical/modern synthesis. *IEEE Transactions on Automatic Control*, AC-26(1):4–16, 1981.

[72] M. G. Safonov, A. J. Laub, and G. L. Hartmann. Feedback properties of multivariable systems: The role and use of the return difference matrix. *IEEE Transactions on Automatic Control*, 26(1):47–65, 1981.

[73] S. H. Lane and R. F. Stengel. Flight control desing using non-linear inverse dynamics. *Automatica*, 24(4):478–483, 1988.

[74] D. Enns, D. Bugajski, R. Hendrick, and G. Stein. Dynamic inversion: An evolving methodology for fight control design. *International Journal of Control*, 51(1):71–91, 1994.

[75] K. Zhou, J. C. Doyle, and K. Glover. *Robust Optimal Control*. Prentice Hall, New Jersey, 1996.

[76] R. E. Roberson. *Dynamics of Multibody Systems*. Springer-Verlag, 1988.

[77] S. P Joshi, Z. Tidwell, W. A. Crossley, and S. Ramakrishnan. Comparison of morphing wing strategies based on aircraft performance impacts. *45th AIAA/ASME/ASCE/AHS/ASC Structures, Structural Dynamics & Materials Conference, AIAA Paper-2004-1726, Palm Springs, California, 19-22 April, 2004.*

[78] N. E. Leonard and J.G. Graver. Model-based feedback control of autonomous underwater gliders. *IEEE Journal of Oceanic Engineering*, 26(4):633–645, October 2001.

[79] C. A. Woolsey and N. E. Leonard. Moving mass control for underwater vehicles. *Proceedings of the American Control Conference*, 5:633–645, 2002.

[80] I. M. Roll. Mechanism for precision orbit control with applications to fomuation flying. *Journal of Guidance, Control, and Dynamics*, 25(4):818–820, 2002.

[81] R. D. Robinett, B. R. Sturgis, and S. A. Kerr. Moving mass trim control for aerospace vehicles. *Journal of Guidance, Control, and Dynamics*, 19(5):1064–1070, 1996.

[82] P. K. Menon and G. D. Sweriduk. Integrated guidance and control of moving-mass actuated kinetic warheads. *Journal of Guidance, Control, and Dynamics*, 27(1):118–126, 2004.

[83] T. Petsopoulos and F. J. Regan. A moving mass roll control system for a fixed-trim reentry vehicles. *AIAA Paper 94-0033*, 1994.

[84] W. F. Phillips and C. E. Hailey. Review of attitude representations used for aircraft kinematics. *Journal of Aircraft*, 38(4):718–737, 2001.

[85] P. Tsiotras. On the choice of coordinates for control problems on SO(3). *30th Annual Conference on Information Sciences and Systems, Princeton University, March 20-22*, pages 1238–1243, 1996.

[86] Ahmed A. Shabana. *Dynamics of Multibody Systems.* Cambridge University Press, 1998.

[87] R. L. Huston. *Multibody Dynamics.* Butterworth-Heinemann, Stoneham, MA, 1990.

[88] B. L. Stevens and F. L. Lewis. *Aircraft Control and Simulation.* John Wiley & Sons Inc, 2003.

[89] T. R. Kane. *Dynamics.* Stanford, CA, 1972.

[90] T. R. Kane and D. A. Levinson. *Dynamics: Theory and Applications*. McGraw-Hill Series in Mechanical Engineering, 1st Edition, 1985.

[91] L. A. Pars. *A Treatise on Analytical Dynamics*. Ox Bow Press, 1981.

[92] D. T. Greenwood. *Classical Dynamics*. Prentice Hall Inc, 1977.

[93] L. Merovitch. *Methods of Analytical Dynamics*. McGraw-Hill, 1970.

[94] R. M. Rosenberg. *Analytical Dynamics of Discrete Systems*. Plenum Press, 1977.

[95] A. M. Bloch, N. E. Leonard, and J. E. Marsden. Controlled Lagrangians and the stabilization of Euler-Poincare mechanical systems. *International Journal of Robust and Nonlinear Control*, 11(3):191–214, 1990.

[96] P. C. Mitiguy and T. R. Kane. Motion variables leading to efficient equations of motion. *International Journal of Robotics Research*, 15(5):522–532, 1996.

[97] J. E. Keat. Comment on 'relationship between Kane's equation and the Gibbs-Appell equations. *Journal of Guidance, Control, and Dynamics*, 10(6):594–595, 1987.

[98] D. E. Rosenthal. Comment on 'relationship between Kane's equation and the Gibbs-Appell equations. *Journal of Guidance, Control, and Dynamics*, 10(6):595–596, 1987.

[99] A. K. Banerjee. Comment on 'relationship between Kane's equation and the Gibbs-Appell equations. *Journal of Guidance, Control, and Dynamics*, 10(6):596–597, 1987.

[100] R. L. Huston. Comment on 'relationship between Kane's equation and theGibbs-Appell equations. *Journal of Guidance, Control, and Dynamics*, 11(2):191, 1988.

[101] A. H. Bajodah, D. H. Hodges, and Y. H. Chen. New form of Kane's equations of motion for constrained systems. *Journal of Guidance, Control, and Dyanamics*, 26(1):79–88, 2003.

[102] R. L. Huston. On the equivalence of Kane's equations and Gibbs' equations for multi-body dynamic formulations. *Mechanical Research Communications*, 14(2):123–131, 1987.

[103] I. Sharf, G. M. T. D'eleuterio, and P. C. Hughes. On the dynamics of Gibbs, Appell, and Kane. *European Journal of Mechanics*, 11(2):145–155, 1992.

[104] N. B. Haaser and J. A. Sullivan. *Real Analysis*. Dover Publications, 1971.

[105] J. I. Neimark and N. A. Fufaev. *Dynamics on Nonholonomic Systems*. American Mathematical Society, 1972.

[106] A. Kurdila, J. G. Papastavridis, and M. P. Kamat. Role of Maggi's equations in computational methods for constrained multibody systems. *Journal of Guidance, Control, and Dynamics*, 13(1):113–120, 1990.

[107] J. T. Wang and R. L. Huston. Kane's equations with undetermined multipliers - application to constrained multibody systems. *Journal of Applied Mechanics*, 54:424–429, 1987.

[108] R. L. Huston, C. Q. Liu, and F. Li. Equivalent control of constrained multibody systems. *Multibody System Dynamics*, 10:313–321, 2003.

[109] W. Blajer. Dynamics and control of mechanical systems in partly specified motion. *Journal of the Franklin Institute*, 334B(3):407–426, 1997.

[110] R. L. Huston, C. Q. Liu, and F. Li. Constraint forces and undetermined multipliers in constrained multibody systems. *Multibody System Dynamics*, 3:381–389, 1999.

[111] Bernard Etkin. *Dynamics of Atmospheric Flight*. John Wiley & Sons, 1972.

[112] John H. Blakelock. *Automatic Control of Aircraft and Missiles*. John Wiley & Sons, 1991.

[113] D. P. Raymer. *Aircraft Design: A Conceptual Approach, 3rd Edition*. AIAA, Reston, VA, 1999.

[114] J. D. Anderson, Jr. *Aircraft Performance and Design*. Prentice-Hall, Englewood Cliffs, NJ, 1989.

[115] D. E. Hoak and et al. Fink, R. D. *USAF Stability and Control Datcom*. Flight Control Division, Air Force Flight Dynamics Laboratory, Wright-Patterson Air Force Base, Ohio, 1978.

[116] S. R. Vukelich, S. L. Stoy, K. A. Burns, J. A. Castillo, and M. E. Moore. *Missile Datcom Final Report*. McDonnell Douglas Missile Systems Company, St. Louis, Missouri, 1988.

[117] R. W. Kress. Variable sweep wing designs. *AIAA Paper 83-1051*, 1983.

[118] Bernard Etkin. *Dynamics of Flight: Stability and Control*. John Wiley & Sons, second edition edition, 1982.

[119] T. T. Takahashi, R. J. Spall, D. C. Turner, J. C. Otto, and P. O. Hagan. A multidisciplinary assessment of morphing aircraft technology applied to tactical cruise missile configurations. *45th AIAA/ASME/ASCE/AHS/ASC Structures, Structural Dynamics & Materials Conference, AIAA Paper 2004-1709, Palm Springs, California, 19-22 April, 2004*.

[120] L. Prandtl and O. G. Tietjens. *Applied Hydro and Aeromechanics*. Dover Publications, 1957.

[121] J. J. Bertin and M. L. Smith. *Aerodynamics for Engineers*. Prentice Hall, 1998.

[122] D. McRuer, I. Ashkenas, and D. Graham. *Aircraft Dynamics and Automatic Control*. Princeton University Press, Princeton, NJ, 1990.

[123] Hassan K. Khalil. *Nonlinear Systems*. Prentice Hall, 2002.

[124] Friedland B. Williams, D. E. and A. N. Madiwale. Modern control theory for design of autopilots for bank-to-turn missiles. *Journal of Guidance, Control, and Dynamics*, 10(4):378–386, July-August 1987.

[125] Paul Zarchan. *Progress in Astronautics and Aeronautics: Tactical and Strategic Missile Guidance*, volume 199. AIAA, fourth edition edition, 2002.

[126] Shankar Sastry. *Nonlinear Systems: Analysis, Stability, and Control*. Springer Verlag, 1999.

[127] Z. Qu and D. M. Dawson. Robust control design of a class of cascaded nonlinear uncertain systems. *ASME Control of Systems With Inexact Dynamic Models*, 33:63–71, 1991.

[128] A. Mazur. New approach to designing input-output decoupling controllers for mobile manipulators. *Bulletin of the Polish Academy of Sciences*, 53(1):31–37, 2005.

[129] J. K. Hedrick and S. Gopalswarny. Nonlinear flight control design via sliding methods. *Journal of Guidance, Control, and Dynamics*, 13(5):850–858, 1990.

[130] J. J. Romano and S. N. Singh. I-O map inversion, zero dynamics and flight control. *IEEE Transactions on Aerospace and Electronic Systems*, 26(6):1022–1029, 1990.

[131] K.-Y. Lian, Chung D.-M. Fu, L.-C., and T.-S. Kuo. Adaptive robust autopilot design for bank-to-turn aircraft. *Proceedings of the American Control Conference*, pages 1746–1750, March-April 1993.

[132] C.M. Mickle and J.J. Zhu. Bank-to-turn roll-yaw-pitch autopilot design using dynamic nonlinear inversion and pd-eigenvalue assignment. *Proceedings of the American Control Conference, Chicago, Illinois*, pages 1359–1364, June 2000.

[133] W. C. Durham. Constrained control allocation - three moment problem. *Journal of Guidance, Control, and Dynamics*, 17(2):330–336, 1993.

[134] W. C. Durham. Constrained control allocation. *Journal of Guidance, Control, and Dynamics*, 16(4):717–725, 1994.

# Appendix A

The following appendices give the full equations of motion of a shape-changing aircraft for various dynamic representations. The equations are expressed in coordinates of $\mathcal{F}^1$, that is, the origin of the main body located within the fuselage. The inertial contributions are left undeveloped, but may be easily derived from the vector equations given in Chapter 2.

## Body-Axis Equations

The body axis equations, expressed in the basis of the body frame, are given as:

$$
\begin{aligned}
\dot{U} &- RV + QW = 1/m_T(h_{f_x} + F_x - gm_T s\theta) \\
\dot{V} &+ RU - PW = 1/m_T(h_{f_y} + F_y + gm_T c\theta s\phi) \\
\dot{W} &- QU + PV = 1/m_T(h_{f_z} + F_z + gm_T c\theta c\phi) \\
J_x\dot{P} &- J_{12}\dot{Q} - J_{13}\dot{R} - J_{13}PQ - J_{23}Q^2 + J_{12}PR + (J_z - J_y)QR + J_{23}R^2 \\
&= h_{m_x} + \mathscr{L} + gc\theta(c\phi\ \hat{S}_y - s\phi\ \hat{S}_z) \\
-J_{12}\dot{P} &+ J_y\dot{Q} - J_{23}\dot{R} + (J_x - J_z)PR + J_{13}(P - R)(P + R) + J_{23}PQ - J_{12}QR \\
&= h_{m_y} + \mathscr{M} - g(c\theta c\phi\ \hat{S}_x + s\theta\ \hat{S}_z) \\
-J_{13}\dot{P} &- J_{23}\dot{Q} + J_z\dot{R} + (J_y - J_x)PQ + J_{13}QR - J_{12}P^2 + J_{12}Q^2 - J_{23}PR \\
&= h_{m_z} + \mathscr{N} + g(s\theta\ \hat{S}_y + c\theta s\phi\ \hat{S}_x)
\end{aligned}
$$

# Stability-Axis Equations

The body-axis equations, expressed in the basis of the stability axis are given as:

$$
\begin{aligned}
c\beta\dot{V}_T &- s\beta V_T\dot{\beta} - s\beta V_T R_s = 1/m_T[h^s_{f_x} + F^s_x - gm_T(c\theta\ c\phi\ s\alpha - c\alpha\ s\theta)] \\
s\beta\dot{V}_T &+ c\beta V_T\dot{\beta} + c\beta V_T R_s = 1/m_T[h^s_{f_y} + F^s_y + gm_T c\theta s\phi] \\
V_T c\beta\dot{\alpha} &- c\beta Q V_T + s\beta P_s V_T = 1/m_T[h^s_{f_z} + F^s_z + gm_T(c\alpha\ c\theta\ c\phi + s\alpha\ s\theta)] \\
J^s_x\dot{P}_s &- J^s_{13}\dot{R}_s - (J^s_x R_s + J^s_{13}P_s)\dot{\alpha} - J^s_{13}QP_s + (J^s_z - J^s_y)QR_s \\
&= h^s_{m_x} + M^s_x + g[c\alpha c\theta(c\phi\hat{S}_y - s\phi\hat{S}_z) + s\alpha(s\theta\hat{S}_y + c\theta s\phi\hat{S}_x)] \\
J^s_y\dot{Q} &+ (J^s_x - J^s_z)P_s R_s + J^s_{13}(P_s - R_s)(P_s + R_s) \\
&= h^s_{m_y} + M^s_y - g(c\theta c\phi\hat{S}_x + s\theta\hat{S}_z) \\
-J^s_{13}\dot{P}_s &+ J^s_z\dot{R}_s + (J^s_z P_s + J^s_{13}R_s)\dot{\alpha} - (J^s_y - J^s_x)QP_s + J^s_{13}QR_s \\
&= h^s_{m_z} + M^s_z + g[(c\alpha s\theta\hat{S}_y + c\theta(s\phi c\alpha\hat{S}_x - c\phi s\alpha\hat{S}_y + s\phi s\alpha\hat{S}_z)]
\end{aligned}
$$

# Wind-Axis Equations

The body-axis equations, expressed in the basis of the wind axis are given as:

$$
\begin{aligned}
\dot{V}_T &= 1/m_T[h^w_{f_x} + F^w_x + gm_T(c\beta c\theta c\phi s\alpha - c\beta c\alpha s\theta + c\theta s\beta s\phi)] \\
V_T\dot{\beta} &+ V_T R_w = 1/m_T[h^w_{f_y} + F^w_y + gm_T(c\alpha s\beta s\theta - c\theta c\phi s\alpha s\beta + c\theta c\beta s\phi)] \\
c\beta V_T\dot{\alpha} &- V_T Q_w = 1/m_T[h^w_{f_z} + F^w_z + gm_T(c\alpha c\theta c\phi + s\alpha s\theta)] \\
J^w_x\dot{P}_w &- J^w_{12}\dot{Q}_w - J^w_{13}\dot{R}_w - [(J^w_{13}P_w + J^w_x R_w)c\beta + (J^w_{13}Q_w - J^w_{12}R_w)s\beta]\dot{\alpha} \\
&- (J^w_{12}P_w + J^w_x Q_w)\dot{\beta} - (J^w_{13}P_w + J^w_{23}Q_w)Q_w + [J^w_{12}P_w + (J^w_y - J^w_z)Q_w]R_w \\
&+ J^w_{23}R^2_w = h^w_{m_x} + M^w_x + g[c\beta s\alpha s\theta\hat{S}_y - s\beta c\theta c\phi\hat{S}_x - s\beta s\theta\hat{S}_z + c\beta c\theta s\alpha s\phi\hat{S}_x \\
&+ c\alpha c\beta c\theta(c\phi\hat{S}_y - s\phi\hat{S}_z)] \\
J^w_y\dot{Q}_w &- J^w_{23}\dot{R}_w + c\beta[(J^w_{12}R_w - J^w_{23}P_w) + s\beta(J^w_{23}Q_w + J^w_y R_w)]\dot{\alpha} \\
&+ (J^w_y P_w + J^w_{12}Q_w)\dot{\beta} + J^w_{23}P_w Q_w + (J^w_x - J^w_z)P_w R_w - J^w_{12}Q_w R_w \\
&+ J^w_{13}(P_w - R_w)(P_w + R_w) = h^w_{m_y} + M^w_y - g[c\beta(c\theta c\phi\hat{S}_x + s\theta\hat{S}_z) \\
&+ s\beta c\alpha c\theta(c\phi\hat{S}_y - s\phi\hat{S}_z) + s\beta s\alpha(s\theta\hat{S}_y + c\theta s\phi\hat{S}_x)] \\
-J^w_{13}\dot{R}_w &- J^w_{23}\dot{Q}_w + J^w_z\dot{R}_w + (c\beta J^w_{13}R_w - s\beta J^w_{23}R_w + c\beta J^w_z P_w - s\beta J^w_z Q_w)\dot{\alpha} \\
&+ (J^w_{13}Q_w - J^w_{23}P_w)\dot{\beta} - (J^w_{12}P_w + J^w_x Q_w)P_w + (J^w_y P_w + J^w_{12}Q_w)Q_w \\
&+ (J^w_{13}Q_w - J^w_{23}P_w)R_w = h^w_{m_z} + M^w_z + g[c\alpha s\theta\hat{S}_y - c\theta c\phi s\alpha\hat{S}_y \\
&+ c\theta s\phi(c\alpha\hat{S}_x + s\alpha\hat{S}_z)]
\end{aligned}
$$

# Appendix B - Datcom Aerodynamics

## Loiter Configuration

```
1        ***** THE USAF AUTOMATED MISSILE DATCOM * REV 3/99 *****
            AERODYNAMIC METHODS FOR MISSILE CONFIGURATIONS

   CONERR - INPUT ERROR CHECKING

   ERROR CODES - N* DENOTES THE NUMBER OF OCCURENCES OF EACH ERROR
   A - UNKNOWN VARIABLE NAME
   B - MISSING EQUAL SIGN FOLLOWING VARIABLE NAME
   C - NON-ARRAY VARIABLE HAS AN ARRAY ELEMENTDESIGNATION - (N)
   D - NON-ARRAY VARIABLE HAS MULTIPLE VALUES ASSIGNED
   E - ASSIGNED VALUES EXCEED ARRAY DIMENSION
   F - SYNTAX ERROR

   ************************ INPUT DATA CARDS ************************

  1  $FLTCON NALPHA=13.,NMACH=1.,MACH=0.5,ALT=30000.,BETA=0.,
  2         ALPHA=-2.,-1.,0.,1.,2.,3.,
  3         ALPHA(7)=4.,5.,6.,7.,8.,9.,10.,$
  4  $REFQ XCG=10.7,SREF=46.9288,LREF=2.2566,LATREF=22.3154,$
  5  $AXIBOD LNOSE=4.95,DNOSE=2.33,BNOSE=0.1532,LCENTR=15.0,DCENTR=2.33,
  6          LAFT=2.95,DEXIT=1.13,$
  7  $FINSET1 XLE=8.9121,NPANEL=2.,PHIF=90.,270.,SWEEP=15.9724,STA=0.,
  8           CHORD=2.8816,1.1192,SSPAN=1.1654,11.1577,
  9           SECTYP=NACA,$
             ** SUBSTITUTING NUMERIC FOR NAME NACA
 10 NACA-1-4-0010-53
 11  $FINSET2 XLE=16.9637,NPANEL=3.,PHIF=0.,90.,270.,
 12           SWEEP=43.7736,STA=0.,SSPAN=1.1650,3.9113,CHORD=2.3188,2.0995,
 13           SECTYP=NACA,$
             ** SUBSTITUTING NUMERIC FOR NAME NACA
 14 NACA-2-4-0010-53
 15  $DEFLCT DELTA2=0.,0.,0.,$
 16 DERIV RAD
 17 DAMP
 18 WRITE DB12,1,8
 19 PLOT
 20 SAVE
 21 NEXT CASE
 22  $TRIM SET=2.,$
 23 PRINT AERO TRIM
 24 PLOT
 25 NEXT CASE
1        ***** THE USAF AUTOMATED MISSILE DATCOM * REV 3/99 *****     CASE   1
            AERODYNAMIC METHODS FOR MISSILE CONFIGURATIONS          PAGE   1
   CASE INPUTS
   FOLLOWING ARE THE CARDS INPUT FOR THIS CASE

  $FLTCON NALPHA=13.,NMACH=1.,MACH=0.5,ALT=30000.,BETA=0.,
         ALPHA=-2.,-1.,0.,1.,2.,3.,
```

```
      ALPHA(7)=4.,5.,6.,7.,8.,9.,10.,$
 $REFQ XCG=10.7,SREF=46.9288,LREF=2.2566,LATREF=22.3154,$
 $AXIBOD LNOSE=4.95,DNOSE=2.33,BNOSE=0.1532,LCENTR=15.0,DCENTR=2.33,
      LAFT=2.95,DEXIT=1.13,$
 $FINSET1 XLE=8.9121,NPANEL=2.,PHIF=90.,270.,SWEEP=15.9724,STA=0.,
      CHORD=2.8816,1.1192,SSPAN=1.1654,11.1577,
      SECTYP=1.,$
NACA-1-4-0010-53
 $FINSET2 XLE=16.9637,NPANEL=3.,PHIF=0.,90.,270.,
      SWEEP=43.7736,STA=0.,SSPAN=1.1650,3.9113,CHORD=2.3188,2.0995,
      SECTYP=1.,$
NACA-2-4-0010-53
 $DEFLCT DELTA2=0.,0.,0.,$
DERIV RAD
DAMP
WRITE DB12,1,8
PLOT
SAVE
NEXT CASE
  THE BOUNDARY LAYER IS ASSUMED TO BE TURBULENT
  THE INPUT UNITS ARE IN FEET, THE SCALE FACTOR IS   1.0000
1       ***** THE USAF AUTOMATED MISSILE DATCOM * REV 3/99 *****     CASE   1
          AERODYNAMIC METHODS FOR MISSILE CONFIGURATIONS         PAGE   2
           STATIC AERODYNAMICS FOR BODY-FIN SET 1 AND 2

    ******* FLIGHT CONDITIONS AND REFERENCE QUANTITIES *******
   MACH NO  =      0.50             REYNOLDS NO = 1.419E+06 /FT
   ALTITUDE =    30000.0 FT       DYNAMIC PRESSURE =    110.19 LB/FT**2
   SIDESLIP =      0.00 DEG               ROLL =      0.00 DEG
   REF AREA =    46.929 FT**2       MOMENT CENTER =    10.700 FT
   REF LENGTH =     2.26 FT         LAT REF LENGTH =     22.32 FT

            ----- LONGITUDINAL -----     -- LATERAL DIRECTIONAL --
      ALPHA      CN       CM       CA       CY      CLN      CLL

      -2.00   -0.211    0.004    0.017    0.000    0.000    0.000
      -1.00   -0.106    0.002    0.021    0.000    0.000    0.000
       0.00    0.000    0.000    0.022    0.000    0.000    0.000
       1.00    0.106   -0.002    0.021    0.000    0.000    0.000
       2.00    0.211   -0.004    0.017    0.000    0.000    0.000
       3.00    0.314   -0.007    0.010    0.000    0.000    0.000
       4.00    0.417   -0.010    0.001    0.000    0.000    0.000
       5.00    0.518   -0.012   -0.010    0.000    0.000    0.000
       6.00    0.615   -0.017   -0.023    0.000    0.000    0.000
       7.00    0.706   -0.024   -0.039    0.000    0.000    0.000
       8.00    0.786   -0.036   -0.054    0.000    0.000    0.000
       9.00    0.859   -0.053   -0.063    0.000    0.000    0.000
      10.00    0.930   -0.069   -0.064    0.000    0.000    0.000

      ALPHA      CL       CD      CL/CD     X-C.P.

      -2.00   -0.210    0.024   -8.700   -0.021
      -1.00   -0.105    0.023   -4.672   -0.021
       0.00    0.000    0.022    0.000   -0.021
       1.00    0.105    0.023    4.672   -0.021
       2.00    0.210    0.024    8.700   -0.021
```

| | | | | |
|---|---|---|---|---|
| 3.00 | 0.313 | 0.027 | 11.701 | -0.022 |
| 4.00 | 0.415 | 0.031 | 13.620 | -0.023 |
| 5.00 | 0.516 | 0.035 | 14.607 | -0.024 |
| 6.00 | 0.614 | 0.041 | 14.919 | -0.027 |
| 7.00 | 0.705 | 0.048 | 14.802 | -0.034 |
| 8.00 | 0.786 | 0.056 | 13.983 | -0.046 |
| 9.00 | 0.858 | 0.072 | 11.896 | -0.061 |
| 10.00 | 0.927 | 0.098 | 9.422 | -0.075 |

X-C.P. MEAS. FROM MOMENT CENTER IN REF. LENGTHS, NEG. AFT OF MOMENT CENTER

1 ***** THE USAF AUTOMATED MISSILE DATCOM * REV 3/99 ***** CASE 1
AERODYNAMIC METHODS FOR MISSILE CONFIGURATIONS PAGE 3
STATIC AERODYNAMICS FOR BODY-FIN SET 1 AND 2

******* FLIGHT CONDITIONS AND REFERENCE QUANTITIES *******
MACH NO = 0.50 REYNOLDS NO = 1.419E+06 /FT
ALTITUDE = 30000.0 FT DYNAMIC PRESSURE = 110.19 LB/FT**2
SIDESLIP = 0.00 DEG ROLL = 0.00 DEG
REF AREA = 46.929 FT**2 MOMENT CENTER = 10.700 FT
REF LENGTH = 2.26 FT LAT REF LENGTH = 22.32 FT

---------- DERIVATIVES (PER RADIAN) ----------

| ALPHA | CNA | CMA | CYB | CLNB | CLLB |
|---|---|---|---|---|---|
| -2.00 | 5.9838 | -0.1339 | -0.6103 | 0.0692 | -0.0385 |
| -1.00 | 6.0320 | -0.1276 | -0.6042 | 0.0693 | -0.0422 |
| 0.00 | 6.0562 | -0.1245 | -0.6005 | 0.0691 | -0.0458 |
| 1.00 | 6.0320 | -0.1276 | -0.6026 | 0.0687 | -0.0493 |
| 2.00 | 5.9693 | -0.1373 | -0.6071 | 0.0681 | -0.0525 |
| 3.00 | 5.9012 | -0.1458 | -0.6119 | 0.0672 | -0.0557 |
| 4.00 | 5.8284 | -0.1570 | -0.6165 | 0.0663 | -0.0587 |
| 5.00 | 5.6867 | -0.2040 | -0.6210 | 0.0654 | -0.0618 |
| 6.00 | 5.3997 | -0.3261 | -0.6256 | 0.0645 | -0.0642 |
| 7.00 | 4.9081 | -0.5577 | -0.6305 | 0.0639 | -0.0656 |
| 8.00 | 4.3723 | -0.8217 | -0.6358 | 0.0634 | -0.0658 |
| 9.00 | 4.1133 | -0.9549 | -0.6400 | 0.0626 | -0.0669 |
| 10.00 | 4.0607 | -0.9868 | -0.6434 | 0.0617 | -0.0689 |

PANEL DEFLECTION ANGLES (DEGREES)

| SET | FIN 1 | FIN 2 | FIN 3 | FIN 4 | FIN 5 | FIN 6 | FIN 7 | FIN 8 |
|---|---|---|---|---|---|---|---|---|
| 1 | 0.00 | 0.00 | | | | | | |
| 2 | 0.00 | 0.00 | 0.00 | | | | | |

1 ***** THE USAF AUTOMATED MISSILE DATCOM * REV 3/99 ***** CASE 1
AERODYNAMIC METHODS FOR MISSILE CONFIGURATIONS PAGE 4
BODY + 2 FIN SETS DYNAMIC DERIVATIVES

******* FLIGHT CONDITIONS AND REFERENCE QUANTITIES *******
MACH NO = 0.50 REYNOLDS NO = 1.419E+06 /FT
ALTITUDE = 30000.0 FT DYNAMIC PRESSURE = 110.19 LB/FT**2
SIDESLIP = 0.00 DEG ROLL = 0.00 DEG
REF AREA = 46.929 FT**2 MOMENT CENTER = 10.700 FT
REF LENGTH = 2.26 FT LAT REF LENGTH = 22.32 FT

---------- DYNAMIC DERIVATIVES (PER RADIAN) ----------

| ALPHA | CNQ | CMQ | CAQ | CNAD | CMAD |
|---|---|---|---|---|---|
| -2.00 | 7.981 | -53.218 | -0.459 | 18.747 | -18.070 |

| | | | | | |
|---|---|---|---|---|---|
| -1.00 | 8.044 | -53.447 | -0.488 | 18.747 | -18.070 |
| 0.00 | 8.090 | -53.614 | -0.503 | 18.747 | -18.070 |
| 1.00 | 8.094 | -53.628 | -0.505 | 18.747 | -18.070 |
| 2.00 | 8.080 | -53.571 | -0.497 | 18.747 | -18.070 |
| 3.00 | 8.052 | -53.464 | -0.480 | 18.747 | -18.070 |
| 4.00 | 8.012 | -53.316 | -0.454 | 18.747 | -18.070 |
| 5.00 | 7.963 | -53.130 | -0.421 | 18.747 | -18.070 |
| 6.00 | 7.907 | -52.909 | -0.378 | 18.747 | -18.070 |
| 7.00 | 7.844 | -52.646 | -0.322 | 18.747 | -18.070 |
| 8.00 | 7.768 | -52.323 | -0.249 | 18.747 | -18.070 |
| 9.00 | 7.666 | -51.940 | -0.159 | 18.747 | -18.070 |
| 10.00 | 7.548 | -51.519 | -0.050 | 18.747 | -18.070 |

PITCH RATE DERIVATIVES NON-DIMENSIONALIZED BY Q*LREF/2*V



******* FLIGHT CONDITIONS AND REFERENCE QUANTITIES *******

MACH NO = 0.50 REYNOLDS NO = 1.419E+06 /FT
ALTITUDE = 30000.0 FT DYNAMIC PRESSURE = 110.19 LB/FT**2
SIDESLIP = 0.00 DEG ROLL = 0.00 DEG
REF AREA = 46.929 FT**2 MOMENT CENTER = 10.700 FT
REF LENGTH = 2.26 FT LAT REF LENGTH = 22.32 FT

---------- DYNAMIC DERIVATIVES (PER RADIAN) ----------

| ALPHA | CYR | CLNR | CLLR | CYP | CLNP | CLLP |
|---|---|---|---|---|---|---|
| -2.00 | 0.417 | -0.400 | 0.033 | 0.189 | -0.068 | -0.512 |
| -1.00 | 0.418 | -0.401 | 0.033 | 0.193 | -0.069 | -0.519 |
| 0.00 | 0.419 | -0.401 | 0.033 | 0.195 | -0.070 | -0.522 |
| 1.00 | 0.418 | -0.401 | 0.033 | 0.195 | -0.070 | -0.519 |
| 2.00 | 0.417 | -0.400 | 0.033 | 0.193 | -0.069 | -0.512 |
| 3.00 | 0.415 | -0.400 | 0.033 | 0.190 | -0.068 | -0.505 |
| 4.00 | 0.413 | -0.399 | 0.033 | 0.189 | -0.068 | -0.500 |
| 5.00 | 0.411 | -0.398 | 0.032 | 0.183 | -0.066 | -0.495 |
| 6.00 | 0.409 | -0.398 | 0.032 | 0.168 | -0.060 | -0.471 |
| 7.00 | 0.407 | -0.397 | 0.032 | 0.139 | -0.050 | -0.420 |
| 8.00 | 0.405 | -0.396 | 0.032 | 0.102 | -0.037 | -0.357 |
| 9.00 | 0.403 | -0.395 | 0.032 | 0.088 | -0.031 | -0.331 |
| 10.00 | 0.402 | -0.395 | 0.031 | 0.087 | -0.031 | -0.329 |

YAW AND ROLL RATE DERIVATIVES NON-DIMENSIONALIZED BY R*LATREF/2*V



CASE INPUTS
FOLLOWING ARE THE CARDS INPUT FOR THIS CASE

```
 $TRIM SET=2.,$
PRINT AERO TRIM
PLOT
NEXT CASE
```

THE BOUNDARY LAYER IS ASSUMED TO BE TURBULENT
THE INPUT UNITS ARE IN FEET, THE SCALE FACTOR IS 1.0000

******* FLIGHT CONDITIONS AND REFERENCE QUANTITIES *******
MACH NO = 0.50 REYNOLDS NO = 1.419E+06 /FT
ALTITUDE = 30000.0 FT DYNAMIC PRESSURE = 110.19 LB/FT**2
SIDESLIP = 0.00 DEG ROLL = 0.00 DEG
REF AREA = 46.929 FT**2 MOMENT CENTER = 10.700 FT
REF LENGTH = 2.26 FT LAT REF LENGTH = 22.32 FT

| ALPHA | DELTA | CL | CD | CN | CA |
|---|---|---|---|---|---|
| -2.00 | 0.18 | -0.209 | 0.024 | -0.209 | 0.017 |
| -1.00 | 0.09 | -0.105 | 0.023 | -0.105 | 0.021 |
| 0.00 | 0.00 | 0.000 | 0.022 | 0.000 | 0.022 |
| 1.00 | -0.09 | 0.105 | 0.023 | 0.105 | 0.021 |
| 2.00 | -0.18 | 0.209 | 0.024 | 0.209 | 0.017 |
| 3.00 | -0.29 | 0.311 | 0.027 | 0.312 | 0.010 |
| 4.00 | -0.40 | 0.413 | 0.030 | 0.414 | 0.002 |
| 5.00 | -0.51 | 0.513 | 0.035 | 0.514 | -0.010 |
| 6.00 | -0.69 | 0.609 | 0.041 | 0.610 | -0.023 |
| 7.00 | -0.97 | 0.699 | 0.047 | 0.699 | -0.038 |
| 8.00 | -1.46 | 0.776 | 0.055 | 0.776 | -0.053 |
| 9.00 | -2.10 | 0.843 | 0.070 | 0.844 | -0.062 |
| 10.00 | -2.75 | 0.908 | 0.096 | 0.910 | -0.063 |

PANELS FROM FIN SET 2 WERE DEFLECTED OVER THE RANGE -25.00 TO 20.00 DEG
PANEL 1 WAS FIXED
PANEL 2 WAS VARIED
PANEL 3 WAS FIXED
*** END OF JOB ***

# Dash Configuration

```
1        ***** THE USAF AUTOMATED MISSILE DATCOM * REV 3/99 *****
            AERODYNAMIC METHODS FOR MISSILE CONFIGURATIONS

   CONERR - INPUT ERROR CHECKING

   ERROR CODES - N* DENOTES THE NUMBER OF OCCURENCES OF EACH ERROR
   A - UNKNOWN VARIABLE NAME
   B - MISSING EQUAL SIGN FOLLOWING VARIABLE NAME
   C - NON-ARRAY VARIABLE HAS AN ARRAY ELEMENTDESIGNATION - (N)
   D - NON-ARRAY VARIABLE HAS MULTIPLE VALUES ASSIGNED
   E - ASSIGNED VALUES EXCEED ARRAY DIMENSION
   F - SYNTAX ERROR

   ************************ INPUT DATA CARDS ************************

  1  $FLTCON NALPHA=13.,NMACH=1.,MACH=0.5,ALT=30000.,BETA=0.,
  2          ALPHA=-2.,-1.,0.,1.,2.,3.,
  3          ALPHA(7)=4.,5.,6.,7.,8.,9.,10.,$
  4  $REFQ XCG=13.2,SREF=65.4031,LREF=6.3483,LATREF=12.6058,$
  5  $AXIBOD LNOSE=4.95,DNOSE=2.33,BNOSE=0.1532,LCENTR=15.0,DCENTR=2.33,
  6           LAFT=2.95,DEXIT=1.13,$
  7  $FINSET1 XLE=8.9542,NPANEL=2.,PHIF=90.,270.,SWEEP=60.0008,STA=0.,
  8           CHORD=7.8661,0.9392,SSPAN=1.1654,6.3029,
  9           SECTYP=NACA,$
             ** SUBSTITUTING NUMERIC FOR NAME NACA
```

```
 10 NACA-1-4-0010-53
 11  $FINSET2 XLE=16.9637,NPANEL=3.,PHIF=0.,90.,270.,
 12          SWEEP=43.7736,STA=0.,SSPAN=1.1650,3.9113,CHORD=2.3188,2.0995,
 13          SECTYP=NACA,$
           ** SUBSTITUTING NUMERIC FOR NAME NACA
 14 NACA-2-4-0010-53
 15  $DEFLCT DELTA2=0.,0.,0.$
 16 DAMP
 17 WRITE DB12,1,8
 18 PLOT
 19 SAVE
 20 NEXT CASE
 21  $TRIM SET=2.,$
 22 PRINT AERO TRIM
 23 PLOT
 24 NEXT CASE
1        ***** THE USAF AUTOMATED MISSILE DATCOM * REV 3/99 *****     CASE   1
            AERODYNAMIC METHODS FOR MISSILE CONFIGURATIONS          PAGE   1
   CASE INPUTS
   FOLLOWING ARE THE CARDS INPUT FOR THIS CASE

 $FLTCON NALPHA=13.,NMACH=1.,MACH=0.5,ALT=30000.,BETA=0.,
        ALPHA=-2.,-1.,0.,1.,2.,3.,
        ALPHA(7)=4.,5.,6.,7.,8.,9.,10.,$
 $REFQ XCG=13.2,SREF=65.4031,LREF=6.3483,LATREF=12.6058,$
 $AXIBOD LNOSE=4.95,DNOSE=2.33,BNOSE=0.1532,LCENTR=15.0,DCENTR=2.33,
        LAFT=2.95,DEXIT=1.13,$
 $FINSET1 XLE=8.9542,NPANEL=2.,PHIF=90.,270.,SWEEP=60.0008,STA=0.,
        CHORD=7.8661,0.9392,SSPAN=1.1654,6.3029,
        SECTYP=1.,$
NACA-1-4-0010-53
 $FINSET2 XLE=16.9637,NPANEL=3.,PHIF=0.,90.,270.,
        SWEEP=43.7736,STA=0.,SSPAN=1.1650,3.9113,CHORD=2.3188,2.0995,
        SECTYP=1.,$
NACA-2-4-0010-53
 $DEFLCT DELTA2=0.,0.,0.$
DAMP
WRITE DB12,1,8
PLOT
SAVE
NEXT CASE
   THE BOUNDARY LAYER IS ASSUMED TO BE TURBULENT
   THE INPUT UNITS ARE IN FEET, THE SCALE FACTOR IS   1.0000
1        ***** THE USAF AUTOMATED MISSILE DATCOM * REV 3/99 *****     CASE   1
            AERODYNAMIC METHODS FOR MISSILE CONFIGURATIONS          PAGE   2
             STATIC AERODYNAMICS FOR BODY-FIN SET 1 AND 2

     ******* FLIGHT CONDITIONS AND REFERENCE QUANTITIES *******
    MACH NO  =       0.50             REYNOLDS NO = 1.419E+06 /FT
    ALTITUDE =    30000.0 FT       DYNAMIC PRESSURE =    110.19 LB/FT**2
    SIDESLIP =       0.00 DEG             ROLL =      0.00 DEG
    REF AREA =     65.403 FT**2       MOMENT CENTER =    13.200 FT
    REF LENGTH =     6.35 FT         LAT REF LENGTH =     12.61 FT

                ----- LONGITUDINAL -----     -- LATERAL DIRECTIONAL --
       ALPHA       CN        CM        CA        CY       CLN       CLL
```

| | | | | | | |
|---|---|---|---|---|---|---|
| -2.00 | -0.098 | 0.007 | 0.014 | 0.000 | 0.000 | 0.000 |
| -1.00 | -0.049 | 0.004 | 0.015 | 0.000 | 0.000 | 0.000 |
| 0.00 | 0.000 | 0.000 | 0.016 | 0.000 | 0.000 | 0.000 |
| 1.00 | 0.049 | -0.004 | 0.015 | 0.000 | 0.000 | 0.000 |
| 2.00 | 0.098 | -0.007 | 0.014 | 0.000 | 0.000 | 0.000 |
| 3.00 | 0.148 | -0.010 | 0.012 | 0.000 | 0.000 | 0.000 |
| 4.00 | 0.198 | -0.013 | 0.009 | 0.000 | 0.000 | 0.000 |
| 5.00 | 0.249 | -0.016 | 0.005 | 0.000 | 0.000 | 0.000 |
| 6.00 | 0.300 | -0.018 | 0.001 | 0.000 | 0.000 | 0.000 |
| 7.00 | 0.351 | -0.020 | -0.004 | 0.000 | 0.000 | 0.000 |
| 8.00 | 0.402 | -0.022 | -0.009 | 0.000 | 0.000 | 0.000 |
| 9.00 | 0.454 | -0.024 | -0.011 | 0.000 | 0.000 | 0.000 |
| 10.00 | 0.505 | -0.026 | -0.011 | 0.000 | 0.000 | 0.000 |

| ALPHA | CL | CD | CL/CD | X-C.P. |
|---|---|---|---|---|
| -2.00 | -0.097 | 0.017 | -5.613 | -0.071 |
| -1.00 | -0.048 | 0.016 | -3.008 | -0.073 |
| 0.00 | 0.000 | 0.016 | 0.000 | -0.073 |
| 1.00 | 0.048 | 0.016 | 3.008 | -0.073 |
| 2.00 | 0.097 | 0.017 | 5.613 | -0.071 |
| 3.00 | 0.147 | 0.019 | 7.536 | -0.068 |
| 4.00 | 0.197 | 0.023 | 8.703 | -0.065 |
| 5.00 | 0.247 | 0.027 | 9.232 | -0.063 |
| 6.00 | 0.298 | 0.032 | 9.305 | -0.060 |
| 7.00 | 0.349 | 0.038 | 9.088 | -0.058 |
| 8.00 | 0.400 | 0.047 | 8.466 | -0.056 |
| 9.00 | 0.450 | 0.060 | 7.475 | -0.054 |
| 10.00 | 0.499 | 0.077 | 6.471 | -0.052 |

X-C.P. MEAS. FROM MOMENT CENTER IN REF. LENGTHS, NEG. AFT OF MOMENT CENTER

1 ***** THE USAF AUTOMATED MISSILE DATCOM * REV 3/99 ***** CASE 1
AERODYNAMIC METHODS FOR MISSILE CONFIGURATIONS PAGE 3
STATIC AERODYNAMICS FOR BODY-FIN SET 1 AND 2

******* FLIGHT CONDITIONS AND REFERENCE QUANTITIES *******

MACH NO = 0.50 REYNOLDS NO = 1.419E+06 /FT
ALTITUDE = 30000.0 FT DYNAMIC PRESSURE = 110.19 LB/FT**2
SIDESLIP = 0.00 DEG ROLL = 0.00 DEG
REF AREA = 65.403 FT**2 MOMENT CENTER = 13.200 FT
REF LENGTH = 6.35 FT LAT REF LENGTH = 12.61 FT

---------- DERIVATIVES (PER DEGREE) ----------

| ALPHA | CNA | CMA | CYB | CLNB | CLLB |
|---|---|---|---|---|---|
| -2.00 | 0.0494 | -0.0033 | -0.0079 | 0.0001 | -0.0008 |
| -1.00 | 0.0488 | -0.0035 | -0.0077 | 0.0001 | -0.0009 |
| 0.00 | 0.0485 | -0.0035 | -0.0075 | 0.0000 | -0.0010 |
| 1.00 | 0.0488 | -0.0035 | -0.0074 | 0.0000 | -0.0011 |
| 2.00 | 0.0495 | -0.0032 | -0.0073 | -0.0001 | -0.0012 |
| 3.00 | 0.0502 | -0.0030 | -0.0073 | -0.0002 | -0.0013 |
| 4.00 | 0.0506 | -0.0028 | -0.0072 | -0.0003 | -0.0014 |
| 5.00 | 0.0509 | -0.0026 | -0.0071 | -0.0004 | -0.0015 |
| 6.00 | 0.0511 | -0.0024 | -0.0070 | -0.0005 | -0.0016 |
| 7.00 | 0.0512 | -0.0022 | -0.0069 | -0.0006 | -0.0017 |

| | | | | | |
|---|---|---|---|---|---|
| 8.00 | 0.0513 | -0.0020 | -0.0068 | -0.0007 | -0.0018 |
| 9.00 | 0.0514 | -0.0018 | -0.0067 | -0.0008 | -0.0019 |
| 10.00 | 0.0513 | -0.0017 | -0.0066 | -0.0008 | -0.0019 |

PANEL DEFLECTION ANGLES (DEGREES)

| SET | FIN 1 | FIN 2 | FIN 3 | FIN 4 | FIN 5 | FIN 6 | FIN 7 | FIN 8 |
|---|---|---|---|---|---|---|---|---|
| 1 | 0.00 | 0.00 | | | | | | |
| 2 | 0.00 | 0.00 | 0.00 | | | | | |



******* FLIGHT CONDITIONS AND REFERENCE QUANTITIES *******

MACH NO = 0.50 REYNOLDS NO = 1.419E+06 /FT
ALTITUDE = 30000.0 FT DYNAMIC PRESSURE = 110.19 LB/FT**2
SIDESLIP = 0.00 DEG ROLL = 0.00 DEG
REF AREA = 65.403 FT**2 MOMENT CENTER = 13.200 FT
REF LENGTH = 6.35 FT LAT REF LENGTH = 12.61 FT

---------- DYNAMIC DERIVATIVES (PER DEGREE) ----------

| ALPHA | CNQ | CMQ | CAQ | CNAD | CMAD |
|---|---|---|---|---|---|
| -2.00 | 0.036 | -0.088 | 0.000 | 0.054 | 0.006 |
| -1.00 | 0.036 | -0.089 | 0.000 | 0.054 | 0.006 |
| 0.00 | 0.036 | -0.089 | 0.000 | 0.054 | 0.006 |
| 1.00 | 0.036 | -0.089 | -0.001 | 0.054 | 0.006 |
| 2.00 | 0.036 | -0.089 | -0.001 | 0.054 | 0.006 |
| 3.00 | 0.037 | -0.089 | -0.002 | 0.054 | 0.006 |
| 4.00 | 0.037 | -0.089 | -0.002 | 0.054 | 0.006 |
| 5.00 | 0.037 | -0.089 | -0.002 | 0.054 | 0.006 |
| 6.00 | 0.037 | -0.089 | -0.003 | 0.054 | 0.006 |
| 7.00 | 0.037 | -0.088 | -0.003 | 0.054 | 0.006 |
| 8.00 | 0.037 | -0.088 | -0.002 | 0.054 | 0.006 |
| 9.00 | 0.037 | -0.088 | -0.001 | 0.054 | 0.006 |
| 10.00 | 0.037 | -0.088 | 0.000 | 0.054 | 0.006 |

PITCH RATE DERIVATIVES NON-DIMENSIONALIZED BY Q*LREF/2*V



******* FLIGHT CONDITIONS AND REFERENCE QUANTITIES *******

MACH NO = 0.50 REYNOLDS NO = 1.419E+06 /FT
ALTITUDE = 30000.0 FT DYNAMIC PRESSURE = 110.19 LB/FT**2
SIDESLIP = 0.00 DEG ROLL = 0.00 DEG
REF AREA = 65.403 FT**2 MOMENT CENTER = 13.200 FT
REF LENGTH = 6.35 FT LAT REF LENGTH = 12.61 FT

---------- DYNAMIC DERIVATIVES (PER DEGREE) ----------

| ALPHA | CYR | CLNR | CLLR | CYP | CLNP | CLLP |
|---|---|---|---|---|---|---|
| -2.00 | 0.007 | -0.020 | 0.001 | 0.001 | 0.000 | -0.004 |
| -1.00 | 0.007 | -0.020 | 0.001 | 0.001 | 0.000 | -0.004 |
| 0.00 | 0.007 | -0.020 | 0.001 | 0.001 | 0.000 | -0.004 |
| 1.00 | 0.007 | -0.020 | 0.001 | 0.001 | 0.000 | -0.004 |
| 2.00 | 0.007 | -0.020 | 0.001 | 0.001 | 0.000 | -0.004 |
| 3.00 | 0.006 | -0.020 | 0.001 | 0.001 | 0.000 | -0.004 |
| 4.00 | 0.006 | -0.020 | 0.001 | 0.001 | 0.000 | -0.004 |

```
      5.00     0.006    -0.020     0.001     0.001    -0.001    -0.004
      6.00     0.006    -0.020     0.001     0.001    -0.001    -0.004
      7.00     0.006    -0.020     0.001     0.001    -0.001    -0.004
      8.00     0.006    -0.020     0.001     0.001    -0.001    -0.004
      9.00     0.006    -0.020     0.001     0.001    -0.001    -0.004
     10.00     0.006    -0.020     0.001     0.001    -0.001    -0.004

  YAW AND ROLL RATE DERIVATIVES NON-DIMENSIONALIZED BY R*LATREF/2*V
1       ***** THE USAF AUTOMATED MISSILE DATCOM * REV 3/99 *****     CASE   2
          AERODYNAMIC METHODS FOR MISSILE CONFIGURATIONS         PAGE   1
  CASE INPUTS
  FOLLOWING ARE THE CARDS INPUT FOR THIS CASE

 $TRIM SET=2.,$
PRINT AERO TRIM
PLOT
NEXT CASE
  THE BOUNDARY LAYER IS ASSUMED TO BE TURBULENT
  THE INPUT UNITS ARE IN FEET, THE SCALE FACTOR IS   1.0000
1       ***** THE USAF AUTOMATED MISSILE DATCOM * REV 3/99 *****     CASE   2
          AERODYNAMIC METHODS FOR MISSILE CONFIGURATIONS         PAGE   2
            STATIC AERODYNAMIC COEFFICIENTS TRIMMED IN PITCH

    ******* FLIGHT CONDITIONS AND REFERENCE QUANTITIES *******
   MACH NO  =      0.50             REYNOLDS NO = 1.419E+06 /FT
   ALTITUDE =   30000.0 FT       DYNAMIC PRESSURE =    110.19 LB/FT**2
   SIDESLIP =      0.00 DEG              ROLL =      0.00 DEG
   REF AREA =    65.403 FT**2       MOMENT CENTER =    13.200 FT
   REF LENGTH =     6.35 FT         LAT REF LENGTH =     12.61 FT

      ALPHA     DELTA       CL       CD       CN       CA
      -2.00      1.62    -0.089    0.017   -0.090    0.014
      -1.00      0.83    -0.044    0.016   -0.044    0.015
       0.00      0.00     0.000    0.016    0.000    0.016
       1.00     -0.83     0.044    0.016    0.044    0.015
       2.00     -1.62     0.089    0.017    0.090    0.014
       3.00     -2.36     0.135    0.019    0.136    0.012
       4.00     -3.05     0.182    0.022    0.183    0.009
       5.00     -3.68     0.229    0.026    0.231    0.006
       6.00     -4.26     0.277    0.031    0.279    0.001
       7.00     -4.79     0.326    0.036    0.328   -0.004
       8.00     -5.26     0.374    0.045    0.376   -0.008
       9.00     -5.68     0.422    0.057    0.426   -0.010
      10.00     -6.07     0.469    0.073    0.475   -0.009
  PANELS FROM FIN SET 2 WERE DEFLECTED OVER THE RANGE -25.00 TO  20.00 DEG
  PANEL 1 WAS FIXED
  PANEL 2 WAS VARIED
  PANEL 3 WAS FIXED
  *** END OF JOB ***
```

# Maneuver Configuration

```
1       ***** THE USAF AUTOMATED MISSILE DATCOM * REV 3/99 *****
          AERODYNAMIC METHODS FOR MISSILE CONFIGURATIONS
```

```
  CONERR - INPUT ERROR CHECKING

  ERROR CODES - N* DENOTES THE NUMBER OF OCCURENCES OF EACH ERROR
  A - UNKNOWN VARIABLE NAME
  B - MISSING EQUAL SIGN FOLLOWING VARIABLE NAME
  C - NON-ARRAY VARIABLE HAS AN ARRAY ELEMENTDESIGNATION - (N)
  D - NON-ARRAY VARIABLE HAS MULTIPLE VALUES ASSIGNED
  E - ASSIGNED VALUES EXCEED ARRAY DIMENSION
  F - SYNTAX ERROR

  ************************ INPUT DATA CARDS *************************

  1  $FLTCON NALPHA=13.,NMACH=1.,MACH=0.5,ALT=30000.,BETA=0.,
  2         ALPHA=-2.,-1.,0.,1.,2.,3.,
  3         ALPHA(7)=4.,5.,6.,7.,8.,9.,10.,$
  4  $REFQ XCG=10.3,SREF=45.9381,LREF=2.9157,LATREF=16.6058,$
  5  $AXIBOD LNOSE=4.95,DNOSE=2.33,BNOSE=0.1532,LCENTR=15.0,DCENTR=2.33,
  6          LAFT=2.95,DEXIT=1.13,$
  7  $FINSET1 XLE=8.9115,NPANEL=2.,PHIF=90.,270.,SWEEP=15.0125,STA=0.,
  8          CHORD=3.5672,1.6531,SSPAN=1.1654,8.3029,
  9          SECTYP=NACA,$
            ** SUBSTITUTING NUMERIC FOR NAME NACA
 10 NACA-1-4-0010-53
 11  $FINSET2 XLE=16.9637,NPANEL=3.,PHIF=0.,90.,270.,
 12           SWEEP=43.7736,STA=0.,SSPAN=1.1650,3.9113,CHORD=2.3188,2.0995,
 13           SECTYP=NACA,$
            ** SUBSTITUTING NUMERIC FOR NAME NACA
 14 NACA-2-4-0010-53
 15  $DEFLCT DELTA2=0.,0.,0.,$
 16 DAMP
 17 WRITE DB12,1,8
 18 PLOT
 19 SAVE
 20 NEXT CASE
 21  $TRIM SET=2.,$
 22 PRINT AERO TRIM
 23 PLOT
 24 NEXT CASE
1         ***** THE USAF AUTOMATED MISSILE DATCOM * REV 3/99 *****     CASE   1
            AERODYNAMIC METHODS FOR MISSILE CONFIGURATIONS          PAGE   1
  CASE INPUTS
  FOLLOWING ARE THE CARDS INPUT FOR THIS CASE

 $FLTCON NALPHA=13.,NMACH=1.,MACH=0.5,ALT=30000.,BETA=0.,
        ALPHA=-2.,-1.,0.,1.,2.,3.,
        ALPHA(7)=4.,5.,6.,7.,8.,9.,10.,$
 $REFQ XCG=10.3,SREF=45.9381,LREF=2.9157,LATREF=16.6058,$
 $AXIBOD LNOSE=4.95,DNOSE=2.33,BNOSE=0.1532,LCENTR=15.0,DCENTR=2.33,
        LAFT=2.95,DEXIT=1.13,$
 $FINSET1 XLE=8.9115,NPANEL=2.,PHIF=90.,270.,SWEEP=15.0125,STA=0.,
         CHORD=3.5672,1.6531,SSPAN=1.1654,8.3029,
         SECTYP=1.,$
NACA-1-4-0010-53
 $FINSET2 XLE=16.9637,NPANEL=3.,PHIF=0.,90.,270.,
         SWEEP=43.7736,STA=0.,SSPAN=1.1650,3.9113,CHORD=2.3188,2.0995,
         SECTYP=1.,$
```

NACA-2-4-0010-53
$DEFLCT DELTA2=0.,0.,0.,$
DAMP
WRITE DB12,1,8
PLOT
SAVE
NEXT CASE
THE BOUNDARY LAYER IS ASSUMED TO BE TURBULENT
THE INPUT UNITS ARE IN FEET, THE SCALE FACTOR IS 1.0000
1 ***** THE USAF AUTOMATED MISSILE DATCOM * REV 3/99 ***** CASE 1
AERODYNAMIC METHODS FOR MISSILE CONFIGURATIONS PAGE 2
STATIC AERODYNAMICS FOR BODY-FIN SET 1 AND 2

******* FLIGHT CONDITIONS AND REFERENCE QUANTITIES *******
MACH NO = 0.50 REYNOLDS NO = 1.419E+06 /FT
ALTITUDE = 30000.0 FT DYNAMIC PRESSURE = 110.19 LB/FT**2
SIDESLIP = 0.00 DEG ROLL = 0.00 DEG
REF AREA = 45.938 FT**2 MOMENT CENTER = 10.300 FT
REF LENGTH = 2.92 FT LAT REF LENGTH = 16.61 FT

----- LONGITUDINAL ----- -- LATERAL DIRECTIONAL --

| ALPHA | CN | CM | CA | CY | CLN | CLL |
|---|---|---|---|---|---|---|
| -2.00 | -0.194 | 0.003 | 0.017 | 0.000 | 0.000 | 0.000 |
| -1.00 | -0.097 | 0.002 | 0.021 | 0.000 | 0.000 | 0.000 |
| 0.00 | 0.000 | 0.000 | 0.022 | 0.000 | 0.000 | 0.000 |
| 1.00 | 0.097 | -0.002 | 0.021 | 0.000 | 0.000 | 0.000 |
| 2.00 | 0.194 | -0.003 | 0.017 | 0.000 | 0.000 | 0.000 |
| 3.00 | 0.291 | -0.004 | 0.012 | 0.000 | 0.000 | 0.000 |
| 4.00 | 0.387 | -0.005 | 0.005 | 0.000 | 0.000 | 0.000 |
| 5.00 | 0.483 | -0.006 | -0.005 | 0.000 | 0.000 | 0.000 |
| 6.00 | 0.579 | -0.006 | -0.016 | 0.000 | 0.000 | 0.000 |
| 7.00 | 0.672 | -0.008 | -0.029 | 0.000 | 0.000 | 0.000 |
| 8.00 | 0.755 | -0.014 | -0.040 | 0.000 | 0.000 | 0.000 |
| 9.00 | 0.827 | -0.025 | -0.045 | 0.000 | 0.000 | 0.000 |
| 10.00 | 0.890 | -0.040 | -0.044 | 0.000 | 0.000 | 0.000 |

| ALPHA | CL | CD | CL/CD | X-C.P. |
|---|---|---|---|---|
| -2.00 | -0.193 | 0.024 | -7.995 | -0.016 |
| -1.00 | -0.096 | 0.022 | -4.324 | -0.018 |
| 0.00 | 0.000 | 0.022 | 0.000 | -0.018 |
| 1.00 | 0.096 | 0.022 | 4.324 | -0.018 |
| 2.00 | 0.193 | 0.024 | 7.995 | -0.016 |
| 3.00 | 0.290 | 0.027 | 10.621 | -0.014 |
| 4.00 | 0.386 | 0.032 | 12.166 | -0.013 |
| 5.00 | 0.482 | 0.038 | 12.836 | -0.012 |
| 6.00 | 0.578 | 0.045 | 12.892 | -0.010 |
| 7.00 | 0.670 | 0.053 | 12.599 | -0.011 |
| 8.00 | 0.753 | 0.065 | 11.531 | -0.018 |
| 9.00 | 0.824 | 0.085 | 9.711 | -0.030 |
| 10.00 | 0.884 | 0.111 | 7.940 | -0.045 |

X-C.P. MEAS. FROM MOMENT CENTER IN REF. LENGTHS, NEG. AFT OF MOMENT CENTER
1 ***** THE USAF AUTOMATED MISSILE DATCOM * REV 3/99 ***** CASE 1

******* FLIGHT CONDITIONS AND REFERENCE QUANTITIES *******

MACH NO = 0.50 REYNOLDS NO = 1.419E+06 /FT
ALTITUDE = 30000.0 FT DYNAMIC PRESSURE = 110.19 LB/FT**2
SIDESLIP = 0.00 DEG ROLL = 0.00 DEG
REF AREA = 45.938 FT**2 MOMENT CENTER = 10.300 FT
REF LENGTH = 2.92 FT LAT REF LENGTH = 16.61 FT

---------- DERIVATIVES (PER DEGREE) ----------

| ALPHA | CNA | CMA | CYB | CLNB | CLLB |
|---|---|---|---|---|---|
| -2.00 | 0.0971 | -0.0013 | -0.0108 | 0.0019 | -0.0010 |
| -1.00 | 0.0969 | -0.0016 | -0.0107 | 0.0019 | -0.0010 |
| 0.00 | 0.0968 | -0.0017 | -0.0107 | 0.0019 | -0.0011 |
| 1.00 | 0.0969 | -0.0016 | -0.0108 | 0.0019 | -0.0012 |
| 2.00 | 0.0970 | -0.0012 | -0.0109 | 0.0019 | -0.0012 |
| 3.00 | 0.0967 | -0.0010 | -0.0110 | 0.0019 | -0.0013 |
| 4.00 | 0.0963 | -0.0008 | -0.0111 | 0.0019 | -0.0013 |
| 5.00 | 0.0961 | -0.0004 | -0.0113 | 0.0019 | -0.0014 |
| 6.00 | 0.0941 | -0.0010 | -0.0114 | 0.0019 | -0.0014 |
| 7.00 | 0.0877 | -0.0038 | -0.0115 | 0.0019 | -0.0015 |
| 8.00 | 0.0777 | -0.0085 | -0.0116 | 0.0019 | -0.0015 |
| 9.00 | 0.0677 | -0.0134 | -0.0117 | 0.0019 | -0.0015 |
| 10.00 | 0.0586 | -0.0181 | -0.0118 | 0.0019 | -0.0016 |

PANEL DEFLECTION ANGLES (DEGREES)

| SET | FIN 1 | FIN 2 | FIN 3 | FIN 4 | FIN 5 | FIN 6 | FIN 7 | FIN 8 |
|---|---|---|---|---|---|---|---|---|
| 1 | 0.00 | 0.00 | | | | | | |
| 2 | 0.00 | 0.00 | 0.00 | | | | | |

1 ***** THE USAF AUTOMATED MISSILE DATCOM * REV 3/99 ***** CASE 1



******* FLIGHT CONDITIONS AND REFERENCE QUANTITIES *******

MACH NO = 0.50 REYNOLDS NO = 1.419E+06 /FT
ALTITUDE = 30000.0 FT DYNAMIC PRESSURE = 110.19 LB/FT**2
SIDESLIP = 0.00 DEG ROLL = 0.00 DEG
REF AREA = 45.938 FT**2 MOMENT CENTER = 10.300 FT
REF LENGTH = 2.92 FT LAT REF LENGTH = 16.61 FT

---------- DYNAMIC DERIVATIVES (PER DEGREE) ----------

| ALPHA | CNQ | CMQ | CAQ | CNAD | CMAD |
|---|---|---|---|---|---|
| -2.00 | 0.122 | -0.577 | -0.005 | 0.186 | -0.231 |
| -1.00 | 0.123 | -0.579 | -0.006 | 0.186 | -0.231 |
| 0.00 | 0.123 | -0.581 | -0.007 | 0.186 | -0.231 |
| 1.00 | 0.124 | -0.582 | -0.007 | 0.186 | -0.231 |
| 2.00 | 0.124 | -0.582 | -0.008 | 0.186 | -0.231 |
| 3.00 | 0.123 | -0.581 | -0.009 | 0.186 | -0.231 |
| 4.00 | 0.123 | -0.581 | -0.009 | 0.186 | -0.231 |
| 5.00 | 0.123 | -0.580 | -0.009 | 0.186 | -0.231 |
| 6.00 | 0.122 | -0.579 | -0.009 | 0.186 | -0.231 |
| 7.00 | 0.122 | -0.578 | -0.009 | 0.186 | -0.231 |
| 8.00 | 0.120 | -0.577 | -0.009 | 0.186 | -0.231 |
| 9.00 | 0.119 | -0.576 | -0.008 | 0.186 | -0.231 |
| 10.00 | 0.118 | -0.575 | -0.007 | 0.186 | -0.231 |

PITCH RATE DERIVATIVES NON-DIMENSIONALIZED BY Q*LREF/2*V

1 ***** THE USAF AUTOMATED MISSILE DATCOM * REV 3/99 ***** CASE 1

AERODYNAMIC METHODS FOR MISSILE CONFIGURATIONS PAGE 5

BODY + 2 FIN SETS DYNAMIC DERIVATIVES

******* FLIGHT CONDITIONS AND REFERENCE QUANTITIES *******

MACH NO = 0.50 REYNOLDS NO = 1.419E+06 /FT

ALTITUDE = 30000.0 FT DYNAMIC PRESSURE = 110.19 LB/FT**2

SIDESLIP = 0.00 DEG ROLL = 0.00 DEG

REF AREA = 45.938 FT**2 MOMENT CENTER = 10.300 FT

REF LENGTH = 2.92 FT LAT REF LENGTH = 16.61 FT

---------- DYNAMIC DERIVATIVES (PER DEGREE) ----------

| ALPHA | CYR | CLNR | CLLR | CYP | CLNP | CLLP |
|---|---|---|---|---|---|---|
| -2.00 | 0.010 | -0.013 | 0.001 | 0.003 | -0.001 | -0.008 |
| -1.00 | 0.011 | -0.013 | 0.001 | 0.003 | -0.001 | -0.008 |
| 0.00 | 0.011 | -0.013 | 0.001 | 0.003 | -0.002 | -0.008 |
| 1.00 | 0.011 | -0.013 | 0.001 | 0.003 | -0.002 | -0.008 |
| 2.00 | 0.010 | -0.013 | 0.001 | 0.003 | -0.002 | -0.008 |
| 3.00 | 0.010 | -0.013 | 0.001 | 0.003 | -0.002 | -0.008 |
| 4.00 | 0.010 | -0.013 | 0.001 | 0.003 | -0.002 | -0.008 |
| 5.00 | 0.010 | -0.013 | 0.001 | 0.003 | -0.002 | -0.008 |
| 6.00 | 0.010 | -0.013 | 0.001 | 0.003 | -0.002 | -0.008 |
| 7.00 | 0.010 | -0.013 | 0.001 | 0.003 | -0.001 | -0.007 |
| 8.00 | 0.010 | -0.013 | 0.001 | 0.002 | -0.001 | -0.006 |
| 9.00 | 0.010 | -0.013 | 0.001 | 0.001 | -0.001 | -0.005 |
| 10.00 | 0.010 | -0.013 | 0.001 | 0.001 | 0.000 | -0.005 |

YAW AND ROLL RATE DERIVATIVES NON-DIMENSIONALIZED BY R*LATREF/2*V

1 ***** THE USAF AUTOMATED MISSILE DATCOM * REV 3/99 ***** CASE 2

AERODYNAMIC METHODS FOR MISSILE CONFIGURATIONS PAGE 1

CASE INPUTS

FOLLOWING ARE THE CARDS INPUT FOR THIS CASE

```
 $TRIM SET=2.,$
PRINT AERO TRIM
PLOT
NEXT CASE
```

THE BOUNDARY LAYER IS ASSUMED TO BE TURBULENT

THE INPUT UNITS ARE IN FEET, THE SCALE FACTOR IS 1.0000

1 ***** THE USAF AUTOMATED MISSILE DATCOM * REV 3/99 ***** CASE 2

AERODYNAMIC METHODS FOR MISSILE CONFIGURATIONS PAGE 2

STATIC AERODYNAMIC COEFFICIENTS TRIMMED IN PITCH

******* FLIGHT CONDITIONS AND REFERENCE QUANTITIES *******

MACH NO = 0.50 REYNOLDS NO = 1.419E+06 /FT

ALTITUDE = 30000.0 FT DYNAMIC PRESSURE = 110.19 LB/FT**2

SIDESLIP = 0.00 DEG ROLL = 0.00 DEG

REF AREA = 45.938 FT**2 MOMENT CENTER = 10.300 FT

REF LENGTH = 2.92 FT LAT REF LENGTH = 16.61 FT

| ALPHA | DELTA | CL | CD | CN | CA |
|---|---|---|---|---|---|
| -2.00 | 0.16 | -0.192 | 0.024 | -0.193 | 0.017 |
| -1.00 | 0.08 | -0.096 | 0.022 | -0.096 | 0.021 |
| 0.00 | 0.00 | 0.000 | 0.022 | 0.000 | 0.022 |

| | | | | | |
|---|---|---|---|---|---|
| 1.00 | -0.08 | 0.096 | 0.022 | 0.096 | 0.021 |
| 2.00 | -0.16 | 0.192 | 0.024 | 0.193 | 0.017 |
| 3.00 | -0.21 | 0.288 | 0.027 | 0.289 | 0.012 |
| 4.00 | -0.25 | 0.384 | 0.032 | 0.385 | 0.005 |
| 5.00 | -0.28 | 0.480 | 0.037 | 0.481 | -0.005 |
| 6.00 | -0.30 | 0.576 | 0.045 | 0.577 | -0.016 |
| 7.00 | -0.38 | 0.667 | 0.053 | 0.669 | -0.029 |
| 8.00 | -0.67 | 0.748 | 0.065 | 0.750 | -0.040 |
| 9.00 | -1.21 | 0.815 | 0.084 | 0.818 | -0.045 |
| 10.00 | -1.97 | 0.870 | 0.109 | 0.876 | -0.043 |

PANELS FROM FIN SET 2 WERE DEFLECTED OVER THE RANGE -25.00 TO 20.00 DEG
PANEL 1 WAS FIXED
PANEL 2 WAS VARIED
PANEL 3 WAS FIXED
*** END OF JOB ***

# Vita

Thomas Michael Seigler was born in Greenville, South Carolina on October 13, 1975. He received the Bachelor of Science degree in Mechanical Engineering from Clemson University in 2000. He then attended Virginia Polytechnic Institute and State University where he received the Master of Science and Doctor of Philosophy degrees in Mechanical Engineering in 2002 and 2005, respectively. He is currently a post-doctoral researcher for the Center of Intelligent Material Systems and Structures at Virginia Tech.